View metadata, citation and similar papers at core.ac.uk
brought to you by CORE
provided by Helsingin yliopiston digitaalinen arkisto

Structural Analysis of Natural Chlorin Derivatives Utilizing NMR Spectroscopy and Molecular Modelling

Juho Helaja

University of Helsinki
Faculty of Science
Department of Chemistry
Laboratory of Organic Chemistry
P.O. Box 55, FIN-00014 University of Helsinki, Finland

ACADEMIC DISSERTATION

To be presented, with the permission of the Faculty of Science of the University of Helsinki, for public criticism in Auditorium A129of the Department of Chemistry, A. I. Virtasen Aukio 1, on June 30th, 2000 at 12 o'clock noon.

Helsinki 2000

ISBN 952-91-2286-1 (PDF version)
Helsingin yliopiston verkkojulkaisut
Helsinki 2000

Preface

The experimental work of this thesis was carried out at the Laboratory of Organic Chemistry in the University of Helsinki and at the NMR laboratory of the Institute of Biotechnology, University of Helsinki, during the years 1994 - 2000.

I sincerely thank my supervisor Professor Paavo Hynninen for introducing me into the field of chlorophyll chemistry, his endless patience for providing advice and criticism, during these years.

I am very grateful to Docent Ilkka Kilpeläinen for his expertise in NMR spectroscopy and the access to the NMR laboratory at the Institute of Biotechnology. The researchers in the NMR laboratory are thanked for their assistance and creating cosy working atmosphere.

I wish to thank Professor Tapio Hase for providing me working facilities in the Laboratory of Organic Chemistry.

Professors Franz-Peter Montforts in the University of Bremen and Helge Lemmetyinen in the Tampere University of Technology are acknowledged for pleasant collaboration. I am also grateful to Docent Henrik Konschin for his advice and expertise regarding the molecular modelling.

My sincere thanks are due to the members of the chlorophyll research group, especially to Doctors Kristiina Hyvärinen, Maria Stabelbroek-Möllmann and Docent Andrei Tauber, for excellent collaboration and scientific discussions. In particular, I would like to thank Andrei for his innovative and encouraging support.

Professors Reino Laatikainen and Erkki Kolehmainen are thanked for critically pre-examining this manuscript.

Financial support from the Graduate School of Bio-organic Chemistry, Academy of Finland, Finnish Chemical Society, and Magnus Ehrnrooth Foundation is acknowledged.

My warmest thanks are to my parents and parents-in-law for their support.

Above all, the love provided by Tuulamari and Thomas let me carry out this work over the barriers and dark valleys during these years.

Abstract

Chlorophylls are involved in the primary photosynthetic processes in nature. The utilization of chlorophyll derivatives as models for excitation energy transfer and electron transfer processes, as well as their medical applications requires a detailed structural knowledge. In this investigation, the solution structures of natural chlorins were analyzed utilizing NMR spectroscopy supported by molecular modelling.

In the literature review of the thesis, solution NMR spectroscopy and computer-aided molecular modelling are briefly reviewed. Their applications to chlorins are inspected through various examples of conformational analysis of chlorin compounds. In addition, chemical and structural properties of chlorins are discussed, as well as the NH tautomerism in porphyrins and chlorins.

The experimental part of the thesis is composed of five publications. They include conformational investigations of 13^2-methoxychlorophyll *a* epimers and electron-transfer model compounds. The latter are referred to as chlorin–anthraquinone and chlorin–C_{60} dyads. In addition, two publications focus on the NH tautomerism in natural chlorins.

Modern 2D NMR techniques were utilized to determine spectral assignments and structural parameters for the chlorins. Dynamic NMR spectroscopy was used to determine energy barriers for the conformational isomerism and NH tautomerism of the chlorins. The 2D ROESY NMR experiment proved to be a useful tool for determining the proton spectral assignments for the chlorins, as well as the stereochemistries of the modified parts of the chlorins. The computer-aided molecular modelling was based on the structure parameters obtained from the NMR data. Thus, the calculated 3D structures of the natural chlorin derivatives are related to their solution structures. The lowest-energy structural models for chlorin–anthraquinone and chlorin–C_{60} dyads were facilely deduced by molecular mechanics calculations with an MM+ force-field. In the cases of Mg-complexed chlorins and NH tautomers, reliable energy minima were found by the PM3-UHF method.

The results of molecular modelling indicated that the NH tautomers in which the nitrogen of the reduced chlorin subring is protonated, are energetically disfavoured due to their lower aromaticity. For the first time, an intermediate *trans* NH tautomer of a chlorin was detected by NMR spectroscopy at a low temperature. An important conclusion was that the total NH exchange of chlorins proceeds by a stepwise mechanism via aromatic *cis*-tautomers and the less aromatic *trans*-tautomer.

Abbreviations

A	acceptor
ARCS	aromatic ring current shielding
AM1	Austin method 1
B_0	static magnetic field
BChl	bacteriochlorophyll
Chl	chlorophyll
CTOCD	continuous transformation of ring current density
COSY	correlation spectroscopy
δ	chemical shift (ppm)
D	donor
DFT	density functional theory
DMSO	dimethyl sulfoxide
$\Delta G^{\ddagger}$	free energy of activation (Gibbs)
DEPT	distortionless enhancement by polarization transfer
$\Delta H^{\ddagger}$	enthalpy of activation
ΔH_f	heat of formation energy
DNMR	dynamic NMR
$\Delta S^{\ddagger}$	entropy of activation
gs	gradient selected
HF	Hartree-Fock
HMQC	heteronuclear multiple quantum coherence
HMBC	multiple-bond heteronuclear multiple-quantum coherence
HSQC	heteronuclear single quantum coherence
INDOR	internuclear double resonance
IUB	International Union of Biochemistry
IUPAC	International Union of Pure and Applied Chemistry
J	scalar coupling
E_A	activation energy (Arrhenius)
LSPD	long-range selective proton decoupling
NICS	nucleus-independent chemical shift
NMR	nuclear magnetic resonance
NOE	nuclear Overhauser effect
NOESY	NOE spectroscopy
MM	molecular mechanics
MNDO	modified neglect of diatomic overlap
MO	molecular orbital
MP2	second-order Møller-Plessed
PSI	photosystem I
PSII	photosystem II
PM3	parametric method 3
RC	reaction centre
RHF	restricted HF
ROE	NOE in rotating frame
ROESY	rotating frame NOE spectroscopy
SCF	self-consistent field
SFORD	Single frequency on- and off- resonance decoupling
S/N	signal-to-noise
T_1	spin-lattice relaxation time
T_C	coalescence temperature
τ_c	motional correlation time
τ_m	mixing time
THF	tetrahydrofuran
TMS	tetramethylsilane
TOCSY	total correlation spectroscopy
T-ROESY	transverse ROESY
TS	transition state
UFF	universal force-field
UHF	unrestricted HF
v/v	volum/volum
ω	Larmor frequency
1D	one-dimensional
2D	two-dimensional
3D	three-dimensional

List of original publications

This thesis is based on the following original publications.

I J. Helaja, K. Hyvärinen, S. Heikkinen, I. Kilpeläinen and P. H. Hynninen: Solution structures of 13^2-methoxychlorophyll *a* epimers, *J. Mol. Struct.* **1995**, *354*, 71.

II J. Helaja, A. Y. Tauber, I. Kilpeläinen and P. H. Hynninen: Novel Model Compounds for Photoinduced Electron Transfer: Structures of the Folded Conformers of Zinc(II)-Pyropheophytin–Anthraquinone Dyads, *Magn. Reson. Chem*. **1997**, *35*, 619.

III J. Helaja, A. Y. Tauber, Y. Abel, N. V. Tkachenko, H. Lemmetyinen, I. Kilpeläinen and P. H. Hynninen: Chlorophylls. IX. The First Phytochlorin–Fullerene Dyads: Synthesis and Conformational Studies, *J. Chem. Soc., Perkin Trans 1* **1999**, 2403.

IV J. Helaja, F.-P. Montforts, I. Kilpeläinen and P. H. Hynninen: NH Tautomerism in the Dimethyl Ester of Bonellin, a Natural Chlorin, *J. Org. Chem*. **1999**, *64*, 432.

V J. Helaja, M. Stabelbroek-Möllmann, I. Kilpeläinen and P. H. Hynninen: NH Tautomerism in the Natural Chlorin Derivatives, *J. Org. Chem*. **2000**, *65*, 3700.

Contents

1 Introduction

Natural chlorins have been subjected to extensive structural investigations in the 20th century due to their specific chemical properties and fundamental importance in nature.[1-5] The absolute configurations of chlorophyll (Chl) *a* were first elucidated by a combination of synthetic and spectroscopic methods.[6] Later, the three-dimensional (3D) structure was established by the X-ray studies of chemically modified chlorophyll *a*.[7] The X-ray analysis of the crystallized photosystems I[8] and II[9] (PSI and PSII) has revealed how Chl *a* molecules are organized in the photosynthetic machinery.

In the photosynthetic systems of green plants, the Chl *a* and Chl *b* molecules participate in light-induced excitation transfer in the light-harvesting complexes.[1] In the PSI and PSII, the Chl *a* molecules contribute to the charge separation and transfer processes.[10] To date, the detailed structures of the photosystems in green plants, have been obscure. However, it is known that the reaction centres (RC) of green plants resemble bacterial RCs.[8] The latter have been structurally investigated in detail by high-resolution X-ray methods.[11,12] At present, detailed structural features, such as the mutual orientations and distances of the Chl molecules in the PS of green plants, are under investigations, because the exceptionally efficient energy and electron transfer mechanism of green plants is evidently connected to them.[13,14]

Studies of various Chl-derivatives and porphyrins have been motivated by their importance in the primary photosynthetic events. Firstly, a great number of artificial models for natural photosynthetic processes have been constructed.[15-18] However, most of the model tetrapyrroles other than Chl derivatives, poorly mimic their natural counterparts. Secondly, an important aspect in the synthesis of Chl derivatives is their potential use as photosensitizers in the photodynamic cancer therapy.[19] Recently, nanodevices, operating as molecular-size electronic components, have been discussed in the literature.[20]

Nuclear magnetic resonance (NMR) spectroscopy offers an effective tool for the structural analysis of Chl derivatives. Modern NMR spectroscopy can provide information about the absolute configurations and conformations of a Chl derivative. In addition, molecular dynamics and electronic surroundings of the measured nuclei can be inspected by high-resolution NMR spectroscopy. In computer-aided molecular

modelling, structures can be examined based on either empirical or quantum mechanical methods. The present thesis focuses on the 3D structural analysis of Chl compounds in solution using NMR spectroscopy, supported by computer-aided molecular modelling.

The literature review comprises investigation methods of solution NMR (Chapter 2) and molecular modelling (Chapter 3). The application of these methods to the structural analysis of chlorin compounds is reviewed in Chapter 4. This chapter also introduces the chemical properties of Chls, assignment of their NMR spectra and conformational analysis. Specifically, the structural analysis of dyad or dimer compounds including a chlorin or porphyrin substructure is inspected. Finally, the NH tautomerism of porphyrins and chlorins is reviewed briefly.

In the experimental part of the thesis, Chl derivatives originating from Chl *a* (**1**) or *b* (**2**) were studied. The Chls were isolated from clover leaves (Chapter 6). Additionally, the bonellin dimethyl ester (**3**) was studied. Compound **3** is derived from bonellin, a green sex-differentiating pigment of the marine echiuroid worm *Bonnelia viridis*.[21] The primary focus of this study was to analyze the 3D structures of Chl derivatives, such as the Chl allomers or compounds used for electron transfer studies. The secondary interest was to investigate the existence and nature of NH tautomerism in the natural chlorins.

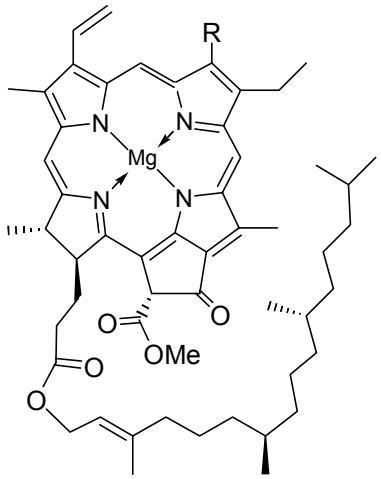

1 Chl *a*, R = Me
2 Chl *b*, R = CHO

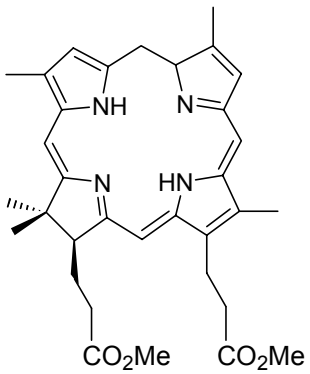

3 Bonellin dimethyl ester

2 Solution NMR methods

In modern solution NMR spectroscopy, the structural information of the molecules is basically extracted from chemical shifts (δ), scalar couplings (*J*) and various relaxation phenomena. Among the lastmentioned, the most important regarding this work is the nuclear Overhauser effect (NOE).[22,23] Moreover, the longitudinal, spin-lattice relaxation time (T_1) can also provide information about molecular structure and surroundings. The δ-value of a nucleus provides information about the electronic surrounding, mediated either via chemical bonding or through space. Scalar couplings are transmitted through chemically bonded nuclei by bonding electrons. The strength of these couplings depends on the number of chemical bonds between the coupled nuclei and molecular conformations. NOE arising from dipolar couplings between nuclei can be used as a measure of spatial distance.

The direct measurement methods of NMR active nuclei, utilizing Fourier-transform NMR spectroscopy, have been established as routine techniques two decades ago. However, the assignment of chemical shifts and couplings for relatively complicated organic molecules, *e.g*. chlorophylls has been laborious. Thus, the two-dimensional (2D) NMR techniques, introduced in the 1980´s, have greatly improved and facilitated the assignment of various organic compounds.[24,25]

The sensitivity, *i.e*. signal-to-noise ratio (S/N), for a one-dimensional (1D) NMR experiment can be expressed by equation 1.[25]

$$\mathrm{S/N} \sim N\gamma_{exc}\gamma_{det}B_0^{3/2}(\mathrm{NS})^{1/2}T_2/T \qquad (1)$$

N is the number of molecules in the active sample volume,
γ_{exc} is the gyromagnetic ratio of the excited spin,
γ_{det} is the gyromagnetic ratio of the detected spin,
B_0 is the static magnetic field,
NS is the number of scans,
T_2^{-1} is the homogeneous line width,
T is temperature

In the case of Chl compounds, a sufficient S/N ratio is often difficult to achieve, especially for the low natural abundance nuclei ^{13}C and ^{15}N. The S/N ratio and signal resolution can often be improved by using a high magnetic field, B_0, and a narrow line-shape giving sample. The latter is related to sample concentration, *i.e.* due to possible aggregation effects, a high concentration may destroy the narrow line-shape

properties of a corresponding dilute sample, in which Chls are in monomeric form. In addition, the choice of NMR experiment affects the sensitivity of the measurements, especially in heteronuclear NMR techniques (2.1).

In the next two sections, 2.1 and 2.2, some basic and advanced 2D techniques, needed for extraction of the NMR parameters *J*, δ and NOE, are reviewed.

2.1 Basic 2D techniques for spectral assignment

The homonuclear proton *J*-couplings can be revealed by correlation spectroscopy (COSY)[26] experiments. Total correlation spectroscopy (TOCSY)[27] affords the *J*-coupled proton pattern, whereas NOE correlations are measured by NOE spectroscopy (NOESY).[28] However, in the case of Chls, the molecular weights are often in the region of reduced NOE intensity, due to their molecular correlation times in the applied static magnetic field, B_0. Hence, the use of the rotating-frame NOE spectroscopy (ROESY)[29] is often favoured, since it is less dependent of molecular correlations times (2.3.3).

According to equation 1, the best sensitivity for ^{1}H-^{13}C or ^{1}H-^{15}N heteronuclear coherence magnetization can be obtained by applying NMR experiments, in which both the excited and detected nucleus is a proton. Thus, the γ of the proton is high compared with that of a heteronucleus, ^{13}C or ^{15}N. The heteronuclear multiple-quantum coherence (HMQC)[30] and heteronuclear single-quantum coherence (HSQC)[31] techniques utilize this principle, *i.e.* correlations peaks between the heteronuclei directly bonded to protons are detected. In the former technique, the observed multiple quantum correlations include homonuclear proton couplings in the heteronuclear dimension also. One advantage of HSQC is the absence of the aforementioned couplings. This allows better separation for correlations in the case of spectral crowding in a heteronuclear dimension. On the other hand, the fine structures of HMQC correlations can provide useful information for the analysis of ^{1}H spectral multiplets.

The multiple-bond heteronuclear multiple-quantum correlation (HMBC)[32] technique is a long-range variant of the HMQC. The longer evolution time for heteronuclear couplings in the HMBC pulse sequence allows the detection of couplings over 2-3 bonds, or in some cases even more. Nowadays, this technique is routinely applied for spectral assignment of organic molecules.

During the acquisition of the aforementioned experiments, most of the recorded signal contain other magnetization in addition to the coherence of interest. This is true especially in the case of heteronuclear experiments with low natural abundance nuclei such as ^{13}C and ^{15}N. Traditionally, the unwanted, ^{12}C- or ^{14}N-bound magnetization is cancelled by phase cycling and combining single transients with different magnetization phases. In the modern instruments, the coherence selection can be performed by using pulsed field gradients which dephase the undesired magnetization.[33] Thus, spectra with improved S/N ratio can be obtained in a shorter accumulation time in comparison with phase-cycled experiments, provided that sample concentrations are high enough. The advantage becomes evident, when a highly concentrated sample is set up for gradient selected(gs)-experiments, in which the strength of coherence magnetization is weak compared with that of undesired magnetization. One drawback of the basic gs-pulse sequences is the fact that only half coherence can be selected. Hence, the sensitivity suffers particularly in low concentration samples. There exist, however, some sensitivity-enhanced heteronuclear techniques, in which both coherence pathways are selected.[34]

2.2 Some advanced 2D techniques for spectral assignment

Recently, new versions of the aforementioned 2D techniques have been developed in order to improve sensitivity or provide more information in one spectral dimension.[33] These novel methods are, in fact, combined 2D hetero- and homonuclear techniques such as HSQCTOCSY or HSQCNOESY. They are based on the assumption that a better separation of signals prevails in the heteronuclear than in the homonuclear dimension. Hence, spectral resolution is enhanced, and thus an unambiguous assignment is achieved even when the corresponding TOCSY or NOESY experiment fails due to increased signal overlapping. In some cases, however, the conversion of the two or multiple dimension experiment into the corresponding 1D version with selective pulses provides shorter acquisition times and better resolution of the spectra.

Yet another example of the combined techniques is the so-called multiplicity-edited HSQC-based experiment.[34] It includes DEPT (distortionless enhancement by polarisation-transfer)-type information in the recorded spectra. Hence, the positive

phasing of the CH_2 signals produces CH and CH_3 signals with negative phases in the multiplicity-edited ^{1}H-^{13}C HSQC spectrum.

Various long-range heteronuclear shift correlation techniques have been introduced recently.[35] Zsu *et al*.[36] have published sensitivity-enhanced versions of the HMBC technique, and have demonstrated its performance even for large biomolecules. In the constant-time (CT) HMBC experiment,[37] the separation of cross peaks is improved, because the homonuclear proton couplings are removed from the heteronuclear axis. The evolution time in the HMBC experiment is generally adjusted according to the long-range couplings, being typically in the range of 6 – 10 Hz. These are rather arbitrary values, because the actual couplings are seldom known. Therefore, these set-up couplings can be far from the real values and may lead to small or even undetectable correlation peaks. This problem can be circumvented by utilizing the experiment of Wagner and Berger,[38] named ACCORD-HMBC which uses couplings optimized for a specific range. The ACCORD-HMBC experiment has been reported to be highly beneficial in terms of the increasing number of observed long-range responses relative to the statically optimized techniques.[39] However, Hadden *et al*.[40,41] have utilized the accordion principle in two new experiments, the IMPEACH-MBC[40] (improved performance accordion heteronuclear multiple-bond correlation) and CIGAR-HMBC[41] (constant time inverse-detected gradient accordion rescaled long-range heteronuclear multiple-bond correlation) experiments. The common improvement in both tehniques is the suppression of ^{1}H-^{1}H couplings in the heteronuclear dimension. In the CIGAR-HMBC method, the couplings can be suppressed by user-determined frequency modulation.

2.3 Structural analysis on the basis of NMR parameters

The focus in the following three sections is on the analysis of the solution conformations of organic molecules utilizing NMR parameters, *i.e*. chemical shift, scalar coupling and NOE.

2.3.1 Chemical shift

There exists a great amount of tabular data in the NMR literature, according to which the chemical shift of a nucleus is indicative of a specific chemical structure. Nowadays, there are some computer programs available which can predict the

chemical shift of a certain nucleus that is part of a defined structural subunit. However, chemical shifts provide information not only about the chemical structure of the studied molecule, but also about its surroundings. Since the chemical shift of a nucleus depends on the local magnetic field around it, δ is affected by magnetic and electrostatic effects exerted by the surroundings of the nucleus. One example of this is the magnetic anisotropic effect of a neighbouring group, which can lead to a shielding or deshielding of the nucleus. In practice, δ-values of protons are the most sensitive for detecting anisotropy effects of molecular surroundings in organic compounds.

Typical shielding or deshielding cones for groups of common anisotropy sources in organic molecules are depicted in Figure 1. The magnetic susceptibilities of the chemical bond, *e.g*. a carbonyl group and a carbon-carbon double bond, lead to the magnetic anisotropy effect in an external B_0-field. In aromatic compounds, such as benzene, the B_0-field induces a ring current that generates an additional magnetic field. The resulting anisotropy effect is stronger than those arising from the double bonds. The strength of anisotropy is proportional to $\sim 1/r^3$, r being the distance from the anisotropy source. Thus, the δ_H-value of a proton-containing group can provide information about the spatial proximity of an other group having a known anisotropy effect. The ring-currents of larger π-systems produce such strong anisotropic effects in their proximity that they cover even more distance in space than NOE (see section 4.5).

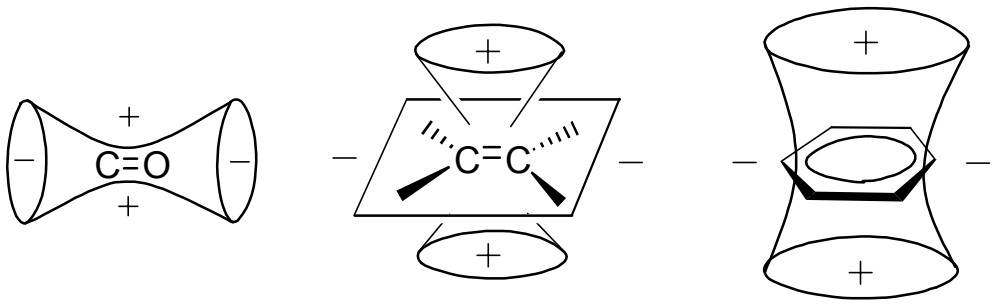

Figure 1. Schematic representation of the magnetic anisotropic effect of the carbonyl group, carbon-carbon double bond and benzene ring.[22] Shielding effect is denoted with (+)-sign and deshielding with (–)-sign.

Electric fields influence the electron densities of nuclei, and thus polarized charges, *e.g*. in amino, carbonyl and nitro groups affect their surroundings. The proton chemical shift can be strongly affected by hydrogen bonding. In a hydrogen bonded

proton, the electron density is formally increased, but the electrostatic dipole field of the hydrogen bond produces a deshielding effect on the bonded hydrogen.[23]

2.3.2 Scalar coupling

In modern NMR spectroscopy, spectral assignment is largely based on the observed scalar couplings between NMR active nuclei in the molecules studied. Scalar spin couplings are mediated by bonding electrons, and thus the couplings are not only sensitive to the chemical structure, but also to bond conformations.

The dependence of a vicinal coupling constant ($^3J_{H\text{-}H}$) on the dihedral angle ϕ between H–C–C–H protons has been first theoretically formulated by Karplus[42] with equation 2:

$$^3J_{H\text{-}H} = A + B\cos\phi + C\cos 2\phi \qquad (2)$$

$A = 4.22$, $B = -0.5$ and $C = 4.5$

Experimentally, the Karplus equation (Eq. 2) has been found to predict ϕ-angles relatively well when the molecular fragment studied resembles ethane. However, it has been shown that the vicinal coupling constant ($^3J_{H\text{-}H}$) depends on electronegative substituents, solvent effects, bond-angles and bond-lengths. A number of variations for equation 2 exist in the literature in which the constants A, B and C are readjusted, and/or trigonometric functions are added or altered to improve empirical correlation.[43-45]

The $^{2 \text{ or } 3}J_{C\text{-}H}$ values provide information similar to that given by the $^3J_{H\text{-}H}$ values about the dihedral angle, but the former couplings have been more difficult to obtain until recent developments in the NMR techniques. Matsumori *et al.*[46] have shown that the determination of the stereochemistry for acyclic natural products is possible utilizing the $^{2 \text{ or } 3}J_{C\text{-}H}$ values. Since the vicinal proton-carbon spin coupling constants ($^3J_{C\text{-}H}$) obey a Karplus-type equation, the conformations of C–C–H fragments can be evaluated. Also geminal $^2J_{C\text{-}H}$ values provide conformational information. Small $^2J_{C\text{-}H}$ values have been measured for the β-alkoxy CH_2 group when the proton is in the *gauche* position with respect to the oxygen functionality of a neighbouring carbon atom, whereas for the *anti* conformation, large $^2J_{C\text{-}H}$ values have been measured.[46]

2.3.3 Nuclear Overhauser effect (NOE)

In NMR spectroscopy, NOE is a direct way to obtain structural information as the effect is proportional to ~ $1/r^6$, r being the distance between the NMR active nuclei.[47] NOE can be quantified when it occurs between two isolated spins. Quantification can be performed by analyzing the NOE build-up rates, which are, in turn, obtained from the cross-peak intensities in the 2D-NOESY spectra measured, with various mixing times (τ_m). With one known proton-proton distance, obtained *e.g.* from a molecular model or an X-ray structure, the other distances can be defined from the NOE build-up rates. However, some additional consideration should be taken into account in NOE spectroscopy, especially in the quantitative distance analysis. In the case of a multiple spin system, the NOE can evolve indirectly via dipolar coupled neighbouring spins, *i.e.* via spin-diffusion. In addition, all external dipole-dipole interaction can quench the NOE of interest. Therefore, the sample solution should be free of magnetic nuclei other than those of the molecule studied, and the sample concentration should not be too high. In the multiple spin system, the scalar spin–spin couplings may also interfere with the accurate measurement of NOE.

Furthermore, the NOE depends on the motional correlation time (τ_c) and the Larmor frequency (ω), indicating that the NOE intensity depends on the B_0-field strength and particularly on the molecular weight.[43] At the edge, when the condition $\omega\tau_c = 1$ is fulfilled, the laboratory-frame NOE is near zero. It is positive, when the product $\omega\tau_c$ is below 1 and negative, when $\omega\tau_c > 1$.[43,23] In a ROESY experiment, the rotating-frame affects the intensity dependency. In fact, the ROE effect is always positive, being, however, stronger for large molecules. Under the spin-lock conditions of the ROESY experiment, scalar couplings may produce TOCSY-type magnetization transfer.[48] However, in the ROESY spectra, TOCSY signals are in the opposite phase with respect to the ROESY signals. In a modified ROESY experiment, called transverse ROESY (T-ROESY), the unwanted TOCSY cross-peaks are eliminated.[49]

3 Computer-aided molecular modelling methods

In modern chemistry, molecular modelling is an essential tool for understanding molecular properties. Computer-aided molecular modelling enables the calculation of molecular geometries, energies and physical properties with varying accuracy, depending on the calculation method and on the level of the theory. Some modelling methods are briefly examined in following chapter.

3.1 Molecular mechanics

Molecular mechanics (MM) methods are based on the parameters obtained from experimental data. Most of the molecular mechanic force-fields are constructed in a similar way as for the MM2 force-field shown in equation 3, in which the total energy, E_{total}, comprises various interaction terms.[50] Allinger's MM2[51] (or MM3) force-field is a standard MM-method nowadays, and it has been applied for a number of organic structures and energies with good accuracy, as compared with those measured experimentally.[50]

$$E_{\text{total}} = E_{\text{R}} + E_{\theta} + E_{\phi} + E_{\text{s}\theta} + E_{\text{el}} + E_{\text{vdW}} \qquad (3)$$

E_{R} = bond stretchings
E_{θ} = angle bendings
E_{ϕ} = dihedral angle torsional interactions
$E_{\text{s}\theta}$ = stretching bending interactions
E_{el} = electronic interactions
E_{vdW} = van der Waals interactions

In addition, various force-fields exist, in which some energy terms are formed from factors different from those in MM2. In the MM-methods, atoms are treated according to different atom types, which take into account different bonding types and hybridizations of a specific atom. An extreme example of atom typing is a generic Dreiding force-field developed by Mayo *et al.*,[52] in which the elements of force-field are purely of atom type, and the atoms of the same type are treated identically in the force-field. The Universal force-field (UFF) is capable of calculating structures that can include any of the elements across the periodic table, based on the element, its hybridization, and its connectivity.[53] The MM+ is an all-atom force-field which is constructed on the basis of the MM2 terms.[54] Hence, the MM+ is an extension of MM2, although some energy terms are calculated with a slightly different approach. The MM+ force-field utilizes MM2 parameters, when they are available, but uses

parameters from Dreiding or UFF force-fields to cover all the elements in the periodic table. The MM-methods function best when they are applied to structures resembling the ones used in the parameterization set. The greatest advantage in molecular mechanics is the method's feasibility to calculate large molecular structures with low computational capacity. The fact that the MM-methods are parameterized for ground state systems and for a common bonding type, is the major defect of these methods. In unusual bonding situations that are fundamentally quantum chemical in nature, *e.g.* electronically excited states, relevant calculation methods are required.

3.2 Quantum chemical methods

Quantum chemical methods are principally based on the approximate solution of the stationary state Schrödinger equation (Eq. 4).[55]

$$H\Psi = E\Psi \qquad (4)$$

H = Hamiltonian (kinetic and potential energy of system)
Ψ = wave function
E = the total energy of system

3.2.1 *Ab initio* methods

In the *ab initio* methods, equation 4 is solved with mathematical approximations.[56] The Hartree-Fock (HF) theory is the most common *ab initio* approximation for equation 4. In the HF approximation, the many-electron wave function Ψ, is split into n single-electron functions $\phi(r)$, *i.e.* molecular orbitals (MO), each having its own energy ε_i (Eq. 5).

$$h^{eff}_{HF}\Sigma\phi_i(r) = \Sigma\varepsilon_i\phi_i(r) \qquad (5)$$

$i = 1,2,...n$
h^{eff}_{HF} = effective one particle HF hamiltonian
ε_i = energy of MO ϕ_i

The MO equation 5 is further reformulated to a matrix equation consisting of elements that are one- and two-electron integrals, being the linear combinations of atomic-like orbitals. The resulting matrix is solved computationally with the self-consistent field (SCF) method. The problem with the HF approximation is that the instantaneous repulsion between electrons is neglected, which causes some error in the resulting energy values. The electron correlation of the HF approximation can be improved by configuration iteration or perturbation techniques, which, however,

increase the calculation time. Another useful *ab initio* approximation method, based on a different solution principle of equation 4, is the density functional theory (DFT).[57,58] In this method, electron density 'orbitals' are calculated instead of the wave functions (MO's). The approximation leads to lower computational effort compared with the HF methods, and thus enables calculation of larger structures.

The complete calculation of MO's or electron densities by *ab initio* methods provides the possibility for theoretical calculation of essential NMR spectral parameters, *i.e.* the nuclear magnetic shielding constants and indirect spin–spin couplings.[59] However, the effects arising from molecular rotations and vibrations in the δ- and *J*-values have to be taken into account in the calculation of fixed-geometry *ab initio* NMR parameters. In addition, in experimental conditions, the system-dependent effects, such as intermolecular interactions and solvation, may contribute significantly to the NMR parameters of a molecule. These effects should be taken into account, when the NMR parameters are computed for a solution structure.

The recent development of *ab initio* calculation methods has also enabled computational quantification of aromaticity. The computational method of continuous transformation of ring-current density (CTOCD)[60] has produced reliable current density maps for polycyclic aromatic hydrocarbons.[61] Von Ragué Schleyer *et al.*[62] have proposed a new method to calculate absolute magnetic shieldings: the nucleus-independent chemical shift (NICS) method. Jusélius and Sundholm[63] have introduced an *ab initio*-based aromatic ring-current shielding (ARCS) method to determine the strength of the ring-current that is related to molecular aromaticity. The ACCS method also enables the determination of the NMR shielding at any arbitrary point in space.

3.2.2 Semiempirical methods

In the semiempirical methods, equation 4 is commonly solved by further approximation of the HF theory.[56,64] This approximation is typically performed by neglecting the most difficult integrals, such as the two-electron integrals of the matrix elements. The resulting error is compensated with parameters obtained from experimental data. The benefit of the approximation is that the size of the computed matrix is reduced in comparison with the *ab initio* solution. Consequently, while the required computer time with respect to number of atoms is proportional to N^4 in the HF *ab initio* methods, it is reduced to N^3 in the semiempirical methods.[56] Thus, the

semiempirical methods are capable of calculating larger molecules in a reasonable computer time. In principle, semiempirical calculations can produce even greater accuracy for the model structure than a similar *ab initio* level calculation, when compared with experimental structure parameters. However, the semiempirical methods may give poor results, when the calculated molecular structure is different from the ones used in the parameterization set.

The modified neglect of diatomic overlap (MNDO)[65] was the first widely applied semiempirical method for organic molecules. Nowadays, the derivatives of MNDO, *i.e.* Austin model 1 (AM1)[66] and parametric method 3 (PM3)[67], are the most commonly applied semiempirical methods for modelling of organic molecules in their ground state. The methods are free from the main defect of MNDO, which is that the method gives spurious results for bonding other than chemically covalent. The AM1 method is parameterized using general organic molecules in the parameterization set, but some of the electron integrals are calculated based on atomic spectra. PM3 is basically a reparameterized version of the AM1 method. The reparameterization is performed with a larger number and variety of atoms and molecules. The parameterization set used also includes most of the main group elements in the periodic table, in addition to the common elements in organic structures. Moreover, the PM3 electron integrals are computed purely on a parametrical basis. As a result, the method is capable of calculating a broader variety of organic structures, also those containing some heavier elements of the main groups. In PM3, the non-bonded interactions tend to be more repulsive than in the AM1 method. It has also been found that both semiempirical methods underestimate frontier interaction with respect to sterical repulsion in comparison to *ab initio* methods. When the two semiempirical methods were tested for various organic structures, PM3 produced structural parameters that were closer to the corresponding *ab initi*o results than the ones obtained by the AM1 method.[68] However, the AM1 method produced energies that were closer to experimental values than the ones obtained by PM3.

4 Structural analysis of chlorin compounds

The following chapter presents the structural analysis of chlorins, as studied by NMR or NMR combined with computer-aided molecular modelling. The examples include mainly chlorophyll (Chl) *a* and *b*, and their derivatives. However, some porphyrin and bacteriochlorophyll (BChl) examples are included, when the research methods could also be useful for related chlorins.

4.1 Nomenclature

Several kinds of nomenclature have been historically applied in the chemistry of tetrapyrroles. In this work, compounds are primarily named according to the IUPAC/IUB[69] semisystematic nomenclature, with the exception that the pyro-prefix is used. Thus, *e.g.* compound **7** is named pyropheophorbide *a* methyl ester (Figure 2), whereas the IUPAC/IUB semisystematic name for **7** is 13^2-(demethoxycarbonyl)-pheophorbide *a* methyl ester.[69] The atoms are numbered according to the IUPAC/IUB semisystematic numbering as exemplified in Figure 2.[69]

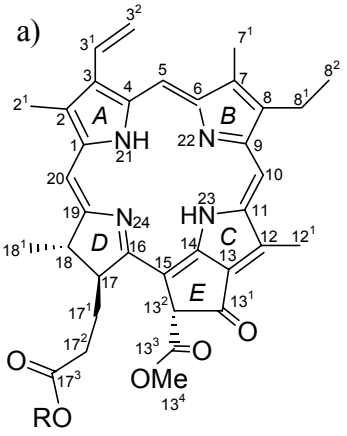

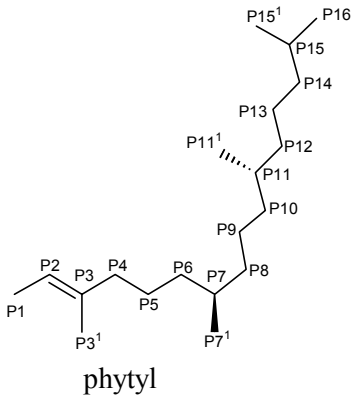

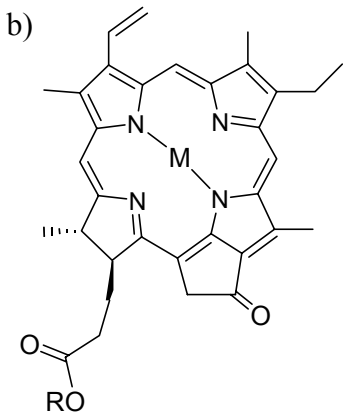

4 pheophytin *a,* R = phytyl
5 pheophorbide *a,* R = H
6 pheophorbide *a* methyl ester, R = Me

7 pyropheophorbide *a* methyl ester, M = 2H, R = Me
8 pyropheophyllide *a*, M = Mg, R = H
9 pyroChl *a*, M = Mg, R = phytyl

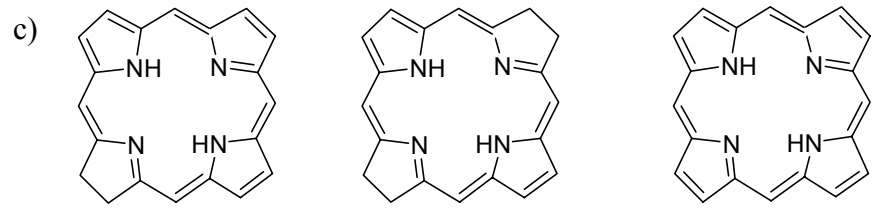

chlorin bacteriochlorin porphyrin

Figure 2. a) IUPAC/IUB accepted semisystematic names and numbering[69] for Chl *a* derivatives **4**-**6**, b) compounds **7**-**9** named with the trivial pyro-prefix c) the names and structures of cyclic parent tetrapyrrole macrocycles.

In the trivial names accepted by IUPAC/IUB,[69] the metal-free Chl derivatives are named pheophytins, whereas the dephytylated Chls are chlorophyllides (Figure 2). Pheophorbide *a* is a Chl *a* derivative that is both demetallated and dephytylated. A chlorin is a dihydroporphyrin, in which two addional hydrogens are at the peripheral (β-pyrrolic) positions of subring *D* (Figure 2). In a bacteriochlorin, subring *B* is also saturated, whereas in a porphyrin, the tetrapyrrolic macrocycle is fully conjugated.

4.2 Special structural and chemical features of chlorins

4.2.1 Chemical reactivity of chlorophyll-related chlorins

Chlorins are chemically amphiprotic compounds. A free-base chlorin with two NH groups can loose both NH protons under basic conditions, whereas in acidic conditions, the inner nitrogens have been claimed to be capable of taking up four protons, *i.e*. each nitrogen then becoming positively charged.[70] Further, it is known that some free-base chlorins exhibit NH tautomerism.[71] The NH tautomerism of the natural chlorin derivatives is discussed in section 7.4.

In the Chl compounds, the Mg(II) is weakly chelated to the inner nitrogens of the tetrapyrrolic macrocycle. The Mg(II) ion is so weakly bonded that even in a dilute acid, it is easily replaced by two protons.[4] The coordination number of the central Mg(II) can be either five or six, indicating that one or two ligands can be coordinated to the metal in solution.[72] However, in Chl derivation, the magnesium is often replaced by other metal atoms. For structural studies, Zn(II) has been a practical alternative, because it forms more stable complexes than Mg(II). In addition, Zn(II) can be easily inserted with a good yield and is strictly five-coordinative.

In the case of Chl compounds, the β-ketoester functional group in the isocyclic ring *E* is prone to chemical reactions during purification and analytical procedures. Firstly, the acidic 13^2-hydrogen can enolize in a polar organic solvent which acts as a Lewis base.[4,73] The enolization equilibrium leads to epimerization of the 13^2-carbon. However, Chls are soluble in monomeric form only in polar solvents such as acetone, alcohols, diethyl ether, pyridine and THF. In all of the aforementioned solvents, interconversion occurs between the 13^2-epimers. Secondly, the allomerization (autoxidation) of the 13^2-carbon can lead to a number of oxidized derivatives when

Chl is allowed to stand in an alcohol solution in contact with air.[4] In addition, Chls are easily photo-oxidized when they are exposed to light in the presence of oxygen.[4] Consequently, the isolation of Chls from natural sources and their chemical modification is demanding, as is the preparation of pure Chl samples.

The chemical stability of Chls can be improved by chemical modifications such as the change or removal of the central metal as previously discussed (*vide supra*). Methyl pyropheophorbide *a* (**7**) can be obtained via the pyrolysis,[74] demetallation and transesterfication of Chl *a*. Chlorin **7** is a relatively stable Chl derivative, still having the isocyclic ring *E*. Therefore, in a number of studies, chlorin **7** has been used instead of authentic Chl, when the properties of a natural chlorin have been an objective.

In the photosynthetic antenna systems, Chls exist predominantly in oligomeric form bound to protein structures. In solution, Chls tend to form oligomers by chlorin–chlorin π–π interaction[75] and the coordination of the central metal to the carbonyl group of a neighbouring Chl molecule.[72,76] Thus, especially in concentrated samples, Chl self-aggregates are easily formed.

4.2.2 Aromaticity

In NMR spectroscopy, the delocalized electrons of an aromatic tetrapyrrole macrocycle induce a ring-current in an external magnetic field, B_0. This effect is observed as deshielding or shielding for the NMR active nucleus experiencing the ring-current (see Figure 1, p. 12). The proton chemical shifts are especially sensitive to the effect, and characteristic chemical shifts (4.3.1) can be observed for the protons located in different positions of the chlorin. The protons of a coordinated molecule, which is located above or below the macrocycle (4.5) plane, can also be effected by the ring-current effect through space.

The chlorin macrocycle is also aromatic, according to the two classical aromaticity criteria used in organic chemistry.[77] Firstly, the macrocycle is planar allowing maximal p–p-orbital overlap. Secondly, there are enough electrons available to fulfil Hückel's $(4n + 2)$-rule for the π-electrons in a delocalization pathway. There are several possibilities for the aromatic delocalization pathway in the chlorin macrocycle, as well as in the porphyrin macrocycle. However, for these molecules, the delocalization of 18 π-electrons in an 18- or 16-membered ring has been mostly

proposed (**A** and **B** in Figure 3).[78,79] In the literature, the 18-atom 18 π-electron system (Figure 3 **A**) is regarded as a traditional delocalization pathway of porphyrins. In the case of free-base porphyrins, this is experimentally supported by NMR measurements, in which the [18]diazaannulene pathway has been deduced on the basis of the chemical shifts and couplings of the *β*-pyrrolic protons.[80,81] Additionally, theoretical evidence has been obtained with semiempirical AM1-UHF calculations, which have produced structures in agreement with the traditional pathway.[82]

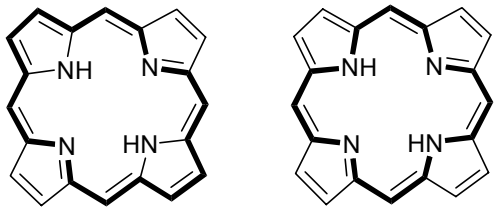

A **B**

Figure 3. Kekulé 18 π-electron delocalization structures for the porphyrin macrocycle. Structure **A** is a [18]diazaannulene and **B** is an internal 16 atom pathway.

The [18]diazaannulene delocalization pathway has also been proposed for chlorins.[71] In the chlorin macrocycle, this pathway can only exist in the way that the *β*-pyrrolic C_7–C_8 double bond and the NH-group nitrogens (N21 and N23) do not participate in the pathway (Figure 4). Supporting evidence for the pathway has been found from protonation titration experiments combined with ^{13}C NMR[83] and UV/Vis[70] spectral measurements upon titration.

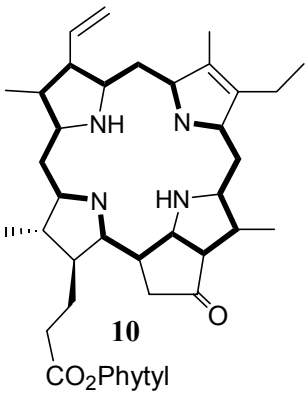

10

Figure 4. The dominating delocalization pathway of pyropheophytin *a* (**10**) as proposed by Lötjönen and Hynninen.[83]

Abraham *et al.*[84,85] have suggested a double dipole ring-current model for chlorophylls and porphyrins in order to estimate chemical shifts for the protons that are exposed to the ring-current. According to their model, the ring currents of the

macrocycles are approximated by dipole vectors which are located in the pentagon and hexagon centres of the tetrapyrrole (Figure 5). In order to obtain the ring-current effect at a specific point in space, the equivalent dipoles can be computationally utilized under the circumstances of a known macrocycle geometry. In the case of chlorin–chlorin dimers, this method has been applied most successfully for estimating the dimer geometries, when the dipoles themselves have been obtained on the basis of the monomer NMR data (4.5.1).

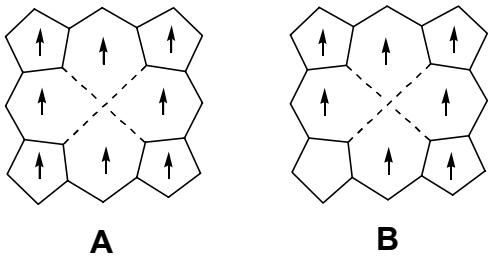

Figure 5. Porphyrin (**A**) and chlorin (**B**) nucleus with the dipole vectors drawn in the ring-current centres.[85]

The results of recent *ab initio* molecular modelling studies on porphyrins and chlorins argue against the traditional [18]diazaannulene pathway. Cyranski *et al.*[86] have supported the 18 π-electron [16]annulene (Figure 3 **B**) pathway to be predominant for porphyrins. In addition, the authors concluded that in the case of free-base porphyrin, the NH pyrrole subrings can be considered as true pyrrole-type rings on the basis of the computed NICS values.[86] This implies that the NH electron lone-pairs are also included in the aromatic pathway. Thus, in total, 22 π-electrons contribute to the aromaticity. Similar NICS calculation results were obtained for bonellin (**3**) dimethyl ester, but those results were interpreted to confirm the traditional delocalization pathway.[87] However, a very recent study applying ARCS and NICS methods (3.2.1) for calculations of porphyrins, chlorins and bacteriochlorins concluded that all the available π-electrons take part in the aromatic delocalization, and that the total aromatic pathway is in fact a linear combination of possible ($4n$ + 2) pathways.[88] In the case of chlorins, it was suggested that 24 π-electrons participate in the aromatic pathway by superposition of several 22 π-electron pathways.[88] Overall, it appears that the aromaticity pathways of chlorins and porphyrins are still a subject of debate.

The induced ring-currents cause diamagnetic behaviour for aromatic molecules in a static magnetic field, B_0. Consequently, the porphyrin and chlorins orient slightly in solution by the magnetic interaction.[89] In these conditions, the dipolar splittings evolve in NMR spectra with a quadratic dependency on the strength of B_0. Dipolar splittings strongly contribute to couplings between nuclei, *e.g.* in one-bond proton-carbon couplings. Their effect becomes significant, when the spectrum of a large aromatic system is measured in a high magnetic field. The dipolar splittings comprise information about orientation of the group from which they are measured. For instance, in the case of porphyrins, the orientation of the vinyl group with respect to the porphyrin macrocycle plane has been estimated using the couplings.[89] The anisotropy effect is also present in chlorins, and for chlorin **7**, only a slightly lower anisotropy effect has been measured as compared with that for a corresponding porphyrin.[90]

4.3 NMR assignments of chlorophylls

A great number of NMR works has been focused on Chls and their derivatives. The magnetic properties of Chls are relatively well documented in the literature.[91,92] In the following sections (4.3.1 – 4.3.2), the principles of assignment for the NMR spectra of Chls are presented.

4.3.1 ^{1}H NMR spectra

The assignment of the proton spectrum of a natural chlorin is quite a straightforward task, when the signals are well resolved. The ring-current distributes the chlorin proton signals over a wide spectral range, and some signals, arising from a certain position in the macrocycle, can be found by their characteristic δ_H-values in the spectra. The *meso*-C*H* signals are typically in the lowest field, covering the spectral region 11.0 – 8.0 ppm. The CH_2 and CH_3 substituents attached to subrings *A*, *B* and *C* normally produce signals appearing at 3.0 – 4.0 ppm. The Chl *a* derivative, 13^2(*R*)-HO-Chl *a* (**11**) in Figure 6,[93] shows a typical ^{1}H NMR spectrum that can be almost completely assigned solely on the basis of the δ_H and $J_{H\text{-}H}$ values.

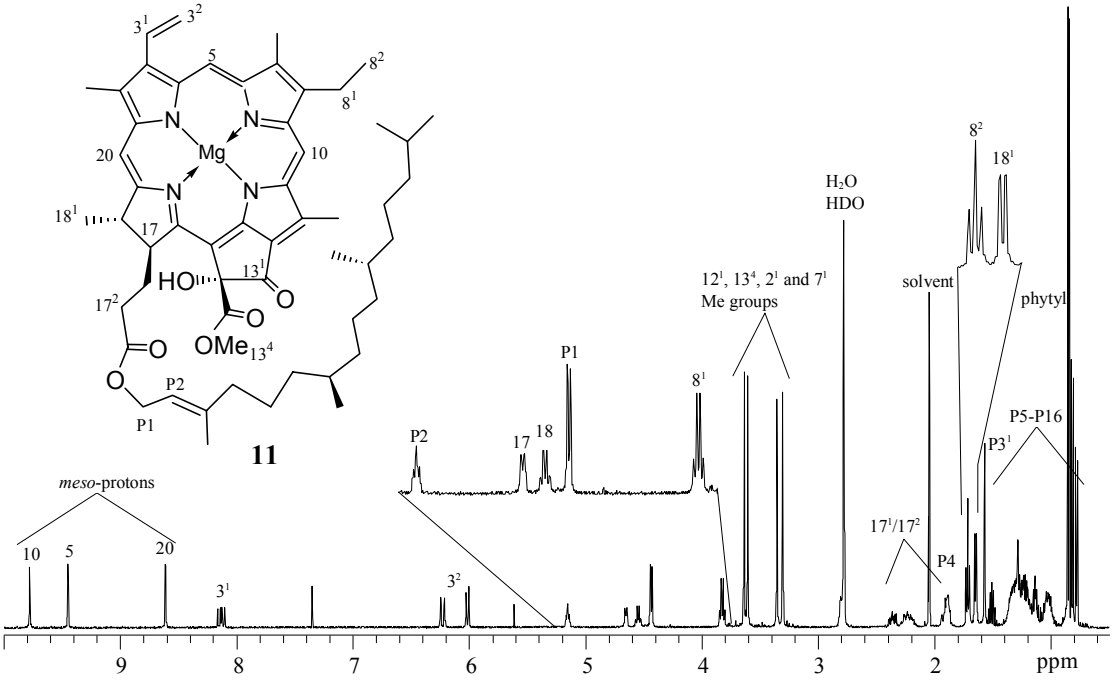

Figure 6. 500 MHz ^{1}H NMR spectrum of 13^2(*R*)-HO-Chl *a* (**11**) in acetone-d_6 (16mM).[93] The signals, assigned using the δ and $J_{H\text{-}H}$ values, are marked in the 1D proton spectrum.

For Chl *a* derivatives, the *meso*-proton signals are in the order of 10, 5 and 20, starting the low field. However, a substituent in the macrocycle, such as the formyl group in Chl *b* derivatives, alters the order of the 5-C*H* and 10-C*H* signals. The demetallation of Chl derivatives only slightly effects the proton chemical shifts. Yet, in a free-base chlorin, the NH protons are commonly strongly shielded, thus appearing in the spectral region of 1 – -3 ppm. When measuring the ^{1}H NMR spectra of Chls, one has to take into account the fact that chemical shifts are sensitive to the sample concentration and the solvent. $CDCl_3$ has been used as a solvent in a number of ^{1}H NMR measurements of chlorins. In the case of metallated (*e.g.* Mg or Zn) chlorins, a small amount of nucleophilic solvent such as CD_3OD or pyridine-d_5, is frequently added in order to disaggregate the sample.[91] Metalled chlorins are often soluble in a pure pyridine-d_5 solution, but it is noteworthy that the chemical shifts of the chlorin macrocycle protons are affected by the pyridine ring-currents.

A rather unambiguous assignment of a Chl compound can be facilely obtained by the concerted use of 2D ROESY, COSY and TOCSY experiments.[94] The spin-systems of the chlorin ring substituents can be identified with TOCSY and COSY spectra, whereas the spatial ROE correlations reveal the connectivities between these substituents. In the chlorin proton spectra, the characteristic spin-system of the 3-vinyl or 8-ethyl group is a practical starting point, when the assignment is performed by

ROESY. After having assigned the 3-vinyl proton signals, the assignment can proceed around the macrocycle (section 7.1), since the neighbouring groups in a chlorin ring usually are within the ROE distance (< 5 Å).

4.3.2 ^{13}C NMR spectra

The complexity of the chlorin **11** structure is clearly visible in its ^{13}C NMR spectrum (Figure 7).[93] Only a few signals can be assigned with sufficient reliability by inspecting the δ_C-values and signal intensities. The 13^1-carbonyl carbon is distinctly separated into the low-field region of the spectrum. This feature is common for all Chl *a* derivatives. The intensive NOE enhanced signals in the middle of the spectrum belong to the CH and CH_2 carbons, and thus these signals can be tentatively assigned on the basis of their chemical shifts. The rest of the signals belong to quaternary carbons appearing at δ-values > 90 ppm, or to saturated carbons having δ-values < 60 ppm. In general, this kind of appearence is typical for the carbon spectra of Chl *a* and *b* derivatives, with some exceptions. For instance the Chls with a *β*-ketoester system in ring *E* exhibit a recognizable 13^2-carbon signal at *ca*. 65 ppm in the spectra, when a proton is attached to the 13^2-carbon. However, in order to obtain a more complete assignment, knowledge of proton–carbon connectivities is required.

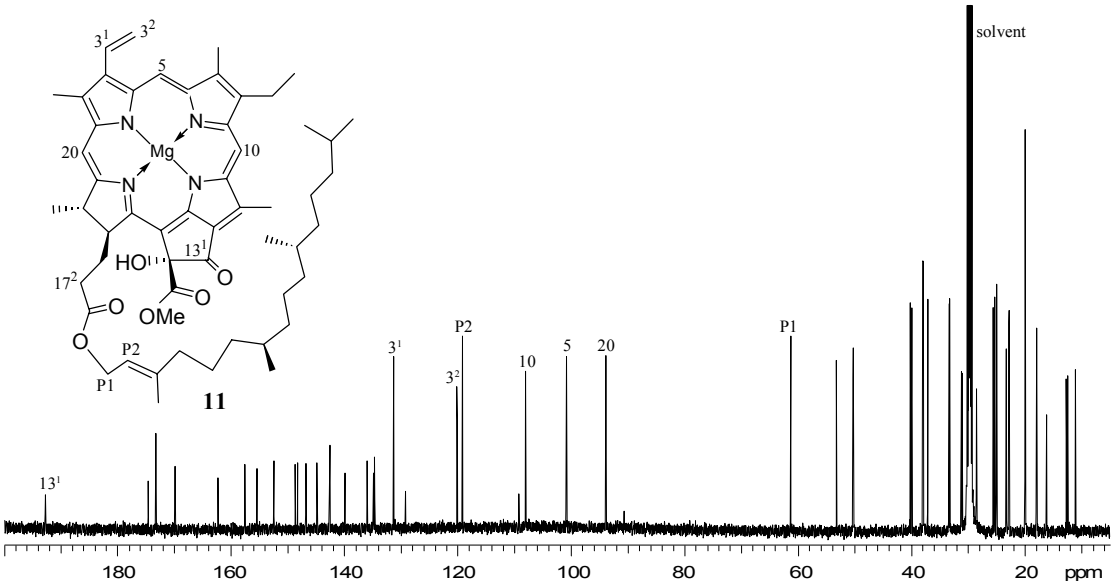

Figure 7. 125 MHz proton decoupled ^{13}C NMR spectrum of 13^2-(*R*)-HO-Chl *a* (**11**) in acetone-d_6 (16mM).[93] The signals labelled with numbers have been tentatively assigned on the basis of δ_C-values and signal intensities.

The first reliable and complete assignment for the ^{13}C NMR spectrum of Chl *a* has been achieved by inspecting the ^{1}H-coupled ^{13}C spectra and the ^{13}C spectra

measured with selective proton decoupling. The long-range selective proton decoupling (LSPD) technique was applied to achieve the complete ^{13}C NMR assignments of Chl *a* (**1**), its 13^2-(*S*)-epimer Chl *a*', pyroChl *a*, and the corresponding pheophytins.[95,96] The single frequency on- and off- resonance decoupling (SFORD)[24] technique was used in the total assignments of Chl *b* (**2**) and its derivatives.[97] The aforementioned assignments are still valid to date, but the methods used have some drawbacks. One disadvantage in the carbon-detected methods is their low sensitivity, and thus there is a need for concentrated samples and long acquisition times. The problem often encountered with concentrated Chl samples is the formation of aggregates. Nevertheless, the ^{13}C nucleus and hence, the recorded carbon spectra are less sensitive to this behaviour than the proton nucleus.

The indirect 2D proton-detected techniques have notably improved the spectral sensitivity and resolution, when the heteronuclear connectivities are of interest. The power of the HMQC and HMBC techniques (2.1) was shown in the nearly complete assignment of the methanolic Chl *a* allomer, 13^2-(*R*)-methoxyChl *a*.[98] The measurements were performed using 500/125 MHz for the $^1H/^{13}C$ frequencies and a sample containing 16 mg of the allomer in 0.6 ml acetone-d_6 (26 mM). Some mutually interchangeable assignments could not be avoided in the case of closely spaced carbon signals with separation less than 0.2 ppm. The combined use of the HMQC and HMBC techniques also afforded the first unambiguous proton and carbon assignments for the phytyl side-chain.[98] Several other methanolic Chl *a* allomers, including the whole macrocycle and the front part of the phytyl chain, have been successfully assigned using these techniques.[91]

The DFT calculations (3.2.1) offer the possibility to calculate geometries and NMR properties of relatively large molecules such as Chls. Facelli[99] has geometry-optimized the structures of bacteriopheophorbide *a*, and bacteriochlorophyll *a* and calculated the chemical shifts of the ^{13}C and ^{15}N nuclei with the DFT method. It was shown that most of the calculated chemical shifts correlated relatively well with the experimental data in the literature.[100] However, a few calculated chemical shifts of the quaternary carbons deviated more than 5 ppm from the experimental literature values assigned without 2D NMR experiments. According to the Facelli's revised assignments,[99] the standard deviation of the calculated *versus* computed ^{13}C chemical shifts decreased from 13 to 4 ppm. Hence, a specific structure obtained in geometry-optimization can be related to the ^{13}C chemical shifts.

4.3.3 ^{15}N NMR spectra

In Chl sample solutions, the natural abundance of ^{15}N nuclei is usually too low to be observed in direct measurements. In the few existing assignments of ^{15}N nuclei in natural chlorins or their derivatives,[101-104] the spectra have mainly been acquired from ^{15}N enriched samples. The subsequent assignments have been performed by techniques similar to those described for the carbon spectra (*vide supra*). The first chlorin ^{15}N assignments were reported for Chl *a* (**1**) and pheophytin *a* (**4**) (Table 1) when internuclear double resonance (INDOR)[22] spectroscopy was used to measure the ^{15}N enriched samples.[101] However, recently the ^{1}H-^{15}N HMQC and HMBC spectra have been measured from a 42 mM sample of mono-L-aspartyl chlorin e_6 (**12**) in DMSO-d_6 at the natural abundance of ^{15}N.[102] The assignments for BChls *a* (**13**) and *c* (**14**) have been obtained by the aforementioned techniques from ^{15}N enriched samples (Table 1).[103,104]

The nature of chemical bonding is clearly visible in the ^{15}N chemical shifts, as can be seen from Table 1. The insertion of Mg reduces the chemical shift differences, when the shifts of **1** are compared with those of **4**. The D_{2h} symmetry element with respect to the saturated bonding in the macrocycle of **13** also effects the chemical shifts (Table 1). In the case of BChl *a*, it was shown that the solvent affects the ^{15}N chemical shifts.[103] Apparently, an increase in solvent polarizability decreases the chemical shift difference between the nitrogens in the lower field (N_{22} and N_{24}) and those in higher field (N_{21} and N_{23}).[103] Unfortunately, unlike the TMS used for ^{1}H and ^{13}C spectra, there is no general standard reference compound available for the ^{15}N NMR spectra, even though the δ_N-value of liquid ammonia at 25 °C has been proposed as a standard ($\delta_N = 0$).[35,105] Hence, the use of various ^{15}N-standards (Table 1) found in the literature hinders the comparison of the absolute values of the ^{15}N chemical shifts.

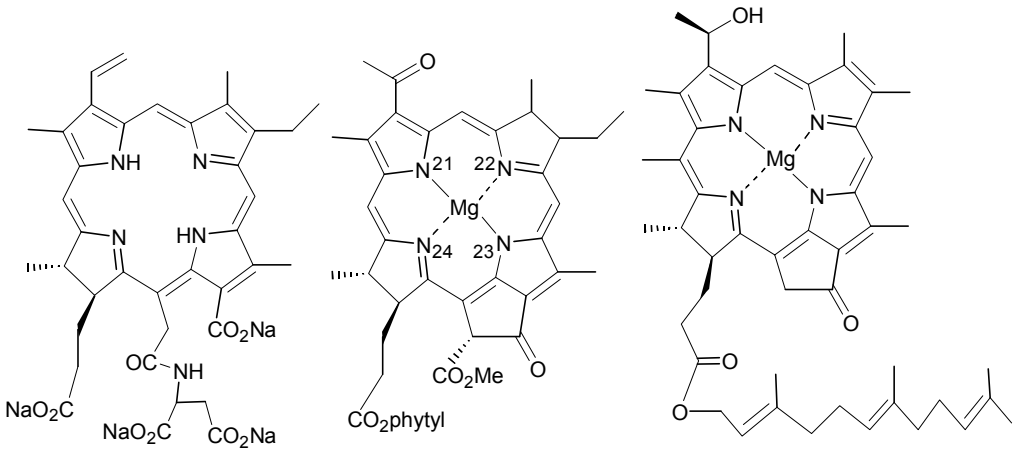

12 **13** **14**

Table 1. Chemical shifts (ppm) of inner nitrogens of various chlorins.

	♣**1**[101] in $CDCl_3$	♣**4**[101] in $CDCl_3$	♦**12**[102] in DMSO-d_6	♥**13**[103] in acetone-d_6	♠**14**[104] in $CDCl_3$
N_{21}	163.6	102.5	128.3	189.6	199.3
N_{22}	183.5	218.5	239.8	191.5	212.5
N_{23}	166.4	110.9	130.0	258.5	196.6
N_{24}	224.0	272.8	282.0	259.1	250.7

reference (external): ♣5M $^{15}NH_4Cl$ in 2M HCl; ♦$NH_4{}^{15}NO_3$ (375.6 ppm);
♥$Me{}^{15}NO_2$ (380.2 ppm); ♠3M $^{15}NH_4Cl$ in 1M HCl (24.9 ppm)

4.4 Solution conformational analysis of monomeric chlorophylls

In several NMR studies of Chls, the conformation of ring *D*,[93] the propionic ester side-chain and/or the front part of the phytyl group have been deduced from proton-proton couplings.[106-109] The methods are discussed in more detail in section 7.2, and in publications I and II. The conformational changes at the lower periphery of the Chl compounds have also been estimated by comparison of the $\Delta\delta_H$-values found between the Chl compounds investigated.[93,110]

4.5 Solution conformational analysis of chlorin-chlorin dimers

In nature, the Chl antennas absorbs light quanta and conduct the singlet excitation energy to the photosynthetic RC, in which a Chl special pair transforms the energy into donation of an electron to the electron acceptor, a pheophytin. The electron is then transferred further to quinones. These charge separation and electron transfer steps have been characterized for bacterial RCs.[11,12] In the case of green plants, the detailed picture of charge separation and electron transfer processes are more obscure. Many biomimetic models have been constructed for investigating the

primary photosynthetic processes.[15-18] Chlorin–chlorin dimer compounds are studied in order to mimic the antenna function and the special-pair interaction of Chls. Electron donor–acceptor (D–A) dyad molecules with a chlorin as the donor are constructed to illuminate the electron transfer processes.

In order to understand the photophysical behaviour of the models, detailed information about the model-compound conformations and relative spatial arrangement of the chlorin and the electron acceptor unit is necessary.[18] NMR spectroscopy offers an excellent tool for the structural analysis of the model compounds, especially when knowledge of solution conformations is required.

In the Chl solution, there are two dominating interaction mechanisms that draw molecules together. Firstly, the π-system of a Chl can interact with the π-system of another Chl or an aromatic molecule by the π–π interaction mechanism. Secondly, a nucleophile, which can be the 13^1-carbonyl group of a neighbouring Chl molecule or a bifunctional solvent molecule, can coordinate to the Chl's central Mg and bring the molecules into close proximity directly or via a solvent bridge. In the next sections (4.5.1 – 4.5.2), the principles for obtaining the chlorin–chlorin and chlorin–electron acceptor compound geometries are reviewed by examining the NMR results alone and the NMR results combined with molecular modelling studies of physically linked and covalently linked chlorin–chlorin dimers.

4.5.1 Physically linked chlorin–chlorin dimers

A chemically simple approach to studying Chl–Chl interaction, is to dissolve the Chl molecules in a non-nucleophilic solvent. In the absence of an external ligand, the central magnesium coordinates to the nucleophilic part of a neighbouring Chl, *i.e.* a carbonyl group, directly or via a water molecule with hydrogen bonding. The nature of this interaction is determined mainly by the solvent, sample concentration and temperature. In polarizable non-nucleophilic solvents such as $CHCl_3$ ($CDCl_3$) or CCl_4, Chl *a* exists mainly in the dimeric form, whereas in non-polarizable solvents like benzene or octane, larger aggregates are formed.

In a Chl solution, there are two competing equilibria, namely the association and dissociation of ligand L which can be a solvent molecule or another Chl. The Chl dimer-monomer equilibrium processes are described by equations 6a-c.[91]

$$Chl_2 \rightleftharpoons 2Chl \quad (6a)$$

$$Chl + L \rightleftharpoons ChlL \quad (6b)$$

$$Chl_2 + 2L \rightleftharpoons 2ChlL \quad (6c)$$

In the case of Chl *a*, NMR studies have led to various proposals for the dimer structures, of which the most convincing **A**–**D** are shown in Figure 8.[91] Fong and Koester[111] have proposed the dimer structure **A**, relying on the chemical shift changes between an aggregating solvent (benzene-d_6) and a disaggregating solvent (acetone-d_6). They have also proposed that a similar "face to face" structure can exist in anhydrous form with a direct coordination between the Mg and the 13^4-carbonyl oxygen of the neighbouring Chl *a*.[112]

Abraham *et al.*[113,114] have proposed the piggy-back model, **B**, on the basis of quantitative double-dipole ring-current calculations, which the authors had previously introduced for chlorins. The aggregation-induced chemical shifts ($\Delta\delta_H$) were obtained from measurements, in which methyl chlorophyllide *a* (0.08 M in $CDCl_3$) was titrated with methanol ligands and Chl *a* (0.06M in CCl_4) with pyridine-d_5 ligands.[113,114] When the less symmetric model (**B**) was used instead of the Fong model (**A**), the calculations produced better correlation for the aggregation-induced chemical shifts of the Chl *a* protons. The weakness of model **B** is the direct Mg-carbonyl coordination, indicating a shorter interplane distance between Chls than that reported in literature (*ca.* 6 Å).[113,114]

Kooyman and Schaafsma[115] have measured the ^1H spin-lattice relaxation times (T_1) for Chl *a* in various aggregation conditions. The authors concluded that the skew model, **C**, has good correlation with the obtained rotational diffusion constants. However, only modest correlation between the experimental $\Delta\delta_H$-values and the values obtained from double dipole ring-current calculations could be established for **C**.

Abraham *et al.*[116] have remeasured Chl *a* in $CDCl_3$ at low concentrations (2.8 mM), and titrated the sample with methanol-d_4 using a high-field spectrometer (500 MHz). The $\Delta\delta_H$-values obtained from the ring-current calculations correlated best with the back-to-back model, **D**. It can be applied only for the formation of a dimer structure, whereas the piggy-back model **B** is capable of being a substructure in larger aggregates.

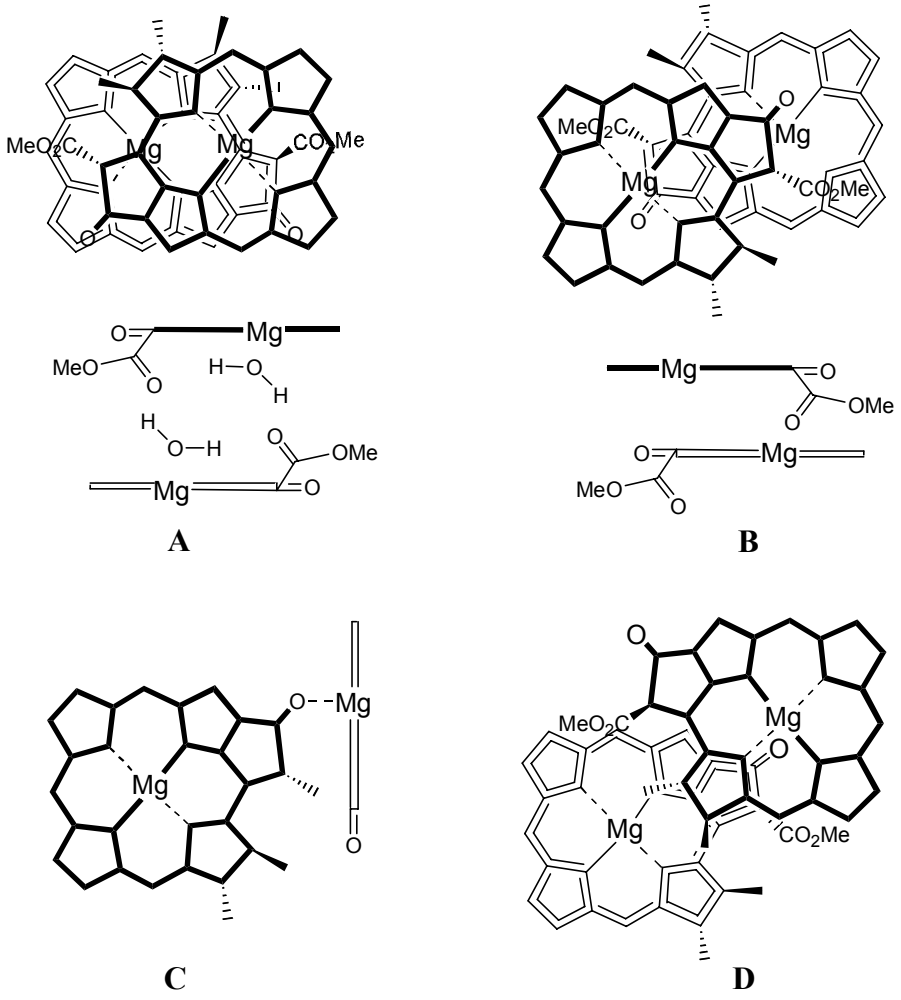

Figure 8. Four schematic models for Chl *a* dimers proposed on the basis NMR studies: **A**, the Fong model; **B**, the piggy-back model; **C**, the skew model and **D**, the back-to-back model.

The dimer formation of methyl pyrochlorophyllide *a* (**15**) at a low concentration (<0.01 M) has been studied in $CDCl_3$ by titrating the sample with methanol-d_4 or pyridine-d_5 using a high magnetic field.[117] The ring-current calculation produced equal correspondence with models **B** and **D**, but only modest correspondence with model **A** (Figure 8).[117] Consequently, it seems that the quantitative double dipole ring-current calculations are not accurate enough to give an unambiguous dimer structure. Nevertheless, the existence of several kinds of dimers or even higher aggregates in $CDCl_3$ can not be excluded. Apparently, the diversity of the experimental system may cause the observed inaccuracy, when the ring-current calculations are based on a single dimer model.

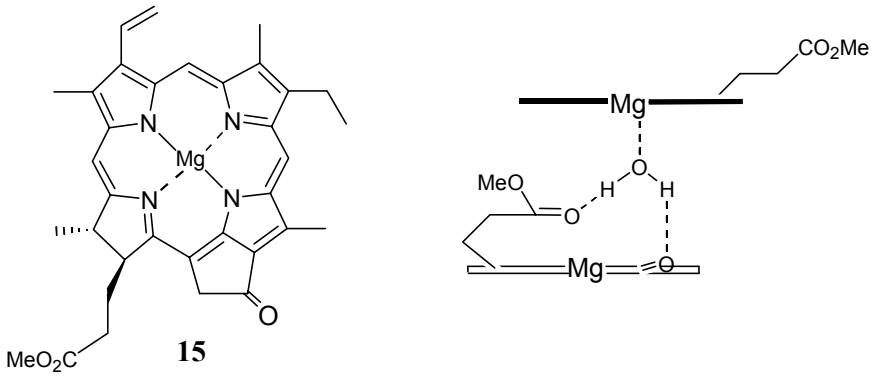

Figure 9. Methyl pyrochlorophyllide *a* (**15**) and the proposed hydrogen bonding network in the dimer.[117]

An early approach to studying molecular association in the case of Chls was to build an aggregation map based on the $\Delta\delta_H$-values between a monomer and an aggregate.[118] The aggregation map of 13^2(*S*)-pheophytin *a*, pheophytin *a'*, (**16**) in Figure 10 shows qualitatively that the ring-current induced shielding effect is strongest around the subring *B* of the chlorin macrocycle.[119] Hence, from the mutual orientation of two chlorin molecules, a dimer structure can be estimated. Two dimer geometries **A** and **B** have been constructed on the basis of the aggregation map (Figure 10).[119]

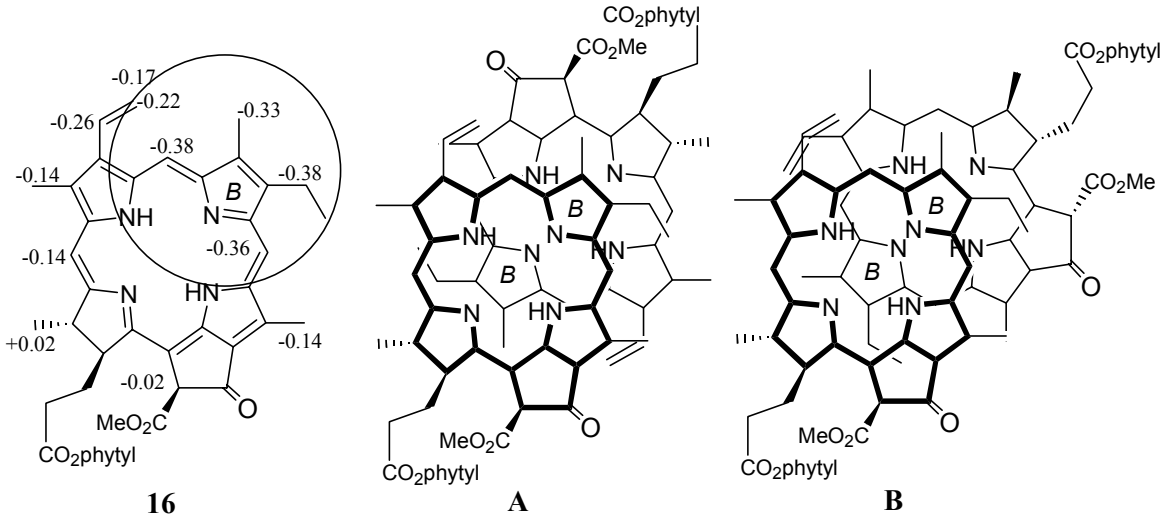

Figure 10. The pheophytin *a*' (**16**) aggregation map, and the proposed symmetrical (**A**) and unsymmetrical (**B**) dimer structures.[119]

In recent NMR studies of BChl *c* (**14**), it was shown that the intact Chl forms a stable dimer in CCl_4 at room temperature.[104,120] In fact, two sets of resonances could be observed in the ^{1}H, ^{13}C and ^{15}N NMR spectra, which could also be completely assigned using modern NMR techniques.[104,120] The dimer conformation could be

evaluated on the basis of the strong intermolecular NOE signals observed between the protons listed in Table 2.[120] The ROESY spectrum was recorded to distinguish the NOE cross-peaks from those due to the exchange in the NOESY spectrum. A slow chemical exchange ($k = 1.8 – 1.9\ s^{-1}$) between the two molecular species over a range of mixing times, $\tau_m = 0.075 – 1.0$ s, was found. The NOESY spectra measured with $\tau_m = 0.2 – 0.4$ s produced the maximum cross-peak intensities. The cross-peak intensities for distance estimation were measured with $\tau_m = 0.15$ s. These were used to calculate quantitative distance information on the basis of a linear rate approximation.[121] The NOE intensities were transformed to distances (Table 2) utilizing the $1/r^6$ distance dependency of NOE, and the known distance for an internuclear NOE reference.[120] The average distance between intramolecular protons 5 and 7^1, assumed to be 2.89 Å in the dimer BChls, was selected as a NOE reference. The distances obtained (Table 2) were subsequently used for building a dimer model. Finally, the dimer structure was geometry-optimized using MM+ molecular mechanics, and the NOE distances were used as restraints in the calculation. The optimized dimer structure is illustrated in Figure 11.

Table 2. The protons showing intermolecular NOE in a BChl *c* dimer and the estimated distances.[120]

Protons of the upper* BChl	Protons of the Lower* BChl	Distance (Å)
10-C*H*	20^1-C*H*$_3$	2.69
	2^1-C*H*$_3$	3.58
20^1-C*H*$_3$	5-C*H*	3.76
	7^1-C*H*$_3$	2.96
18^1-C*H*$_3$	3^1-C*H*	3.15
	7^1-C*H*$_3$	3.68

* see Figure 11.

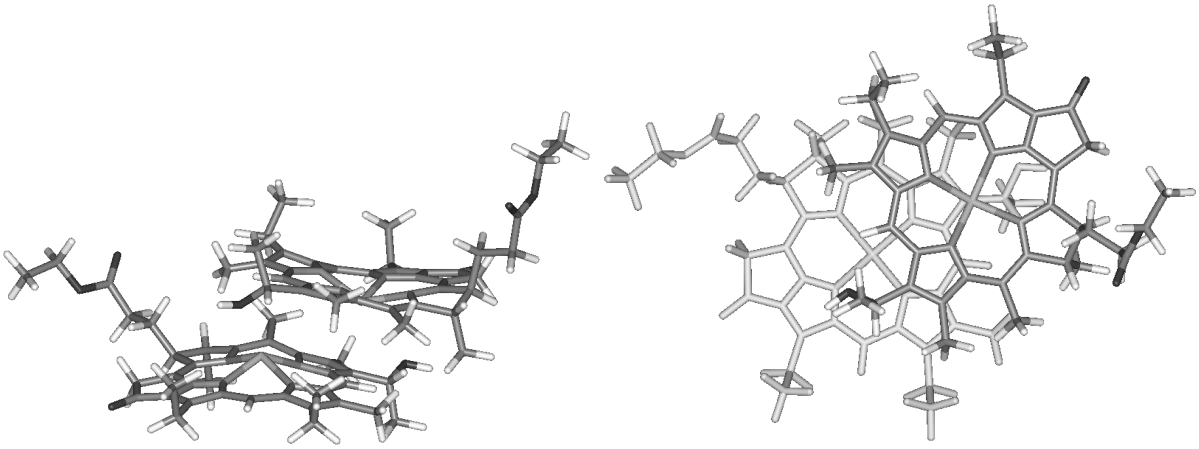

Figure 11. The BChl *c* (**14**) dimer structure with an antiparallel piggy-back conformation. The energy minimized structure has been obtained by MM+ molecular mechanics with six intermolecular distances from NOESY experiments as constraints (Table 2).[120] In the models, the farnesyl side-chains are replaced by ethyl groups.

4.5.2 Covalently linked chlorin–chlorin dimers

An alternative for studying chlorin–chlorin interaction is to link two chlorins with a covalent bond to form a dimer structure. This effectively restricts the molecular diffusion in solution. The interest in the NMR and molecular modelling studies principally involves the dimers with a flexible linkage, allowing the theoretical existence of various conformations. For this kind of covalently-linked molecules, the existing geometries can be basically divided into two classes: folded and extended conformers. In the former class of linked chlorins, the π-electron systems are stacked, whereas in the latter, the π-systems are clearly separated.

A large number of totally synthetic bischlorins has been used for modelling natural photosynthesis.[17] A vast majority of these molecules have been crystallized and structurally analyzed by X-ray diffraction. However, the model molecules based on natural chlorins, *e.g.* Chl derivatives, are seldom crystallizable. In addition, the solution conformation usually differs from the crystal form, as the crystal packing forces may affect the geometry of a molecule. This fact should be noted, especially, when the flexibly linked models are involved.

Several pyroChl- and pyropheophytin-based compounds have been synthesized to model the Chl special-pair interaction in the photosynthetic RC.[15,18] The structural elucidation of the synthesized compounds **17**–**23** has been performed relying solely on qualitative analysis of ring-current induced chemical shifts in the proton NMR spectra.

Boxer and Closs[122] have synthesized the first Chl based bischlorin **17** (Figure 12) from two pyrochlorophyllide units. The ^{1}H NMR spectra of **17** were measured in dry benzene-d_6, in benzene-d_6 saturated with D_2O or in benzene-d_6 with 5% pyridine-d_5. Extremely broad resonances were observed in dry benzene, implying intermolecular aggregation. In contrast, only narrow resonances appeared in the spectrum measured in the pyridine–benzene solvent mixture. Obviously, pyridine coordinates strongly with the central Mg, and thus prevents any specific intramolecular association between the chlorin molecules. The measurement of the ^{1}H NMR spectrum in water-saturated benzene produced one set of mostly narrow proton signals. Characteristically, strong upfield shifts were observed for the 12^1 and 13^2 protons ($\Delta\delta$ = -1.81 and -0.56 ppm, respectively), whereas the signal of protons 8^2

was clearly shifted downfield ($\Delta\delta$ = 0.50 ppm). As a result, the authors concluded that **17** forms a water-linked C_2 symmetric structure (Figure 12) in wet benzene.

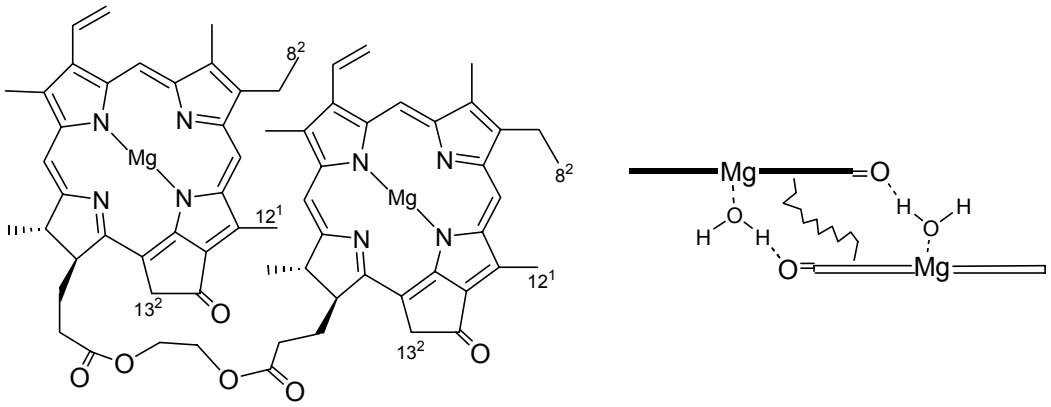

17

Figure 12. The bischlorin **17** and the proposed C_2 geometry with linked H_2O molecules.[122]

Boxer and Bucks[123] have prepared the chlorin trimer **18**. NMR analysis methods, similar to those applied for **17**, were used, except that the specific conformation of **18** was deduced with a 1.8 mM sample in methanol-d_4 (0.6 M) – benzene-d_6. Adjusting the chlorin subunits spatially in such a way that the observed $\Delta\delta_H$-values could be explained by ring-currents, an average 3D-structure shown in Figure 13 was proposed.[123] In fact, the authors also prepared a derivative of **18**, in which Mg atoms were replaced by Zn atoms. For this compound, a similar 3D-structure was suggested.

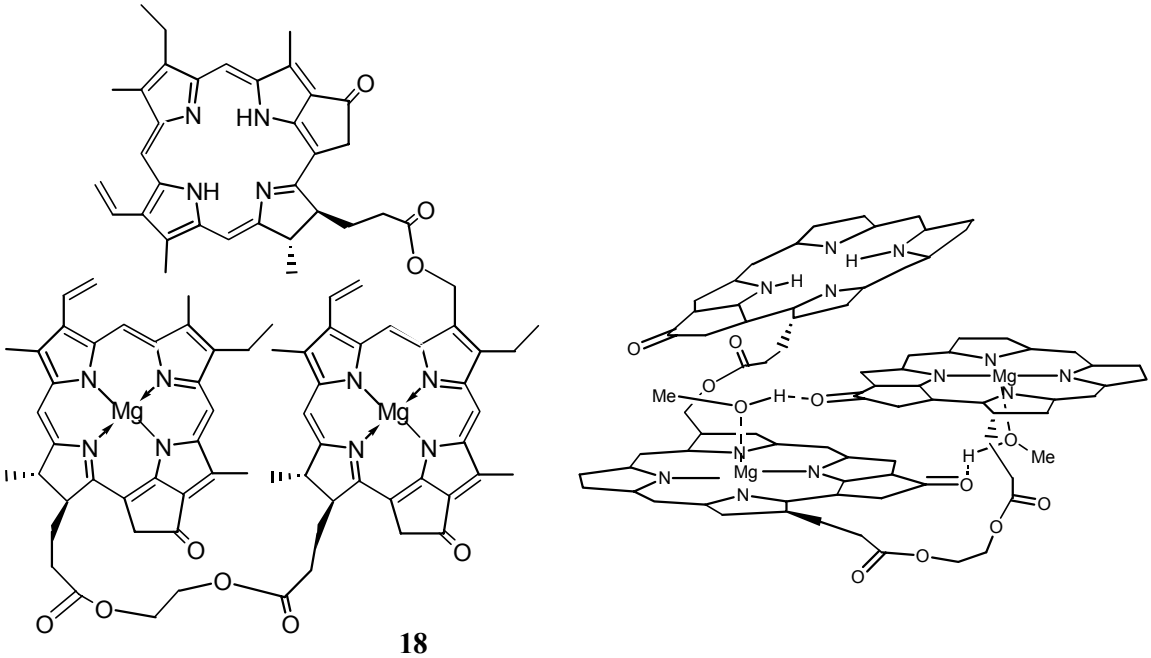

18

Figure 13. The structure **18** and its schematic average conformation in (0.6 M CD_4OD) benzene-d_6 solution.[123]

Wasielewski *et al.*[124] have synthesized the bischlorin cyclophane **19** (Figure 14). The ^{1}H NMR spectrum measured in pyridine-d_5 – benzene-d_6 (1:9 v/v) showed equivalent chemical shifts for the macrocycle protons. The protons at the periphery of the macrocycles experienced only small shift changes compared with the reference compound, methyl chlorophyllide. Consequently, a symmetrically folded 3D-structure (Figure 14) was proposed for **19**. However, the authors concluded from the NMR data that a small tilt angle is possible between the macrocycles. A similar structure was suggested for the corresponding Mg-free derivative.

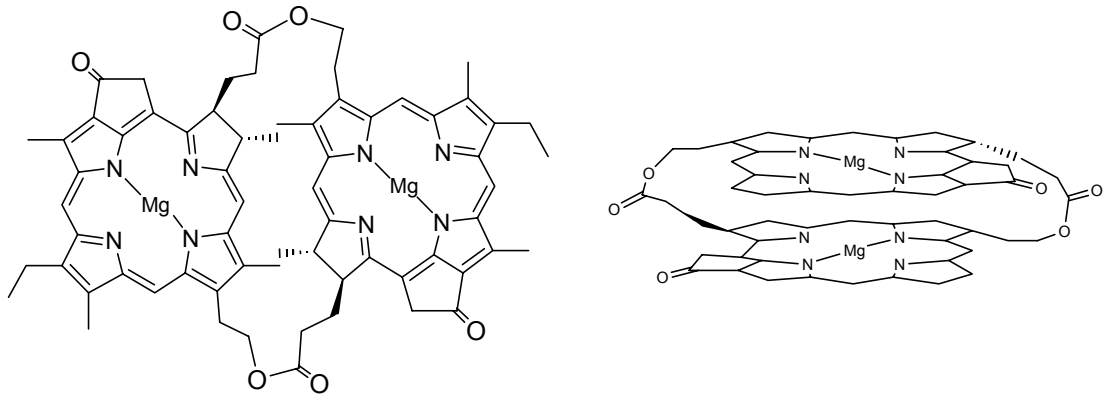

19

Figure 14. The cyclophane structure **19** and its suggested 3D-structure.[124]

Osuka *et al.*[125] have synthesized pyropheophorbide dimers having covalent linkages of various lengths. The aim of the study was to prepare structurally well-defined models with closely stacked face-to-face geometries. The dimer geometry was deduced by analysing the $\Delta\delta_H$-based aggregation maps, which were constructed using monomer-like structures as a reference for comparison. The $\Delta\delta_H$-values of the *meso*-protons demonstrate the degree of macrocycle stacking, since the length of linkage grows gradually in the dimers **20**–**23**. The $\Delta\delta_H$-values of the *meso*-protons varied in the range of -0.02 to +0.30 ppm for **20**, -0.01 to -1.62 ppm for **21**, -0.83 to +1.50 ppm for **22** and -0.50 to -0.64 ppm for **23**. Thus, the anhydride linkage in **20** is too short to allow stacking of macrocycles. The increased linkage length of **21** allows a partial stacking as depicted in model **A** in Figure 15. Both the dimers **22** and **23** exhibit face-to-face geometry, as shown in models **B** and **C**, respectively (Figure 15).

However, the uniformly larger upfield shifts in the macrocycles of **22** indicate closer interplanar distances for this dimer.[125]

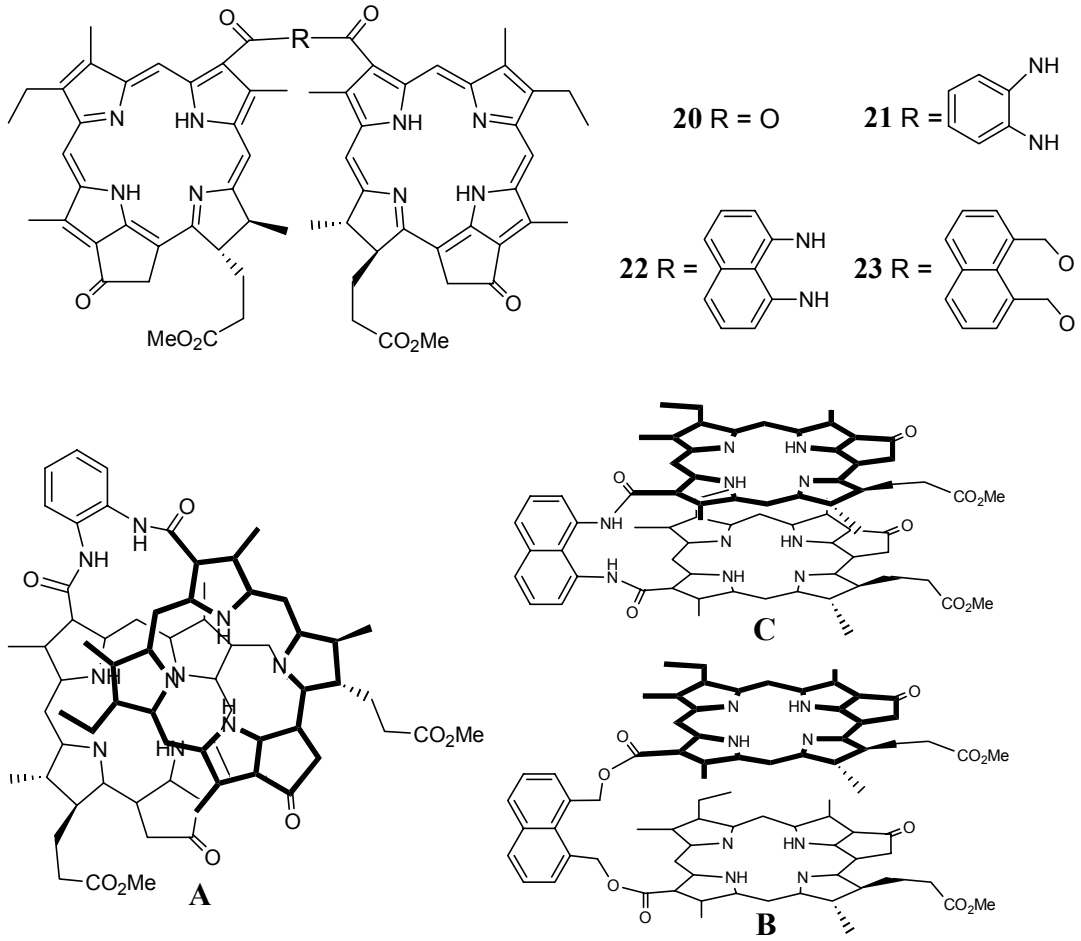

Figure 15. The schematic 3D structures of bispyropheophytins **21**, **A**; **22**, **B** and **23**, **C**, differing recarding the length of the rigid linkage.[125] The models have been constructed on the basis of the $\Delta\delta_H$ aggregation maps obtained from the ^{1}H NMR measurements in $CDCl_3$ or acetone-d_6.

In an attempt to prepare a totally synthetic bischlorin separated by a long unsaturated linker, the chlorin–spirochlorin dimer **24** (Figure 16) was produced instead.[126] Nevertheless, the geometry of **24** and the applied structural analysis methods proved to be highly interesting. The solution structure of **24** was studied in 0.5 % pyridine-d_5/$CDCl_3$, and the ^{1}H NMR spectra were assigned utilizing ROESY and COSY NMR techniques. One ROE correlation was observed between the proton groups of different chlorin subunits (Figure 16) in the ROESY spectrum. In addition, the ring-currents caused notable upfield shifts in the overlaying parts of the chlorin macrocycles. Computer-aided molecular modelling of **24** was performed with MM in a Tripos force-field. The geometry-optimization of **24** was begun from partially refined X-ray coordinates, and performed without constraints. The optimized

geometry was close to that of the X-ray structure. The 3D-model structure in Figure 16 is well in agreement with the NMR data obtained.[126]

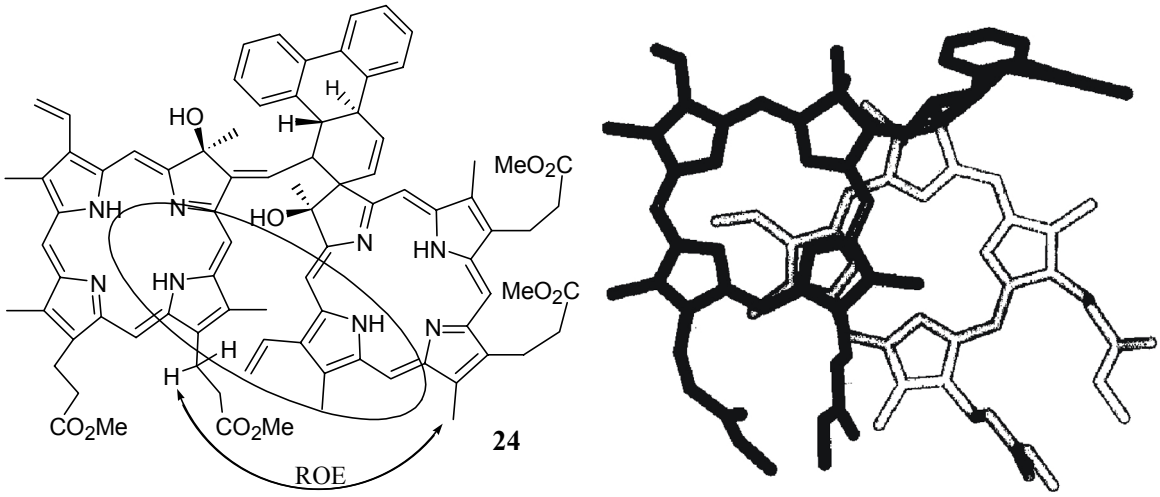

Figure 16. The structure of chlorin–spirochlorin dimer **24**.[126] Significant upfield shifts were observed for protons inside the circled area. The double headed arrow refers to the protons having an interchlorin ROE correlation. The 3D model on the right represents the energy-minimized structure for **24**. Chlorin and spirochlorin are marked with white and dark stick colours, respectively.

In addition to **24**, a more flexible chlorin–chlorin dimer **25** has been synthesized and structurally studied.[127] In the ^{1}H NMR spectrum of **25** clear differences in chemical shifts were observed for some chlorin proton groups. Notably, the protons 10 and 12^{1} were shifted upfield ($\Delta\delta$ = -0.35 and -0.7 ppm, respectively) as compared with the corresponding protons 10' and $12^{1'}$ (Figure 17). The authors did not report any interchlorin ROE correlations. However, the conformation for the vinylic part of the linker group was revealed by the ROE correlations depicted in Figure 17. The dimer **25** can adopt several conformations due to the presence of a flexible linkage in it. Hence, various conformations for the starting structures in the geometry-optimization were created by using a simulated annealing protocol (heating to 700 °C and cooling to 200 °C, with 1000 cycles) in the Tripos force-field.[127] From the resulting 80 structures, 10 were selected for full geometry-optimization on the basis of the relative orientation of the chlorin rings. The preferred geometry for dimer **25**, *i.e.* the structure providing the best correspondence with the NMR data, is presented in Figure 17.

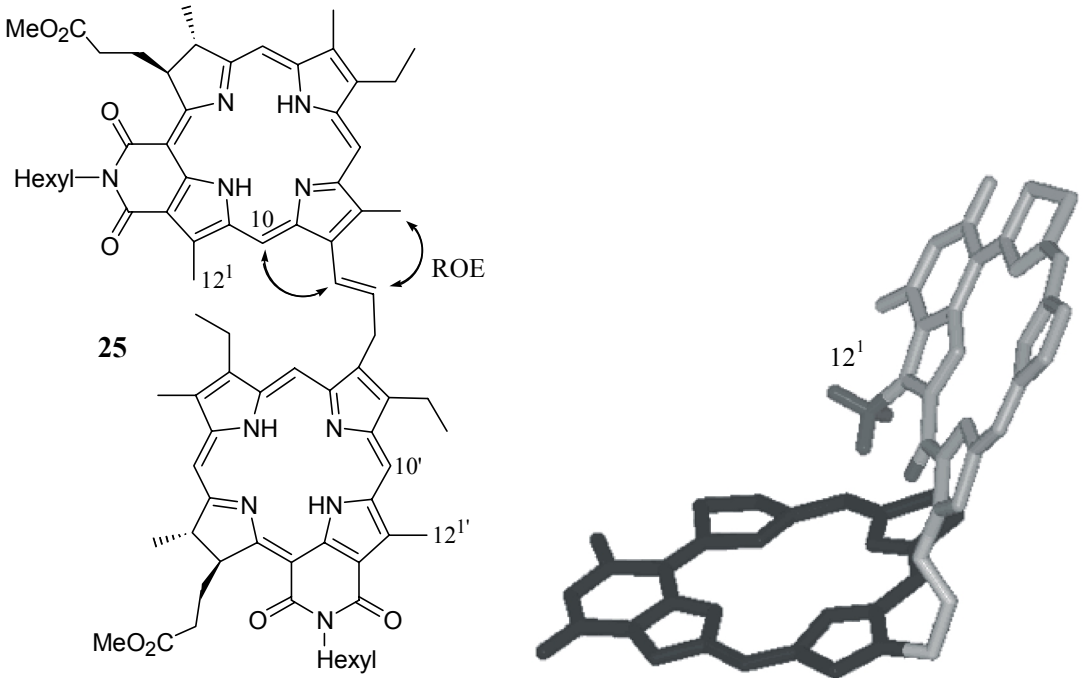

Figure 17. The structure of chlorin–spirochlorin dimer **25**.[127] The double-headed arrows denote ROE correlations that show the orientation of the vinylic part of the linker. The 3D model on the right is the energy-optimized structure of **25**. The hydrogens and most substituents are omitted for clarity.

4.6 Solution conformational analysis of chlorin-related electron donor–acceptor compounds

Only small number of covalently-linked electron donor (D)–acceptor (A) dyads, in which the donor is a chlorin, have been synthetized and structurally analyzed.[15,18] In contrast, a variety of compounds exist in which the electron donor is a porphyrin.[15,16,18] As electron acceptor units, quinones have been widely applied and, more recently, fullerene C_{60}.[15,16,18,128]

4.6.1 Chlorin–quinone and porphyrin–quinone molecules

Porphyrin– or chlorin–quinone interactions are weaker than the previously discussed chlorin–chlorin interactions (*vide supra*).[18] Hence, single-bridged porphyrin– or chlorin–benzoquinones adopt an open or unfolded solution conformation. In order to obtain a defined folded geometry, covalently double-bridged porphyrin–benzoquinones have been prepared.[18] Another approach to achieve a defined geometry is to use a linkage which favours certain conformation(s). Thus, fixed unfolded geometries have been established for synthetic 1,4-cyclohexylene-bridged porphyrin–quinones with a *cis*- or *trans*-configuration (**26a**–**b** and **27a**–**b**).[129-131]

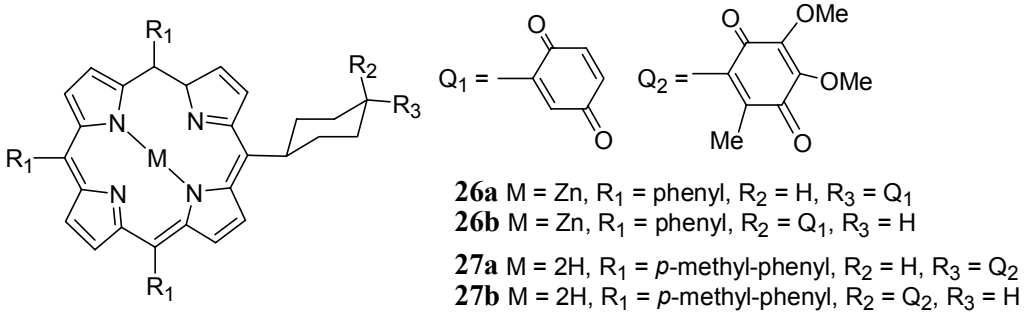

26a M = Zn, R_1 = phenyl, R_2 = H, R_3 = Q_1
26b M = Zn, R_1 = phenyl, R_2 = Q_1, R_3 = H

27a M = 2H, R_1 = *p*-methyl-phenyl, R_2 = H, R_3 = Q_2
27b M = 2H, R_1 = *p*-methyl-phenyl, R_2 = Q_2, R_3 = H

According to the proton couplings obtained from the COSY spectra, the cyclohexylene bridge adopts a chair conformation in the case of porphyrin–quinones **26a**–**b**.[129,130] The NOE enhancements measured between the cyclohexane and porphyrin protons proved that the porphyrin and quinone are in an orthogonal orientation. Semiempirical AM1 molecular modelling calculations were used to estimate the favourable quinone orientation with respect to the cyclohexane ring. The resulting potential energies for the **26** isomers showed that the quinones have a deep potential energy well when being in an orthogonal orientation (Figure 18), for which the energy barrier is less than 1 kcal/mol at $\phi = 0 \pm 50°$. Nevertheless, another feasible local energy minimum (*ca.* 1 kcal/mol higher ΔH_f) was found for the *trans*-compound **26a** ($\phi = 180°$). The rotation barrier between the minima was 7 kcal/mol. In contrast, the *cis*-compound **26b** exhibited a local energy minimum when $\phi = 180°$. However, this rotamer was 5 kcal/mol energetically higher than the rotamer in a global energy minimum.

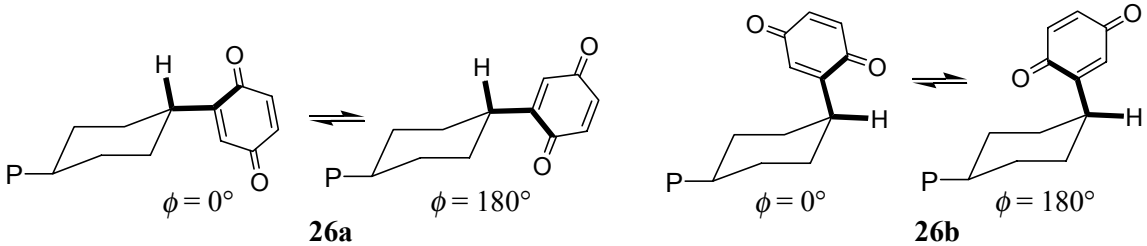

Figure 18. Orthogonal conformations of cyclohexane-quinone *trans*- (**26a**) and *cis*-isomers (**26b**). The bonds forming the torsion angle ϕ are in bold. [129,130]

In the case of substituted quinones **27a** and **27b**, the cyclohexane–quinone conformations could also be analyzed on the basis of NOE enhancements (Figure 19).[131] In fact, the NOE observed proton irradiation experiments clearly indicated that the quinone of the *trans*-isomer **27a** can adopt two orthogonal conformations with $\phi =$

0 or 180° (Figure 19). For the *cis*-isomer **27b**, the observed NOE between the protons 1 and 4 in the cyclohexane ring suggested a twisted-boat conformation for the ring. A chair conformation of the cyclohexane ring could be ruled out, since the protons are too distant for NOE observation. Supporting evidence for the NMR evaluated conformation was obtained from semiempirical MNDO molecular modelling calculations, which produced energy minima for all the deduced conformers.[131]

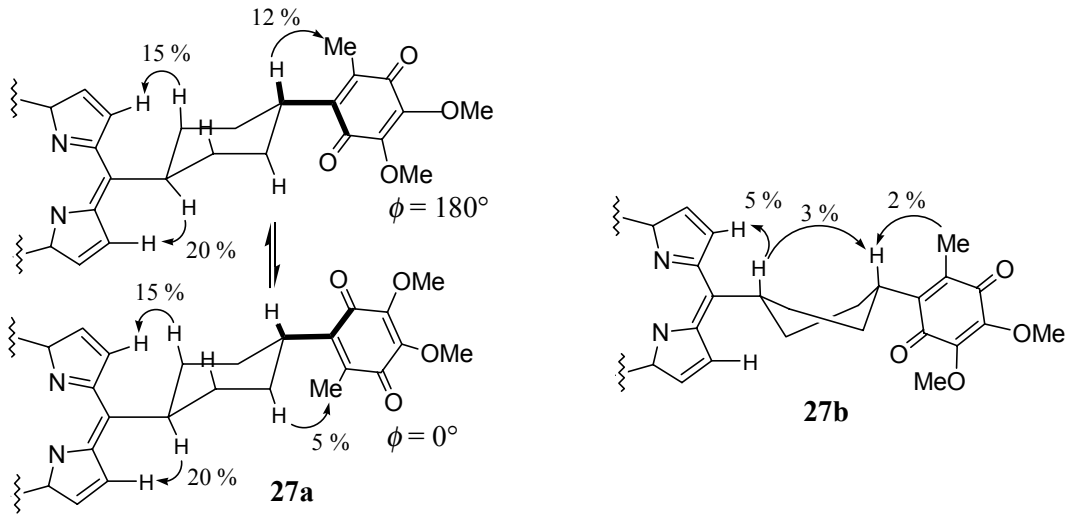

Figure 19. The observed conformations in $CDCl_3$ for the cyclohexane–quinone *trans*- (**27a**) and *cis*-isomers (**27b**).[131] The bonds forming the torsion angle , ϕ, are in bold. The numerical values (in %) of NOE enhancements between different protons are marked with arrows.

The larger π-system of an anthraquinone compared with that of a benzoquinone also indicates stronger π–π interaction in porphyrin– or chlorin–antraquinone dyad structures. Consequently, conformational folding has been observed for flexibly linked porphyrin– or chlorin–anthraquinones.

Sanders *et al.*[132] have synthesized sulphonyloxy-linked porphyrin–anthraquinones **28** and **29** (Figure 20), and have studied their structures by ^{1}H NMR spectroscopy in $CDCl_3$. These studies were based on the antraquinonyl proton upfield shifts, observed when δ-values of the dyad were compared with those of a like anthraquinonyl monomer. By inspecting molecular models, the authors suggested that the anthraquinone ring is folded over the porphyrin macrocycle in **28** and **29**, as depicted in models **A** and **B** (Figure 20). However, time averaging can occur under the experimental conditions and, therefore, the measured data suggest the presence of several conformations in equilibrium besides **A** and **B**. It is notable that the Zn(II) coordination affects the quinone folding mechanism in **29**. When a sample of **29** was

titrated with pyridine-d_5 ligands, a gradual change from conformation **B** to conformation **A** was observed.

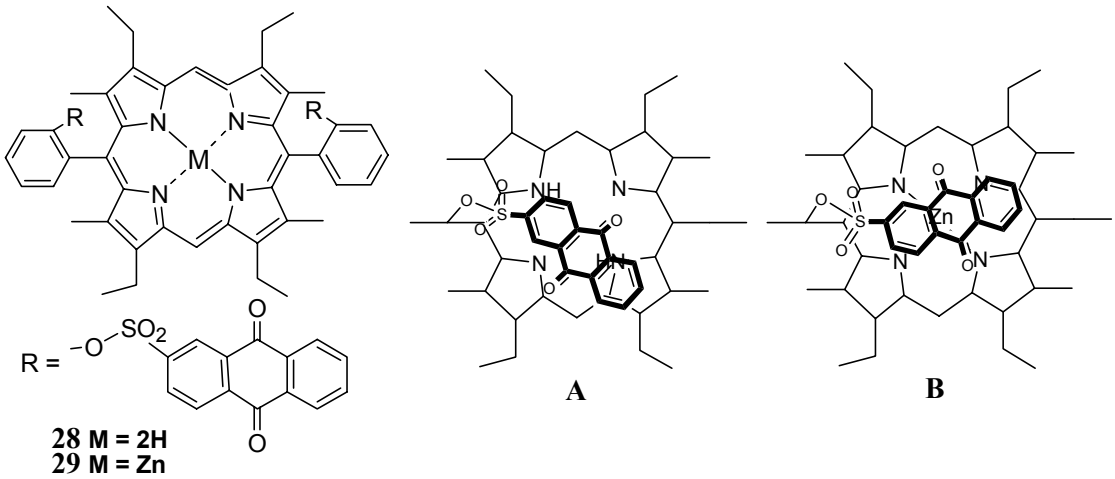

Figure 20. The suggested average conformations for **28** (**A**) and **29** (**B**) on the basis of the $\Delta\delta_H$-values observed for the anthraquinonyl group.[132]

Tauber *et al.*[133,134] have synthesized two pyropheophytin–antraquinone dyads, the P4-stereoisomers **30a**–**b**, both of which experienced conformational folding in $CDCl_3$. The preliminary conformational analysis was performed by calculating the $\Delta\delta_H$-values for both the phorbin and the quinone moieties in the dyads, and constructing molecular models that explain the $\Delta\delta_H$-values. The proposed models for the P4(*S*)- and P4(*R*)-epimers **A** and **B**, respectively, are illustrated in Figure 21. It was concluded that conformational folding contributes significantly in the solution, and that the constructed models do not represent a single folded conformation, but are a result of time-averaging processes between several conformations in equilibrium. A more detailed conformational analysis for **30a**–**b** and their the Zn(II) complexes are presented in section 7.3 and publication III.

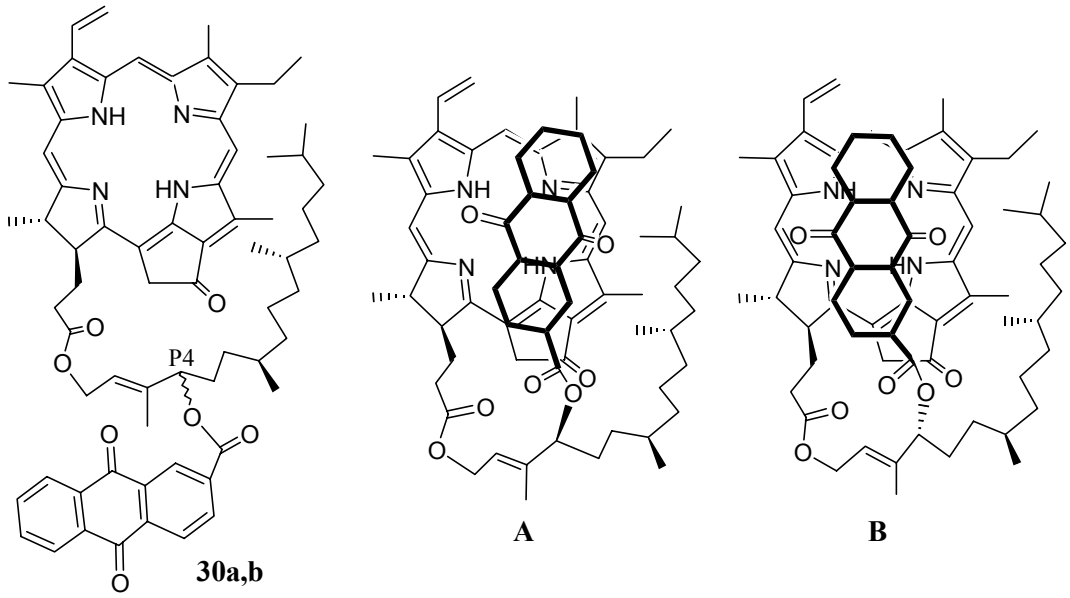

Figure 21. The pyropheophytin–antraquinone P4-epimers **30a**,**b** and the models proposed as a result of conformational analysis for **A** (P4(*S*)-**30a**) and **B** (P4(*R*)-**30b**).[133]

Interestingly, dyads **30** and **31**, although consisting of the same donor and acceptor units, did not show any significant folding, when there was a short four-atomic ether bridge between the pyropheophorbin and anthraquinone.[134,135] This finding was attributed to the shortness and rigidity of the spacer group.[134]

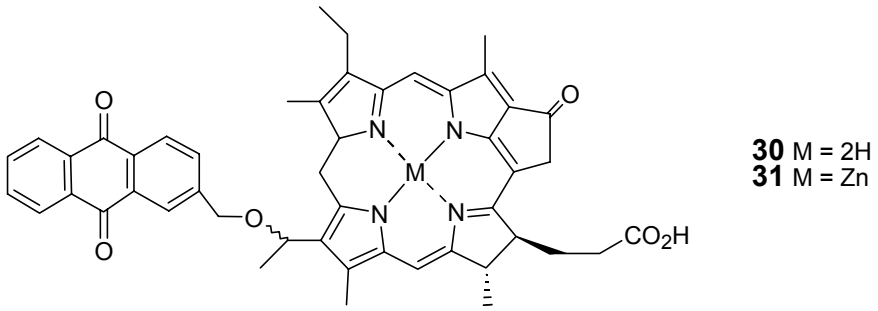

4.6.2 Porphyrin–C_{60} dyads

Fullerenes have been shown to function well as electron acceptors in artificial electron D–A systems.[128] The fullerene C_{60} is a fully-conjugated structure exhibiting a football-like construction in which 20 cyclohexene and 12 cyclopentene-rings are fused to form a sphere, as depicted in Figure 22. In the external magnetic field, the 6-membered rings exhibit diamagnetic ring-currents, while the 5-membered rings induce strong paramagnetic ring-currents.[136] The overall ring-current of the C_{60} is neutral, but the average effect of the C_{60} sphere is essentially deshielding on the NMR chemical shifts of nuclei in it's proximity.[136] In the case of fixed geometries, both

shielding and deshielding effects can be experienced by the nuclei in the vicinity of C_{60}.

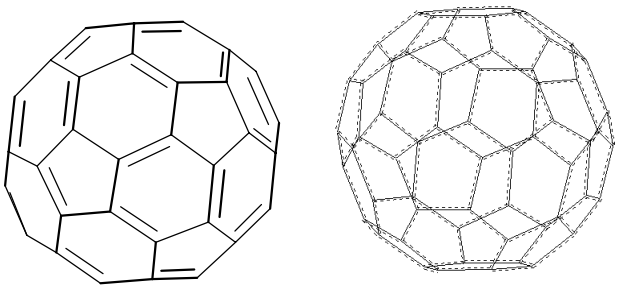

Figure 22. The 2D and 3D view of C_{60} fullerene.

The curved π-surface of C_{60} tends to interact with other molecules. NMR, X-ray and molecular modelling investigations of unlinked tetraphenylporphyrin and C_{60} have proven that the electron rich C–C of the 6,6-ring juncture interacts closely with the core of tetraphenylporphyrin (Figure 23).[137] In the crystal structure, the shortest measured distance between the porphyrin plane and a C_{60} carbon was 2.7 Å, whereas the distance in a typical porphyrin–arene π–π interaction lies in the range of 3.0 – 3.5 Å.[137] The former distance could not be reproduced by the PM3 semiempirical calculations or *ab initio* minimal basis set calculations.[137] A separation of 3.3 – 3.4 Å between porphyrin and C_{60} was found as expected, since the electron correlation was neglected in these calculations. The close interaction (2.7 Å) may originate primarily from forces that are van der Waals in nature. In fact, the density functional calculation with a nonlocal correction for correlations produced a model, in which the porphyrin–C_{60} separation was 2.8 Å. The distance, indicative of close interaction (2,85 – 2.90 Å), was also obtained by using UFF and PCFF[138] MM force-fields which adequately take into account the van der Waals interaction.[137] Moreover, the formation of a porphyrin–C_{60} complex in toluene-d_8 was established by NMR studies, since both the ^{13}C δ-values of fullerene and the ^{1}H δ-values of the NH protons of the porphyrin showed upfield shifts.[137]

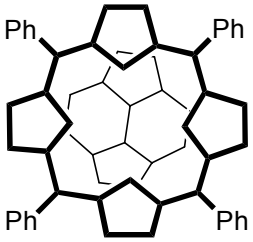

Figure 23. The interaction between unlinked tetraphenylporphyrin and C_{60} as determined by X-ray, NMR studies and molecular modelling calculations.[137] The electron-rich C-C bond of the 6,6-ring juncture, lies over the centre of the porphyrin ring.

The porphyrin–C_{60} dyads **32** and **33** show some conformationally interesting features.[139-142] The flexible bi-linkage of dyad **32** allows the existence of various conformations. However, the ^{1}H NMR spectrum of **32** in $CDCl_3$ shows that the porphyrin *meso*-protons 5 and 15 are clearly shifted upfield with $\Delta\delta_H$-values of 0.5 and 0.3 ppm, respectively.[139] Apparently, the dyad exhibits essentially a folded conformation. Molecular mechanics calculations produced a folded lowest-energy conformation (Figure 24) in which the C_{60} is lying in van der Waals contact over the centre of the porphyrin plane.[141]

In the case of dyad **33**, the short linkage effectively restricts the number of possible conformations. Thus, the C_{60} can be located on either side of the porphyrin plane. Furthermore, the high symmetry of the tetraphenyl porphyrin signifies that similar chemical shifts are expected for both conformers. Consequently, the ^{1}H NMR spectrum measured in CS_2 gave only one set of signals for **33**.[140] The MM calculations showed that the energy minimum is found with the conformation depicted in Figure 24.[141,142] Interestingly, the porphyrin–C_{60} centre–centre separations are *ca*. 7 Å and 9.9 Å for dyads **32** and **33**, respectively.[141]

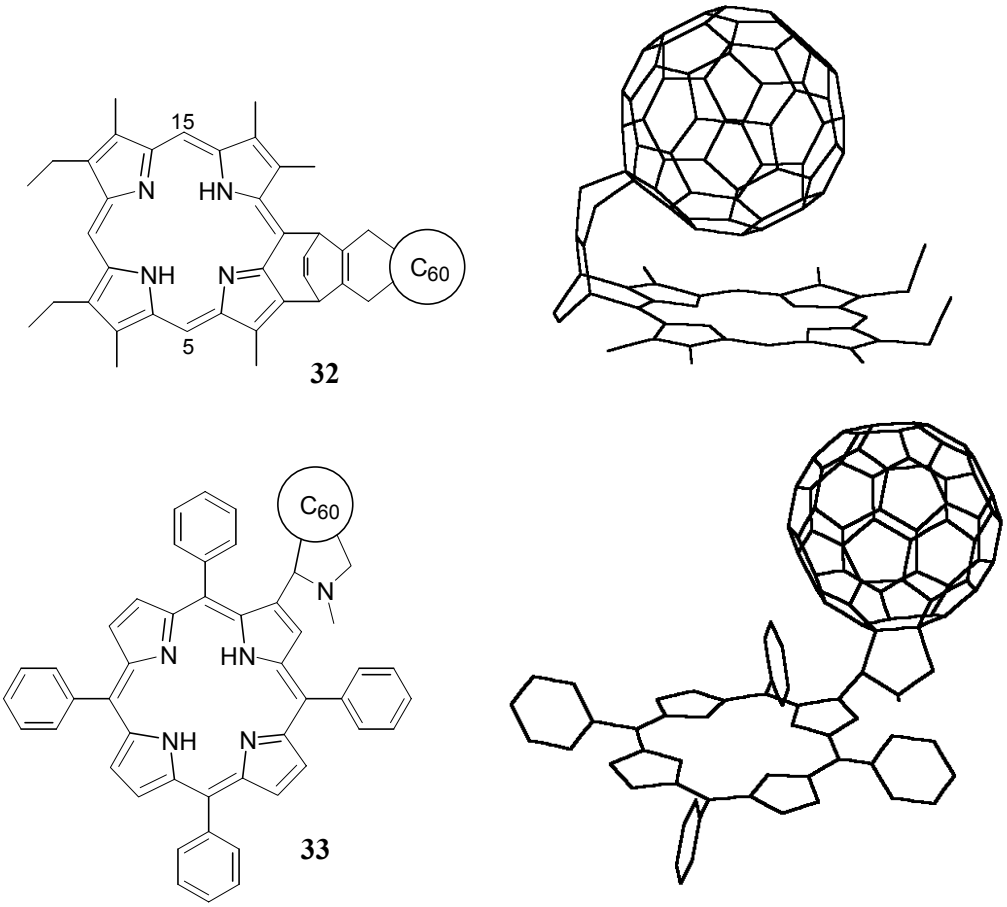

Figure 24. The porphyrin–C_{60} structures **32** and **33**, and their conformations obtained by MM calculations (Discover/Insight II program, Biosym Technologies).[141,142] The pyrrolidine *N*-methyl substituent is in *trans*-orientation with respect to the porphyrin plane in the model of **33**.[142]

Imahori *et al*.[143] have synthesized zinc-tetraphenylporphyrin–C_{60} dyads **34**–**37**, in which C_{60} is covalently linked via an amido group to the *ortho* (**34**), *meta* (**35**) or *para* (**36** and **37**) position of one phenyl ring of the porphyrin. In addition, the cyclohexene ring, fused to the 6,6-ring C–C bond of C_{60}, is attached to the 3,4 or 2,3 position of the phenyl spacer group. The ^{1}H NMR spectrum of the *ortho* dyad **34** in $CDCl_3$ showed exceptional behaviour.[143] The proton resonances of its porphyrin moiety and cyclohexane ring were expanded over a wider spectral region than in the case of dyads **35**–**37**. Obviously, the mutual ring-currents of the porphyrin and C_{60} caused the observed range of chemical shifts in **34** due to conformational folding.

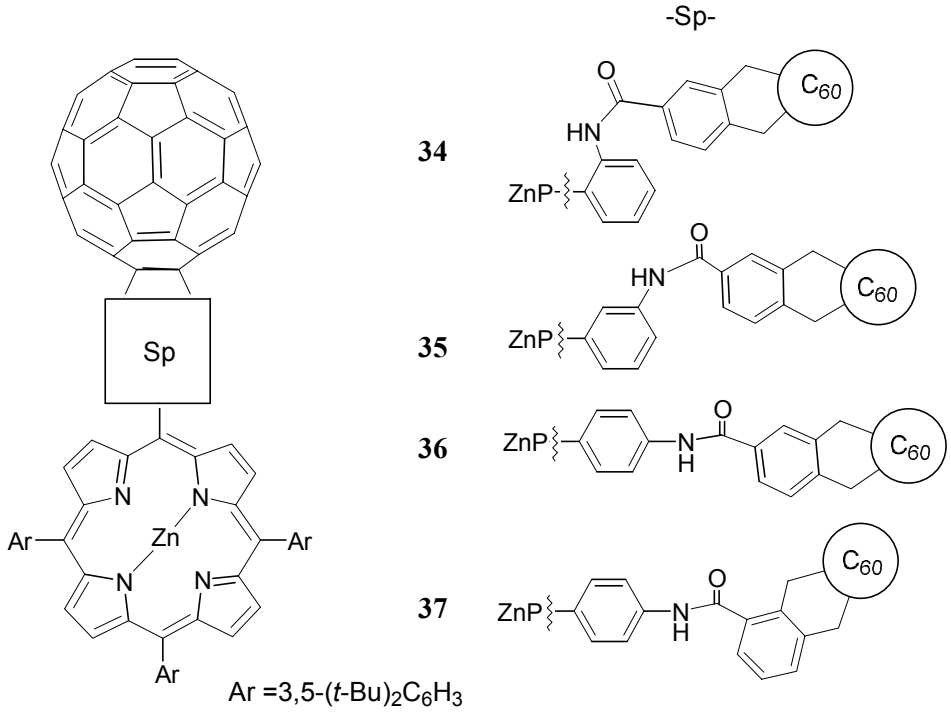

Molecular mechanics calculations were performed in a CHARMm force-field to find the lowest-energy conformations for **34**–**37**.[143] The conformational search was performed by individually rotating three single bonds (ϕ_1,ϕ_2 and ϕ_3, Scheme 1) in the linker group in steps of 30°. Each of the 1728 conformations generated was energy-minimized by constraining the geometry of the porphyrin macrocycle to be planar. As a result, a lowest-energy, folded conformation was obtained only for the dyad **34**, in which C_{60} is located 3.2 Å above the porphyrin plane (Table 3). The molecular modelling calculations showed that dyad **36** favours a stretched conformation, whereas the dyads **35** and **37** adopt chair-like conformations.[143]

Scheme 1

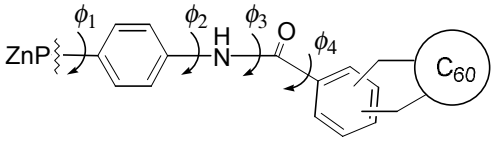

Table 3. Molecular mechanics calculated conformations for porphyrin–C_{60} isomers **34**–**37**.[143]

Compound	ϕ_1	ϕ_2	ϕ_3	ϕ_4	R_{ee}[a]	R_{cc}[b]
34	-78.27	133.02	174.50	-129.15	3.2	7.6
35	95.86	51.17	-175.73	3.10	9.8	14.4
36	86.95	-48.64	179.07	-10.82	11.3	18.6
37	96.68	52.14	-175.81	-131.67	5.9	12.5

[a]Edge-to-edge distance (Å). [b]Centre-to-centre distance (Å).

4.7 NH tautomerism in porphyrins and chlorins

According to literature sources,[71,87,144-147] only a few studies exist about the NH tautomerism in chlorins. In contrast, the elaboration of the mechanism of the NH tautomerism in porphyrins (Figure 25) has been an important objective in numerous experimental and theoretical investigations.[148-150] In the following, the NH tautomerism of porphyrins, investigated by solution NMR and molecular modelling, is briefly discussed.

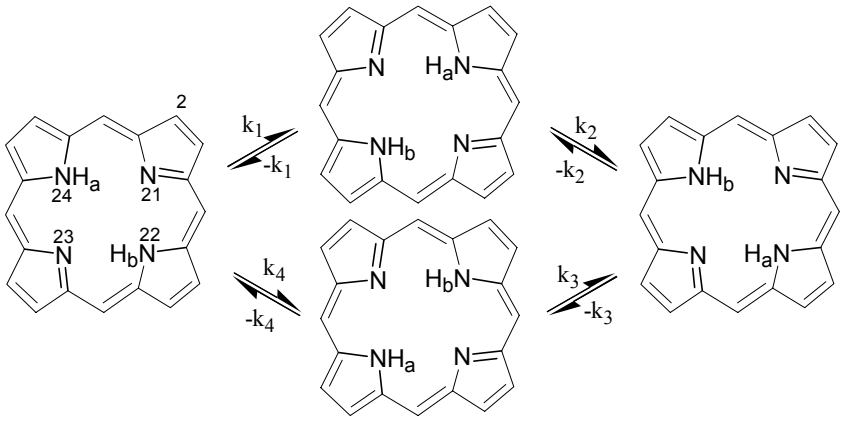

Figure 25. The spectroscopically (NMR) detected porphyrin *trans* NH tautomers and the NH exchange reactions between them.

Storm and Teklu[71] obtained the first experimental evidence by dynamic NMR (DNMR) spectroscopy that NH tautomerism occurs in both chlorins and porphyrins. The tautomerism was investigated by variable-temperature ^{1}H NMR measurements with or without deuterium labelling. The exchange reaction was detected directly in the behaviour of the NH proton signals or indirectly in the behaviour of the porphyrin β-pyrrolic proton signals. Since the pioneering work of Storm and Teklu, the NH tautomerism of porphyrins has been widely investigated by ^{1}H, ^{13}C and ^{15}N DNMR methods.[148-150] The activation free-energy ($\Delta G^{\ddagger}$) can be calculated in terms of the coalescence temperature (T_C) and exchange rate-constant (k_C) using the Eyring equation (Eq. 7 in section 7.4).[22,151] Variable-temperature spectra can also be analyzed by the line-shape analysis, which can afford the coalescence temperature more accurately.[151] The line-shape analysis can also result in the kinetic exchange rate-constants between the tautomers.[150] The thermodynamic parameters, enthalpy of activation ($\Delta H^{\ddagger}$) and entropy of activation ($\Delta S^{\ddagger}$), can be derived from the aforementioned rate-constants.[150,151] Under slow NH-exchange rate conditions (the

rate still being of the same order of magnitude as the reciprocal of T_1), saturation transfer experiments can be used to define the rate constants.[150,151]

Only *trans* NH tautomers (N_{22}-H, N_{24}-H and N_{21}-H, N_{23}-H; Figure 25) of porphyrins have been detected experimentally by NMR spectroscopy.[150] In the case of unsymmetric, 2-substituted 5,10,15,20-tetraphenylporphyrins, two tautomeric barriers have been observed between the major *trans*-tautomers.[150] The calculated rate constants indicated that a directional preference prevails in the NH tautomeric process, *i.e*. the exchange proceeds via the k_1/-k_1 and k_3/-k_3 rather than the k_2/-k_2 and k_4/-k_4 pathways (Figure 25).

The kinetic evidence obtained from NMR spectroscopy and the quantum mechanical calculations have led to the generally accepted conclusion that the NH tautomerism proceeds via *cis*-tautomer intermediates with a stepwise proton or hydrogen transfer mechanism.[148-150] The semiempirical MNDO, AM1 and PM3 calculations in the RHF mode have produced heat of formation energies (ΔH_f) which were 6 – 10 kcal/mol higher for the porphyrin *cis*-tautomers than for the *trans*-tautomers (Table 3).[152-154] By these methods, the saddle-point (ΔH_f) energy, *i.e*. transition state (TS) energy between the *trans*- and *cis*-tautomers has been calculated to be 28-43 kcal/mol. The calculations by advanced *ab initio* methods such as the second order Møller-Plessed (MP2) and the DFT methods, produced energy values 8.1 – 9.1 and 13.1 – 18.6 kcal/mol for the *cis* and TS structures, respectively.[148,155,156] The experimental activation energy obtained for the NH tautomerism of the unsubstituted porphyrin by the ^{1}H and ^{3}H DNMR line-shape analysis is *ca*. 9.0 kcal/mol at 300 K.[157] However, the proton (and triton) tunnelling effects contribute to this energy value.[157] When the tunnelling was taken into account in the calculation, an activation energy of 10.8 kcal/mol was produced instead of 18.6 kcal/mol in the DFT method (DFT(4) in Table 3).[148]

Table 3. The $\Delta\Delta H_f$ energies ($\Delta\Delta H_f$ = [ΔH_f(*cis*) or ΔH_f(TS)] - ΔH_f(*trans*) in kcal/mol) of unsubstituted porphyrin relative to the lowest-energy *trans*-tautomer calculated by semiempirical and *ab initio* methods.

	Semiempirical			*ab initio*				
	MNDO[152] (RHF)	AM1[153] (RHF)	PM3[154] (RHF)	MP2[155]	DFT(1)♣	DFT(2)♣	DFT(3)♣	DFT(4)♣
cis	10	7	6	10.7	8.2-8.4♠	8.7-8.9♠	8.1-8.3♠	9.1
TS	43	35	28	16.7	13.7-16.8♠	13.9-17.0♠	13.1-16.2♠	18.6

♣DFT(1) = B3-LYP/6-31G(d),[156] DFT(2) = MP2/6-31G(d)//B3-LYP/6-31G(d),[155] DFT(3) = B3-LYP/TZ2P,[155] DFT(4) = BH&H-LYP/6-31G(d,p).[148]

♠In the ranges, the lower energy-values have been calculated with zero-point vibrational energy correction, whereas the higher energy-values have been produced without the correction.

The comparison of the energies in Table 3 demonstrates that the semiempirical methods estimate relatively well the energy values for *cis*-tautomers, but for the TS-structures the energies are clearly overestimated. It has been reported that the semiempirical methods show similar qualitative behaviour as the *ab initio* methods in the calculations of the porphyrin structure. However, the former methods clearly tend to distort the symmetry.[155] The calculations with semiempirical methods produced C_{2v} symmetry-broken structures for the porphyrin macrocycle in the ground state, whereas the inclusion of electron correlation in the *ab initio* methods restored the higher D_{2h} symmetry.[155]

In a recent *ab initio* dynamics study of a free-base porphyrin, it was found that NH tautomerization prefers a stepwise mechanism, in which a hydrogen migration step consists of two separate stages of motions.[148] In the first stage, the porphyrin macrocycle is deformed so that the donor and acceptor sides are brought into such a close proximity that a local hydrogen atom transfer can occur in the second stage. The deformation is reported to account for nearly 50 % of the total activation energy.

5 Aims of the present study

The principal aim of the present work was to analyze the solution structures of the natural chlorin derivatives utilizing NMR spectroscopy, supported by computer-aided molecular modelling. A primary objective in the analysis was to define the three-dimensional structures of Chl derivatives. The definition of the 3D structures included the determination of the stereochemistries of the chemically modified parts in the Chl derivatives, as well as the conformational analysis of the propionic acid residue, of the front part of the phytyl group and of ring *D*. In addition, the intramolecular orientation and distances between the electron donor and acceptor subunits in the dyad molecules were targeted for analysis. A secondary goal was to elucidate some fundamental structure-dependent properties of the natural chlorins, such as their NH tautomerism and aromaticity.

The basic approach in the structural analysis involved utilization of modern NMR techniques to obtain experimental data. The NMR data, comprising the measured spin-spin couplings, the NOE (ROE) enhancement correlations and the chemical-shift values, formed the basis for the structural elucidation. The NMR data were supported by the computer-aided molecular modelling. The molecules studied were geometry-optimized by performing the energy-minimization using the MM+ molecular mechanics method or the AM1 and PM3 semiempirical methods.

6 Experimental

The experimental conditions for NMR measurements are described in publications I – V. The parameters of the HMBC spectra of **11** are given in Table 4 and Figure 27.

All the NMR measurements were performed using a Varian UNITY 500 MHz or a Varian INOVA 300 MHz NMR spectrometer. The spectra were measured from freshly prepared samples to avoid signal line-broadening observed for aged samples. Chloroform co-distillation was used to remove the water from the Chl derivatives, prior to vacuum drying and dissolving the sample.

The computer-aided molecular modelling calculations were performed by the methods included in the HyperChem 4.5 software package. The calculations were run on various 486 and Pentium PC computers during the course of the studies.

The molecular modelling methods and equipment are described in publications II –V for the studied compounds, the exception being compounds **38a**,**b**. The molecular modelling parameters for **38a**,**b** and methyl chlorophyllide *a* mono-hydrate are given below. The structures presented in Figure 29 were energy-optimized by the PM3-UHF method. The optimizations were performed using a Polak-Ribiere conjugate gradient algorithm by setting the convergence of the gradient to 0.01 kcal x $Å^{-1}$ x mol^{-1}. The starting structures for the optimization were constructed on the basis of the conformational data obtained from NMR. However, a H_2O ligand was arbitrarily inserted above the chlorin plane (on the same side as the C17 substituent). The calculations were run on an Intel Pentium III PC computer with 128 Mb RAM and 450 MHz clock frequency. For each system studied, the convergence was reached in a few hours.

The chlorophyll derivatives studied in this work have been prepared in the Laboratory of Organic Chemistry at the University of Helsinki. The Chl *a* and *b* were isolated from clover leaves by Hynninen's method,[158] modified for large-scale preparation. The bonellin dimethyl ester (**3**) was prepared by Montforts's group in the University of Bremen.[21]

7 Review of the results

In publications I – III, the solution structures of the chlorophyll *a* derivatives **38**–**40** were analyzed based on complete assignments of the ^{1}H NMR spectra and the utilization of the δ_H and $J_{H\text{-}H}$ values as well as the ROE correlations. In publication I, the absolute configuration was deduced at C13^2 and the conformations of ring *D*, the propionic acid residue and the front part of the phytyl side-chain were determined for the methanolic allomers, *i.e.* the 13^2-methoxyChl *a* epimers **38a**,**b**. In publication II, the conformations of the aforementioned structural subunits were also defined for the dyad epimers **39a**,**b**. Further, the $\Delta\delta_H$ and $\Delta\delta_C$ values were used for constructing the 3D structures for the dyads, which were then energy-optimized by molecular mechanics. In publication III, the atropisomerism and dynamics of chlorin–C_{60} **40** were studied by ^{1}H DNMR and molecular modelling. The principles and results are examined in sections 7.1 – 7.3.

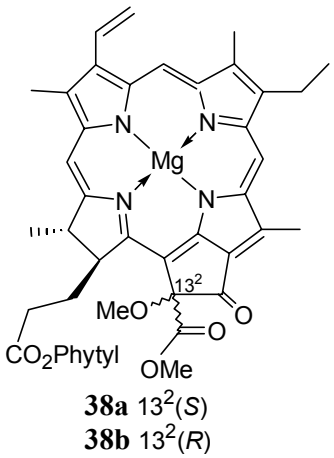

38a 13^2(*S*)
38b 13^2(*R*)

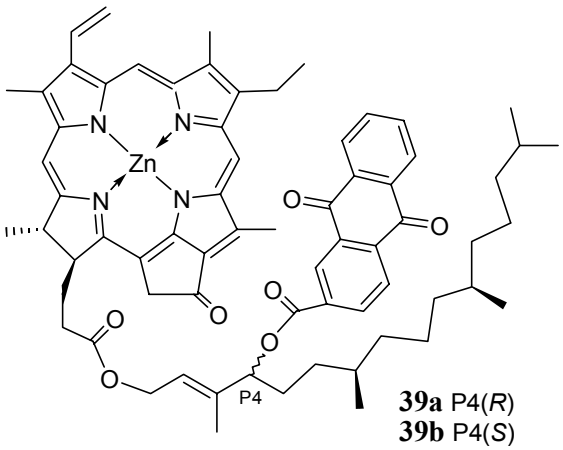

39a P4(*R*)
39b P4(*S*)

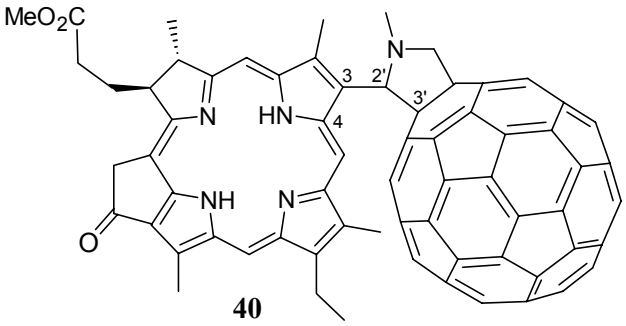

40

In publications IV and V, the nature and existence of NH tautomerism in natural chlorins were studied using bonellin dimethyl ester **3** and Chl *a* and *b*

derivatives **41**–**45**. The results obtained by DNMR in combination with semiempirical molecular modelling for the NH tautomerism are analyzed in section 7.4.

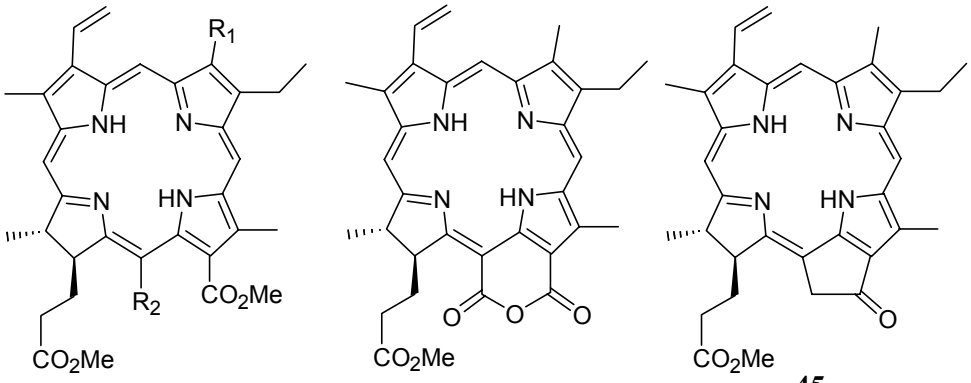

44 **45**

41 R_1= Me, R_2= H,
42 R_1= Me, R_2= CH_2CO_2Me,
43 R_1= HCO, R_2= CH_2CO_2Me

7.1 Assignment of the ^{1}H, ^{13}C, ^{15}N NMR spectra of chlorophyll derivatives and determination of the absolute configuration at C13^{2}

For the proton spectral assignments of Chl *a* derivatives **38**–**40**, the signals arising from the 3-vinyl and/or 8-ethyl spin-systems are easily recognizable due to their typical δ_H and $J_{H\text{-}H}$ values observed in the spectra. The full ^{1}H assignment was further performed by deducing the ^{1}H-^{1}H connectivities in the 2D ROESY spectra. Figure 26 shows that, by starting from any reliably assigned resonance of the chlorin macrocycle, a nearly complete assignment of the macrocyclic protons can be obtained using the ROE connectivities.

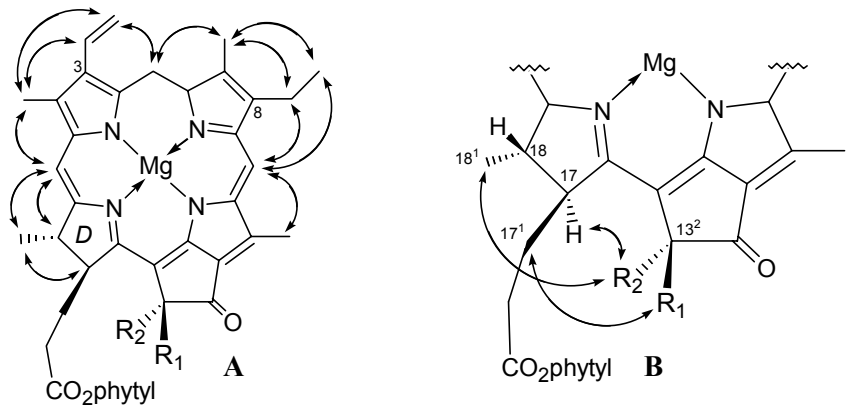

Figure 26. Double-headed arrows drawn between proton groups show the ROE correlations in derivatives **38a** and **38b**. The ROE correlation arrows in structure **B** define the configuration at the 13^{2}-carbon.

The absolute configuration at the 13^2-carbon in the methoxyChl *a* epimers **38a**,**b** could be defined on the basis of the ROE correlations observed between the methyl protons of the 13^2-methoxy substituents and the protons 17, 17^1 or 18^1, as depicted in Figure 26. This principle was utilized later to define the stereochemistry at $C13^2$ or $C15^1$ in other methanolic allomers of Chl *a*.[93]

The performance of ^{1}H spin simulation was a prerequisite for unambiguous assignments of the propionic side-chain 17^1-CH_2 and 17^2-CH_2 protons, as well as for achieving accurate δ_H and $J_{H\text{-}H}$ values (publications I and II). A tentative assignment could be achieved for the aforementioned spin-system by selective proton saturation experiments. The geminal proton pairs (17^1-CH_2 and 17^2-CH_2) could be also identified from an HMQC experiment, which reveals the protons attached to the same carbon. In principle, the mutual assignment of the vicinal proton pairs could be extracted from an HMBC experiment. However, in the present case, the 17^1-CH_2 and 17^2-CH_2 protons showed correlations only to the same carbon nuclei, which was insufficient for assignment.

In general, the HMBC and HMQC (or HSQC) experiments provided a powerful tool for the assignments of the ^{13}C and ^{15}N NMR nuclei in the chlorins studied. In publication II, completely assigned ^{13}C spectra could be obtained for dyads **39a**,**b** by using the HMBC and HMQC techniques. A few interchangeable signals were present due to the lack of resolution in the ^{13}C dimension.

The introduction of gradient selection (gs) has greatly improved the efficiency of the aforementioned indirect heteronuclear techniques. When a sample of bonellin dimethyl ester (72 mM in $CDCl_3$) was set up for an acquisition over the weekend in a conventional ^{1}H-^{15}N HMBC experiment, hardly any signals could be detected from the spectral base-line. However, the use of the corresponding gsHMBC experiment afforded clear correlation signals during an overnight acquisition (publication IV, Figure 2).

In the ^{1}H-^{13}C HMBC experiment, the difference between the phase-cycled and gradient selection versions is less prominent. Nevertheless, the comparison of the spectra of each type recorded for chlorin **11** (Figure 27) demonstrates clearly the advantage of the gs-technique. Despite the fact that gsHMBC was recorded at a lower magnetic field with less than one-third of the transients as compared with the

conventional HMBC spectrum (Table 4), the quality of the former spectrum is superior to the conventional one. The main defect in the conventional spectrum is the t_1-noise, which causes some artefact noise in the spectral region of the intensive methyl resonances. The fact that the correlation signals are narrow in the F2 dimension of spectrum **B** (Figure 27) is due to a larger number of increments used in the acquisition of the spectrum **B** as compared with spectrum **A**. The slightly shorter evolution time, applied for the evolution of long-range couplings in the gsHMBC experiment, probably prevents some weak couplings from becoming visible in the spectrum, *e.g.* the correlations between H18-C16 and H18-C19.

Table 4. The distinctive parameters of the recorded HMBC spectra of **11** (Figure 27).

	HMBC (**A**)	GsHMBC (**B**)
Equipment	Varian Unity 500	Varian INOVA 300
Acquisition time of a single fid*	0.14 s	0.26 s
Evolving delay for long range couplings	70 ms	63ms
Number of transients	110	32
Number of increments	384	512
^{1}H frequency	499.8 MHz	300.1 MHz
^{13}C frequency	125.7 MHz	75.5 MHz
Spectral width in F1	7000 Hz	4000 Hz
Spectral width in F2	30000 Hz	17000 Hz
Receiver gain	41 dB	60 dB
Total acquisition time	14.5 h	6.0 h
Collected data matrix	2 x 384 x 2K	1 x 512 x 2K
Zero-filled to data matrix	2 x 1K x 4K	1 x 1K x 4K

*fid = free induction decay

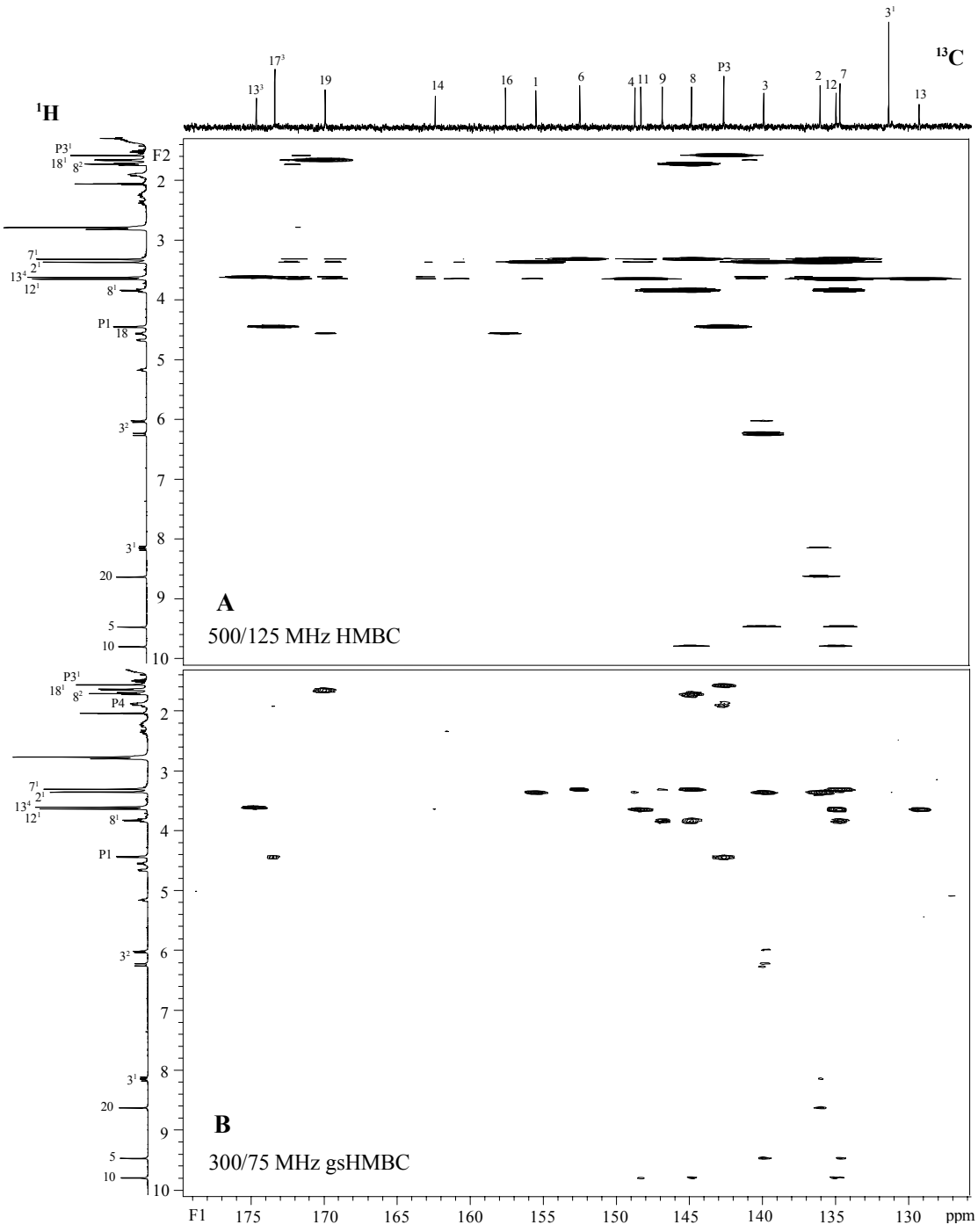

Figure 27. Expansions of the HMBC spectra of 13^2(*R*)-HO-Chl *a* (**11**) containing many quaternary carbons. The spectra were recorded at 300 K using a 16mM sample in acetone-d_6. Spectrum **A** is a conventional HMBC spectrum recorded on a Varian Unity 500 spectrometer.[93] Spectrum **B** is a gradient selected (gs) HMBC spectrum recorded on a Varian INOVA 300 spectrometer. In both spectra, the delay between scans was 1 s, the delay for suppression of the $^1J_{CH}$ couplings was 3.6 ms and the delay for evolving the long-range couplings was 65 ms. The spectra were processed using a $\pi/2$ shifted and a non-shifted sine-bell function in the F1and F2 domains, respectively, prior to Fourier transformations. The distinctive parameters in the spectra are listed in Table 4. The vertical scale is adjusted in the spectral plots to show clear correlations above the base-line noise level.

7.2 Solution conformations of ring *D*, the propionic side-chain and the front part of the phytyl group in the chlorophyll derivatives

The conformations of Chl compounds can be studied by measuring the $^3J_{H\text{-}H}$ values of the propionic acid residue and the front part of the phytyl chain, in which specific conformations dominate on the NMR time-scale. The solution conformation of ring *D* can be estimated by inserting the measured vicinal coupling values between the 17 and 18 protons into the simple Karplus equation (Eq. 6).

$$^3J_{H\text{-}H} = 10\cos^2\phi \qquad (6)$$

The application of the original Karplus equation (Eq. 2) or some more advanced related equations was not justified, since ring *D* is structurally very different from those compounds that are used in the parameterization of these equations. However, the ϕ-values obtained from equation 6 provide at least qualitative information, when the ϕ-values of different Chl derivatives are compared. Thus, the ϕ-values of 106° and 103° obtained for the methoxyChl *a* epimers **38a**,**b** are clearly smaller than the 117°, obtained as the ϕ-value of Chl *a* (publication I), thus indicating increased distortion of ring *D* in **38a**,**b**. Obviously, this is a consequence of increased steric crowding exerted by the C13^2 substituents in **38a**,**b**.

The propionic side-chain was analyzed as an ABCDX (X = H17) spin-system in publications I and II. The computer simulation with LAOCOON-3 type MDL analysis using PERCH software[159] afforded a relatively good correspondence between the simulated and measured spectra as depicted in Figure 4 of publication I and in Figure 4 of publication II. The simulation produced a solid assignment for the side-chain protons and $^3J_{H\text{-}H}$ coupling values, which could be used in the conformational analysis.

The rotamer populations of the propionic side-chain were calculated from the simple equations (publication II, Eqs. 2 and 3). The simulated $^3J_{H\text{-}H}$ couplings were inserted into these equations, in which the model-compound couplings (publication II, Table 3) were used as references for the staggered rotamers. Because the model compound couplings were obtained from similarly substituted cyclohexanes, the non-equivalence of the systems is a possible source of error. This was obvious in the case

of rotamers **1a**–**1c** (Figure 28), for which the model deviates significantly from the structures studied. The rotamers **2a**–**2c** are more distant from the ring effects, being more like the model compound, and hence populations should also be more accurate.

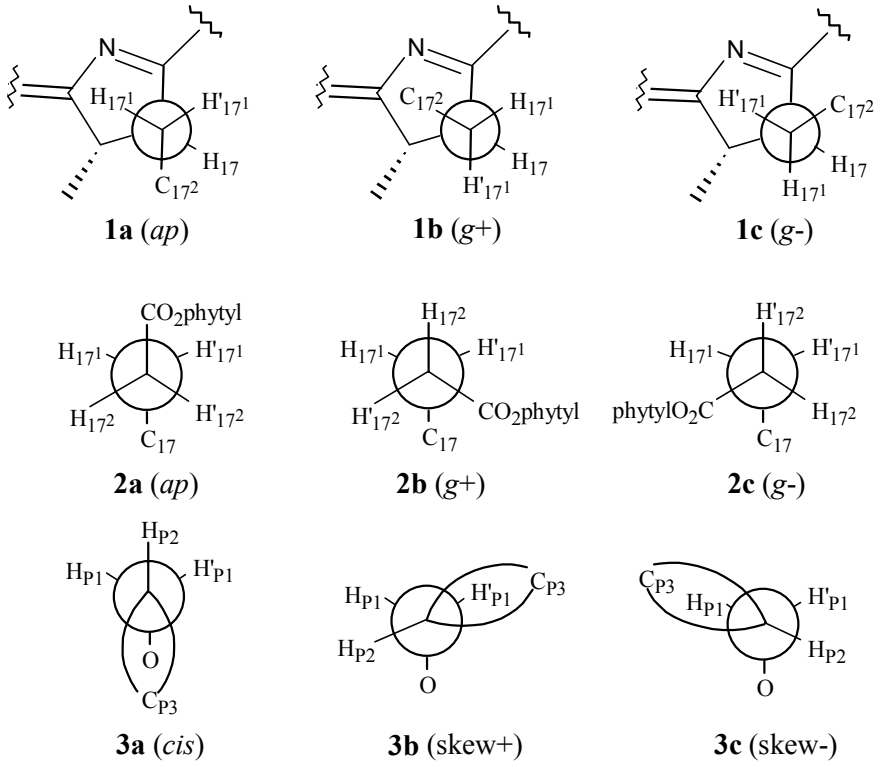

Figure 28. The staggered rotamers of the propionic ester side-chain (**1a**-**2c**) and the front part of the phytyl group (**3a**-**3c**). The *ap* and *g* denote antiperiplanar and *gauche*, respectively.

In publications I and II, the rotamer populations of the front part of the phytyl group (**3a**–**3c**, Figure 28) were analyzed using similar methods. The P1-CH_2 and P2-CH protons form an ABK spin-system, couplings of which could be measured for chlorins **38a**–**b**. However, in the case dyads **39a**,**b**, the line shapes were simulated due to the overlapping of the signals in the ^{1}H NMR spectra. For **38a**,**b**, the measured $^3J_{H\text{-}H}$ of 7.1 Hz for the fragment implies that only the skewed rotamers are populated (50/50) when the populations are calculated using the model-compound couplings (publication II, Table 2). In the simulation of the phytyl front part for **39a**,**b**, two distinct vicinal couplings were obtained for the spin systems. Consequently, the population for each rotamer could be calculated (publication II). However, in the absence of absolute assignment for the P1-CH_2 protons, skewed rotamers **3b** and **3c** could not be identified without molecular models (publication II and section 7.3).

Molecular modelling was performed for the structures **A**–**C** (Figure 29), which were analogical structures for **38a**,**b** and Chl *a*, respectively, in order to illuminate their 3D structures and to test the molecular modelling methods (Figure 29).[160] The starting structures in the modelling were built on the basis of structural parameters presented in publication I. However, one water molecule was added as a ligand for Mg(II) and the phytyl group was replaced by a methyl group to reduce the size of calculation in the modelling. Subsequently, the structures were energy-optimized without constraints using the PM3-UHF method.

In the models obtained (Figure 29),[160] the Mg atom is located *ca*. 0.2 Å above the plane of the nitrogens, whereas the oxygen of the water molecule is situated *ca*. 1.9 Å above the metal. In the analogical models of **38a**,**b**, the crowding in the lower chlorin periphery causes deformations in the macrocycle. Figure 29 shows that this behaviour becomes evident, when the deformed macrocycles of **A** and **B** are compared with the nearly planar macrocycle of **C**. However, there are some differences between the experimentally obtained parameters and the calculated ones, an example being the torsion angle ϕ of ring *D*. In the models, the ϕ-value deviates by 9 – 17° from the experimental values. The observed differences may arise from the reason that the experimental, the dynamic average solution structure differs from the modelled, *i.e.* the lowest-energy monomer structure in vacuum at 0 K. Similar structural parameters can be found between the structure **C** and the crystal structure of ethyl chlorophyllide *a* dihydrate.[7] In the crystal, the Mg is 0.39 Å out of the plane of the nitrogens, whereas the distance between the oxygen atom of the water molecule and the metal is 2.04 Å. In addition, the macrocycle is planar in the crystal, except for ring *D*, which is at a slightly distorted dihedral angle, the ϕ-value being 127.5°.

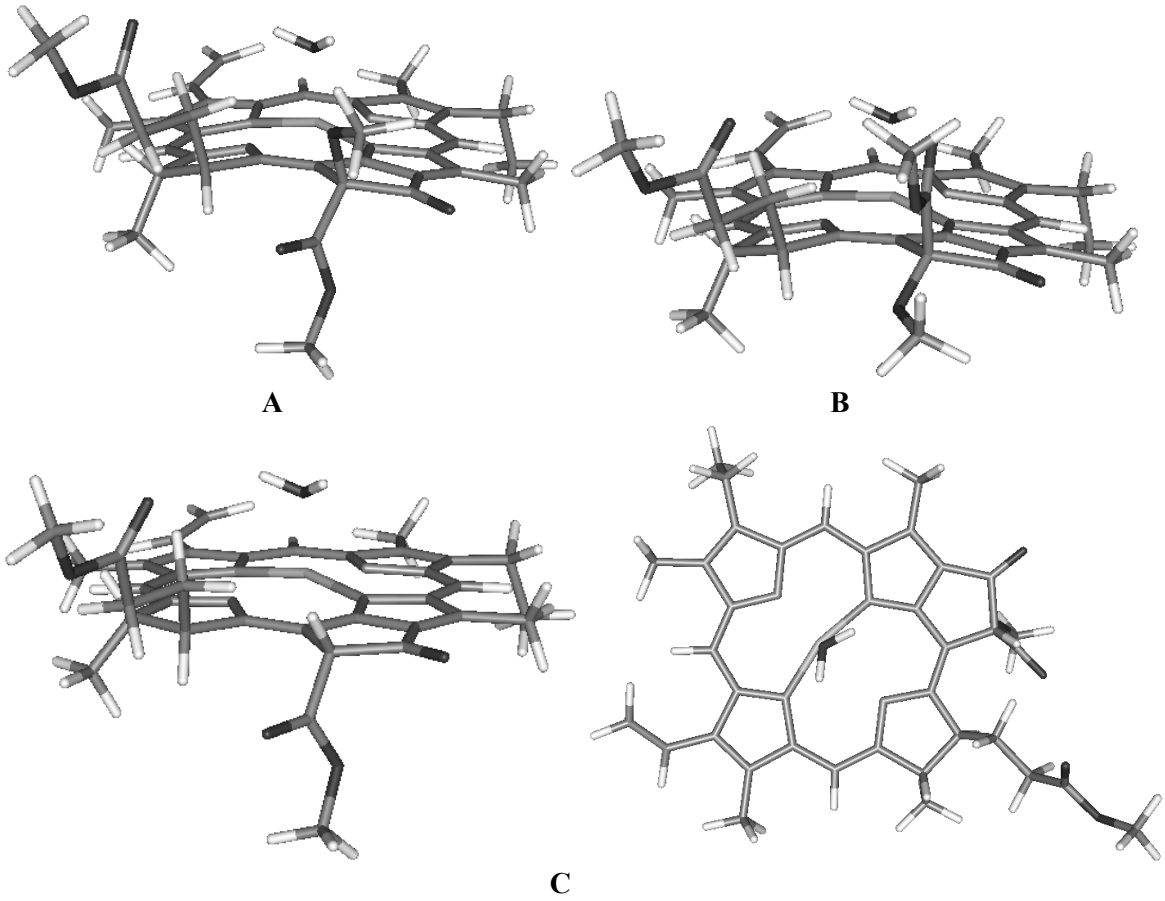

Figure 29. The PM3-UHF energy-optimized geometries for **38a** (**A**), **38b** (**B**) and methyl chlorophyllide **C** (on side and on top view). In the molecular models of **38a** (**A**) and **38b** (**B**) the phytyl was replaced by the methyl group. The torsion angles between the H17 and H18 protons are 115.8°, 120.3° and 126.4° for models **A**, **B** and **C**, respectively.

Of the molecular modelling methods tested, inluding the molecular mechanics MM+ and the semiempirical AM1 and PM3 methods, the latter produced facilely the energy-minima for the above chlorins.[160] In the MM+ energy-optimizations, the chlorin macrocycle geometries were approaching planar structures, but failed finally to converge. Evidently, the poor parameterization of the central Mg is a possible reason for the oscillation, since the corresponding Mg-free chlorins converged easily. The AM1 method could not be used because of the absence of Mg-parameterization for this method.

7.3 Elucidation of the conformations of the chlorin-based electron donor–acceptor dyads

7.3.1 Structures of the folded conformers of Zn(II)-pyropheophytin–anthraquinone dyads

In publication II, the folded geometries of dyads **39a**,**b** were deduced by NMR spectroscopy and molecular modelling. The structure analysis was based on the structural parameters obtained from NMR spectroscopy, which were then used in molecular modelling. For each dyad, the proton spectra showed one set of signals, the δ_H-values of which implied that conformational folding dominates on the NMR time-scale. The most convincing evidence for the mutual geometry of the chlorin and anthraquinone structural units was provided by ROESY experiments. The ROE correlations between the 18^1-CH_3 and Q1-CH protons proved that the anthraquinonyl ring is located below the chlorin macrocycle in both of the epimers. In addition, several ROE correlations were found in the spectra (publication II, Figure 2), indicating mutual geometries for the chlorin, linkage and quinone moieties. Additional information about the geometries was achieved from the aggregation maps based on the $\Delta\delta_H$-values (publication II, Figure 3). The sensitivity of the protons to ring-current, influenced the δ_H-values even at distances so great that ROE signals were too weak to be observed. Thus, the combined use of these methods afforded reliable results. The conformation of the spacer group in the dyads was deduced from the proton couplings according to the methods presented in section 7.2. Furthermore, conformational information could be extracted from the ^{13}C NMR spectra. The deshielding of the anthraquinonyl Q9 carbon ($\Delta\delta$ = 0.49 ppm) in **39a** implied that the coordination of the Q9-carbonyl oxygen to the central Zn(II) was a likely reason.

The energy-optimizations were performed by MM+ molecular mechanics. The structures were freely optimized, except that the torsion angle between H17 and H18 was constrained in the calculations. As a result, conformationally different lowest-energy structures were produced for dyads **39a**,**b** (Figure 30 and Figure 6 in publication II). Consequently, the stereochemical assignments for the P4 carbon could be deduced for dyads **39a**,**b**, being P4(*R*) and P4(*S*), respectively.

By inspecting the model **A** in Figure 30 as well as the side-view of this model (model ZnPQ1 in Figure 6 of publication II), it can be seen that in this structure the mutual geometry of the macrocycles is in good agreement with both the ROESY

spectrum and the aggregation map of **39a**. In contrast, the ROE correlation between 18^1-CH_3 and Q3-CH protons as well as the chemical shielding of the 2^1-CH_3 and 3^1-CH proton resonances in **39b** cannot be explained with model **B** (Figure 30). However, the rotamer populations (publication II, Table 2, ZnPQ2) of **39b** indicate that the linkage exhibits several conformations, probably arising from the various chlorin and quinone macrocycle orientations. Thus, the observed NMR results were produced by time-averaging on the NMR time-scale. Nevertheless, the ROE correlation between the 18^1-CH_3 and Q3-CH protons can be due to the spin diffusion as well.

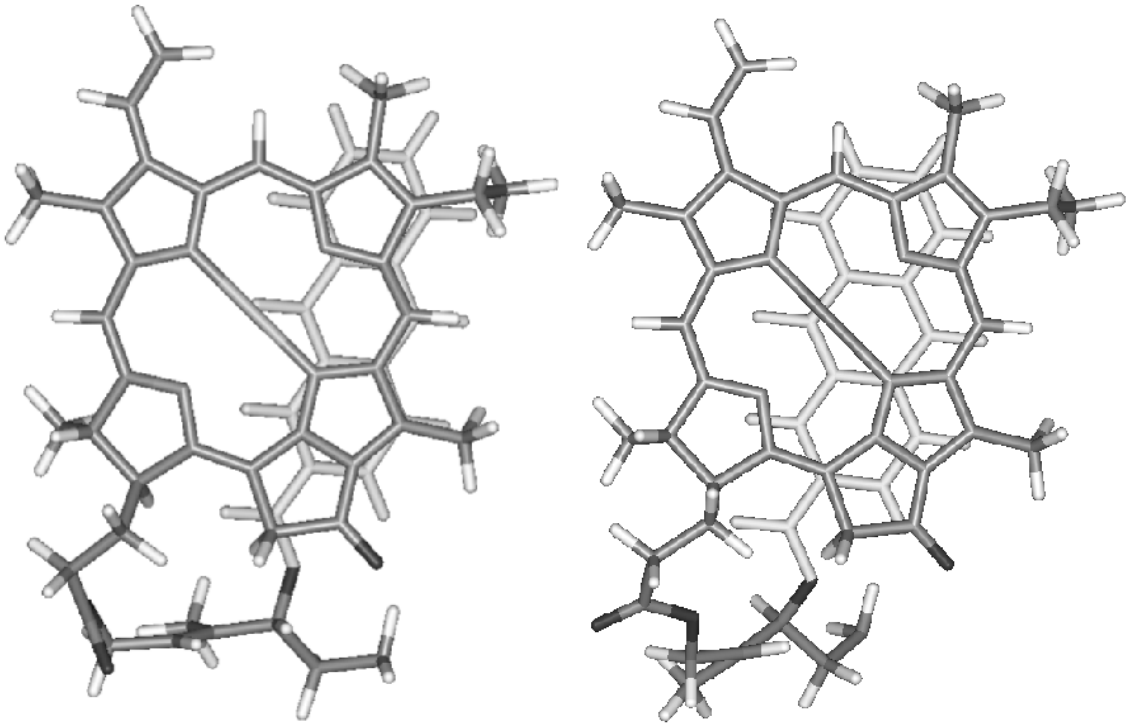

A **B** P4(*S*)

Figure 30. The top views of the folded conformers of the Zn(II)-pyropheophytin–anthraquinone **39a** (**A**) and **39b** (**B**) dyads obtained by NMR spectroscopy and MM+ molecular mechanics. The models **A** and **B** are P4(*R*) and P4(*S*) epimers, respectively.

The structural models of **39a**,**b** are in a good agreement with the results obtained from the photoinduced electron-transfer studies of these molecules.[135] In acetonitrile, the quenching of fluorescence was more effective for **39a** than for **39b**, indicating that the conformational folding is more effective in the former structure.[161] In addition, it was suggested that, in the case of **39b**, the folded conformer dominates, being in a fast exchange with the opened conformer(s).[135]

7.3.2 Conformational studies of the chlorin–C_{60} dyads

The chlorin–C_{60} dyad **40** was synthesized and its isomer pairs (**PF1** and **PF2**, publication III) were separated by column chromatography. Both **PF1** and **PF2** showed two sets of resonances in the ^{1}H NMR spectra (assigned to species *A* and *B*). The two most distinct δ_H-values were established for the chlorin 2^1, 5 and 7^1 proton signals (publication III, Fig. 2). The ring-currents of C_{60} caused mainly deshielding for the δ_H-values, with the exception that the 7^1 protons were shielded in **PF1***B* and **PF1***A*. The isomers **PF1***B* and **PF2***A* produced ROE correlations between the 2'-CH and 5-CH protons, whereas the **PF1***A* and **PF2***B* isomers showed ROE correlations between the 2'-CH and 2^1-CH protons. Inspection of the proton distances in the molecular models revealed that *A* and *B* were different C2' epimers, whereas **PF1** and **PF2** were different atropisomers in respect to the C3–C2' bond rotation. However, the definition of the absolute stereochemistry for the epimers could not be deduced on the basis of the NMR data.

While the samples of the atropisomers, **PF1** and **PF2**, were allowed to stand at room temperature, a slow conversion to a mixture of four isomeric species occurred. The conversion rates of separated **PF1** and **PF2** atropisomers could be investigated by integrating the signal intensities from the ^{1}H NMR spectra, acquired over certain time intervals at each temperature measured. The rate-constants at a specific temperature were obtained by one-exponential fitting of the points representing the relative integration values of the ^{1}H signals. The well-resolved 10-C*H* signal was selected for rate constant determination. Figure 31 illustrates an example of the curve fitting, in which the integration points were plotted as a function of time at 304 K. The rate-constant value of 4.23×10^{-5} s^{-1} was obtained from the fitted curve for the conversion of **PF1***A* to **PF2***A*. Rate-constants were obtained for each isomer at various temperatures. By taking natural logarithms of the various rate-constants and presenting them as a function of inverse temperature, the Arrhenius plots were obtained (Fig. 3 in publication III). In the Arrhenius plot, the gradient of the line is equal to $-E_A/R$, where E_A is the Arrhenius activation energy and R the universal gas constant. Thus, the activation energy obtained was 23.0 ±0.8 kcal/mol for all the **PF1***A*, **PF1***B* and **PF2***A* isomers, whereas for the **PF2***B* isomer, an E_A of 21.5 ±0.5 kcal/mol was calculated.

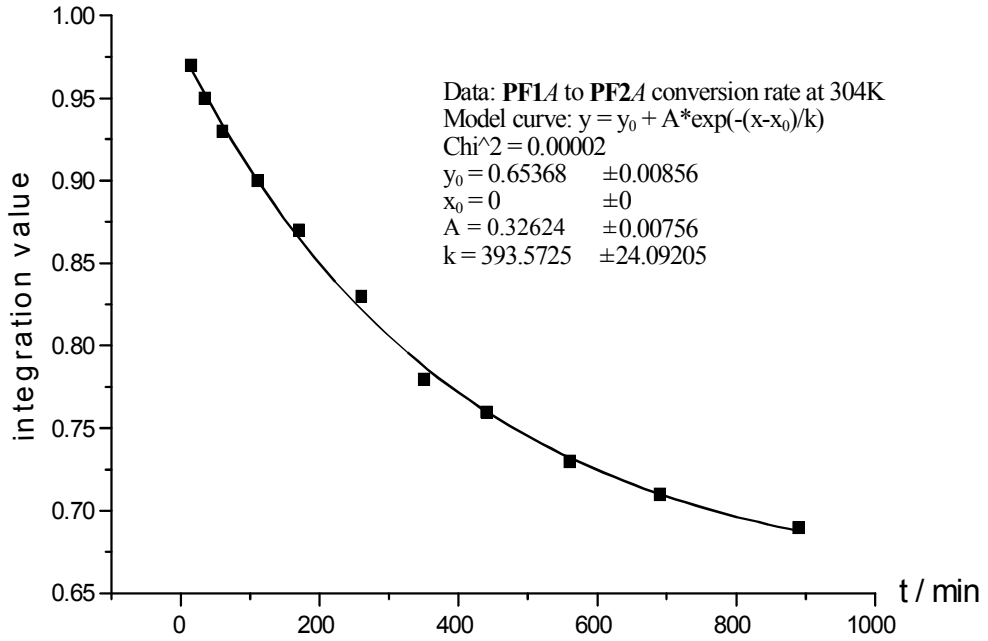

Figure 31. The one-exponential fitting curve and the parameters of the decaying 10-C*H* signal obtained for the conversion of **PF1***A* to **PF2***A* as a function of time at 304 K. The rate-constant obtained is 2.54×10^{-3} $min^{-1} = 4.23 \times 10^{-5}$ s^{-1}.

The MM+ molecular modelling was used to analyze the energy barriers between the atropisomers in order to find an explanation for the experimentally observed differences. The barrier for the rotation about the C3–C2' single bond was calculated by changing the relevant torsion angle ϕ (C4–C3–C2'–C3') in 5° steps and optimizing the rest of the structure. The stepwise optimization was begun from the calculated α and β conformer minima, and incremented in both rotational directions. Consequently, the minimum-energy values found for the 2' *R* and *S* epimers were plotted as a function of ϕ (Fig. 4 in publication III). The symmetric curves show that the lowest rotation barriers are on an equal energy level for the rotamers, *i.e.* 18 – 19 kcal/mol. The atropisomer minimum-energies were *ca*. 1.0 kcal/mol lower for the α-2'*R* and β-2'*S* isomers as compared with the β-2'*R* and α-2'*S* isomers. The AM1-RHF energy optimizations gave similar energy differences for the atropisomers, as can be seen from the ΔH_f-values in Figure 32.

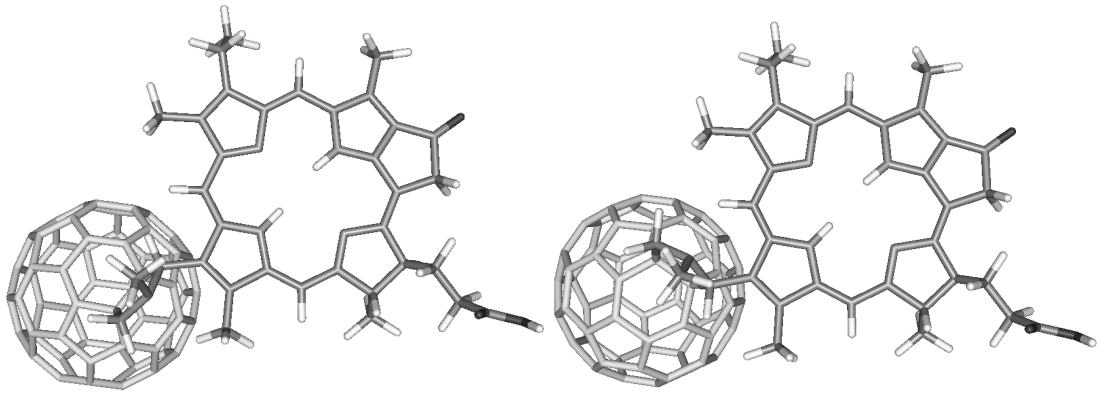

β-2'*S* isomer, ΔH_f = 1004.85 kcal/mol

β-2'*R* isomer, ΔH_f = 1005.85 kcal/mol

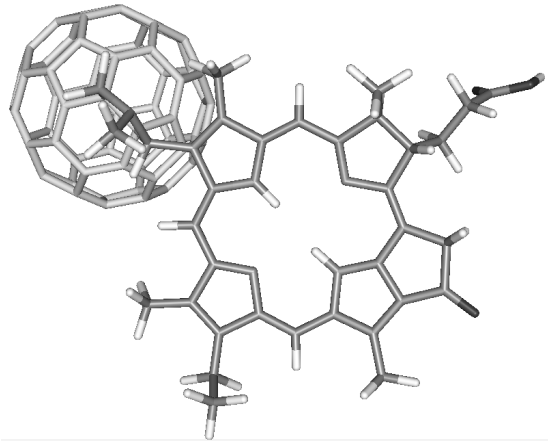

α-2'*R* isomer, ΔH_f = 1005.09 kcal/mol

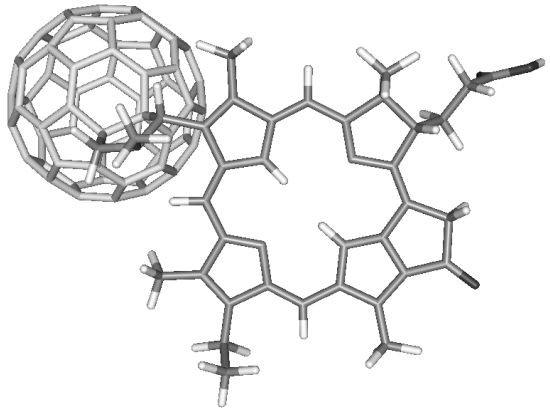

α-2'*S* isomer, ΔH_f = 1005.96 kcal/mol

Figure 32. The AM1-RHF energy-optimized chlorin–C_{60} isomers with respective ΔH_f energies. The chlorins are on the top in the views. In the α-structures, the C_{60} is on the same side of the chlorin-ring plane as the C17 propionic acid residue, whereas in the β-structures these substituents are on different sides of the plane.

In the molecular modelling, the long distance from the C2' to C17 or C2' to C18 chiral centres evidently obscures the diastereomeric differences between the isomers. This may, however, affect the solvation stabilization energies, especially when the solvation is estimated in respect to the coordination of the pyrrolidine nitrogen lone-pair. As shown in Fig. 2 of publication III, there is no space for a ligand in the α-2'*R* and β-2'*S* isomers. In contrast, in the β-2'*R* and α-2'*S* isomers, coordination is spatially possible. In addition, the C17 propionic acid residue is on the same side of the chlorin ring plane in the β-2'*R* isomer, allowing the formation of a solvent bridge via a chain of solvent molecules. By assuming that the stabilization affects the β-2'*R* isomer more than the α-2'*S* isomer, the latter is energetically the least favourable of the isomers. Consequently, the α-2'*S* isomer is the fastest converting isomer of **PF2***B*. This implies that **PF1** and **PF2** correspond to the α and β

atropisomers, respectively, whereas *A* and *B* are the C2' *R* and *S* epimers, respectively.

The photochemical studies in acetonitrile showed an efficient intramolecular electron transfer for all the isomers of **40**.[162] The photochemical behaviour of each atropisomer was the same within experimental error. This observation is in a good agreement with the symmetrical models obtained (Figure 32).

7.4 NH tautomerism in the natural chlorins

In publications IV and V, the NH tautomerism in natural chlorins **3**, and **41**–**45** was studied utilizing NMR spectroscopy and molecular modelling. The ^{1}H-^{15}N correlated 2D gsHSQC and gsHMBC experiments were used to deduce the assignments for the δ_H- and δ_N-values of the NH signals produced by the chlorins. DNMR was applied for the determination of coalescence temperatures (T_C) for each tautomeric exchange reaction. In terms of T_C and k_C, the free-energies of activation ($\Delta G^{\ddagger}$) could be calculated applying the Eyring equation (Eq. 7).

$$\Delta G_C^{\ddagger} = 4.58 T_C(10.32 + \log T_C/k_C) \text{ cal/mol} \qquad (7)$$

T_C = coalescence temperature
k_C = exchange rate-constant at T_C (*Eq. 8*).

$$k_C = \pi\Delta\nu/\sqrt{2} \qquad (8)$$

$\Delta\nu$ = separation of signals with no chemical exchange

The $\Delta G_2^{\ddagger}$-values, calculated for the total tautomeric exchange process (**A** $\rightleftharpoons$ **A'** in Figure 33) were 14.4, 13.6, 17.1, 16.8, 16.8 and > 18.0 kcal/mol for chlorins **3**, and **41**–**45**, respectively. Thus, the lowest energy barriers were found for chlorins **3** and **41**, which are both unsubstituted at C15, whereas for chlorin **45**, which possesses the isocyclic ring *E* in the macrocycle, no NH exchange could be experimentally observed.

At lower temperatures, an intermediate N_{22}-H, N_{24}-H *trans*-tautomer (**B** and **B'** in Figure 33) was found for chlorins **42** and **43**. The exchange barriers ($\Delta G_1^{\ddagger}$) for these tautomers were 10.8 and 10.6 kcal/mol, respectively. Intermediate NH tautomers for chlorins have not been reported before.

The energy differences of the NH tautomers were estimated by the semiempirical molecular modelling calculations. In publication IV, the NH tautomers of bonellin dimethylester **3** were energy-optimized using the AM1 and PM3 methods with RHF or UHF spin-pairing in the calculations. The PM3-UHF optimization produced probably the most realistic structures and energies. The chlorin-ring geometries were planar for all the tautomers of **3** and the energy differences between the tautomers were similar to those that had been obtained in *ab initio* calculations at the MP2 level.[87] Hence, the PM3-UHF method was utilized in energy-optimizations of the tautomers **41**–**45** in publication V.

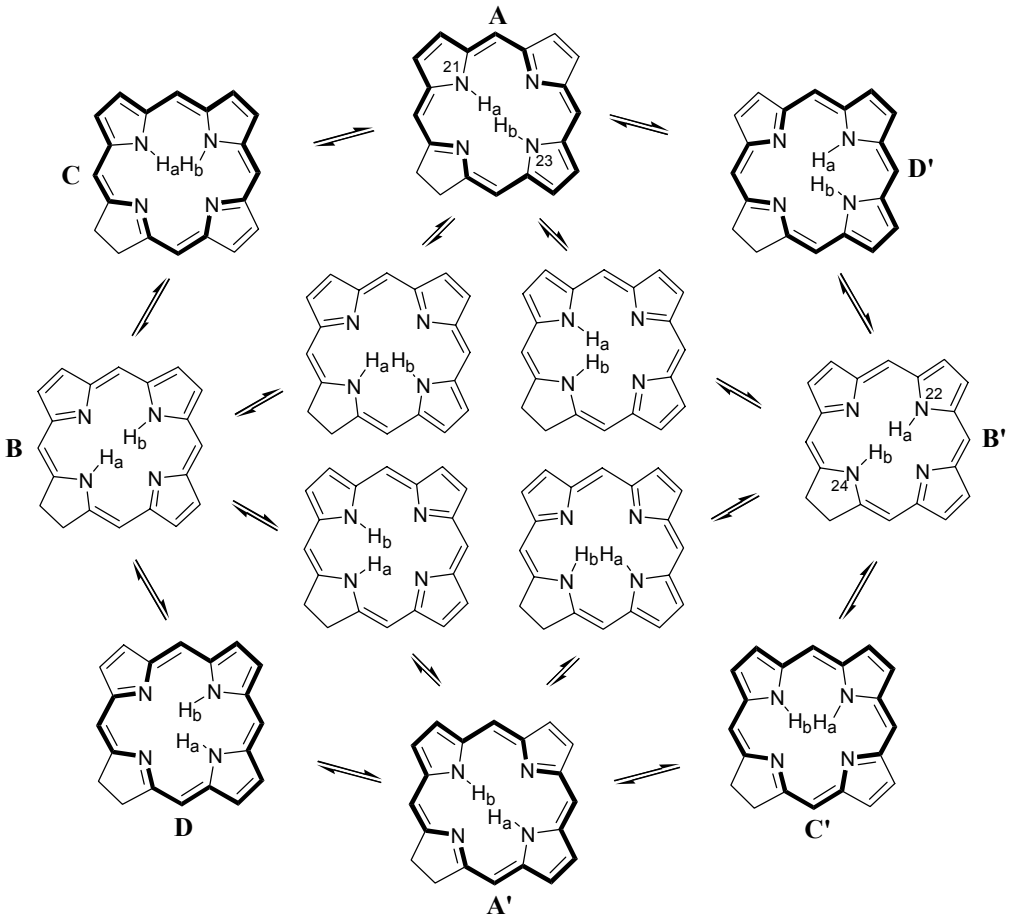

Figure 33. The possible NH-tautomeric pathways for the chlorin NH exchange. The aromatic 18-atom 18 π-electron delocalization pathways are drawn with bold lines in the structures, in which the protonation of N24 does not interrupt the fully-aromatic delocalization pathway.

Inspection of the relative tautomer energies obtained from the PM3-UHF calculations (Table 3 in publication V) shows that the **C** and **D** *cis*-tautomers exist on the energy level closest to the most stable main tautomer **A**. The energy of *trans*-tautomer **B** is regularly on a higher level than that of the *cis*-tautomers **C** and **D**, but is

still clearly at a lower energy level than the energies calculated for *cis*-tautomers **E** and **F**. Obviously, the protonation of N24 significantly raises the tautomerization energy. Thus, the protonation of N24 interrupts the fully-aromatic 18 π-electron delocalization pathway in the chlorin macrocycle. The PM3-UHF calculated spin-density maps of chlorin tautomers (Figure 4 in publication IV and Figure 6 in publication V) illustrate the electron delocalization pathways in the chlorin macrocycle. The spin-density maps demonstrate that the protonation of N24 induces a weak or unobservable spin-polarisation of N24 in tautomers **B**, **E** and **F**. The spin-density maps of the **A**, **C** and **D** chlorin tautomers show similar delocalization pathways, as depicted with bold lines in Figure 33. The PM3-UHF energies calculated for the chlorin **3**, and **41**-**45** tautomers also imply that the chlorin substitution affects tautomeric energies. The substituents in chlorins **42**-**45** cause notable geometry changes in the chlorin macrocycles as compared with chlorins **3** and **41** (Table 5 in publication V). This is an obvious reason for different tautomeric energies observed for the chlorins.

Based on these studies, it could be concluded that the chlorin-ring substituent effects are connected to the NH tautomeric exchange. The NH tautomerization barriers are higher for chlorins, whose macrocycles exhibit steric strain, arising from the substituent effects. Obviously, the total NH tautomeric exchange (**A** $\rightleftharpoons$ **A'** in Figure 33) occurs by a stepwise mechanism via the aromatic *cis*-tautomers (**C** and **D**) and the less aromatic *trans*-tautomer (**B**), and thus, the rate-limiting energy barrier is between these *cis*- and *trans*-tautomers. We suggest that the single steps in the pathway proceed by a mechanism, in which ten electrons are reorganized in a six-membered cycle in the TS structures (Scheme 2 in publication V). The skeletal motions of the chlorin macrocycle are involved in the formation of these TS structures. This is in a good agreement with the lower tautomerization energies observed for the flexible chlorins **3** and **41**.

8 Conclusions

In the present investigation, modern NMR techniques were applied to Chl derivatives to obtain structural data of their solution conformations. The conformations of the rotational fragments of the Chl derivatives, *i.e*. the propionic side-chain and the front part of the phytyl group, could be evaluated based on the $^{3}J_{\text{H-H}}$-values. In addition, the subring *D* conformation of the Chl derivatives could be estimated from the inherent $^{3}J_{17\text{-}18}$ proton coupling in ring *D*. The ^{1}H assignments for the Chl derivatives could be facilely obtained by using the ROESY technique. In addition, the ROE correlations gave information about the spatial proximity of the proton bearing groups. This was successfully utilized in the determination of the absolute stereochemistry at the C13^{2} of the methanolic allomerization products **38a**,**b**, and in the definition of the mutual geometry of the chlorin and anthraquinone moieties in the folded conformers of dyads **39a**,**b**. The energy barriers connected to the conformational isomerism of fullerene–C_{60} dyads **40** and the NH tautomeric exchange of bonellin dimethyl ester **3** and Chl derivatives **41**–**45** were obtained by DNMR.

In the case of the studied chlorins, however, all the structural parameters could not be deduced solely on the basis of the NMR data. Therefore, computer-aided molecular modelling was used to produce 3D structures of the molecules studied. In molecular modelling, the NMR deduced structure parameters were used as starting parameters in the geometry-optimizations. Thus, the structures resulting from the optimization are related to the solution structures. In addition, structural features, such as the conformation of the chlorin macrocycle, could be obtained.

In essence, the NMR spectroscopy and computer-aided molecular modelling gave reliable solution structures for the Chl derivatives studied. Nevertheless, additional *ab initio* calculations involving the NH tautomer TS structures would be highly interesting. However, the simple MM+ molecular mechanics calculations for chlorin–anthraquinone dyads **39a**,**b** and chlorin–C_{60} dyad isomers **40** gave results that explained the experimentally observed behaviour, *i.e.* the conformational folding of **39a**,**b** and the rotational isomerism of **40**. In the case of chlorins **38a**,**b**, **3**, and **41**–**45**, the semiempirical PM3-UHF calculations produced results which were in a good correlation with the experimental data obtained from the NMR spectroscopy.

The investigations of the nature and existence of the NH tautomerism in natural chlorins gave novel information about the fundamental chemical properties of the chlorins. According to the molecular modelling, the NH tautomers in which the nitrogen of the reduced ring (N24) is protonated are clearly energetically disfavoured, because the aromatic delocalization pathway is interrupted in these tautomers. In addition, an intermediate *trans*-tautomer was experimentally detected for the first time by NMR spectroscopy at low temperatures for chlorins **42** and **43**. Consequently, the total NH exchange of chlorins is suggested to proceed by a stepwise mechanism via the aromatic *cis*-tautomers and the less aromatic *trans*-tautomer. Finally, it seems evident that the energy barriers of the NH tautomerization are connected to substituent effects. Thus, the chlorin macrocycles that are distorted or strained by the substituents produce NH tautomeric energy barriers of higher levels.

References

1. H. Scheer, Ed. *Chlorophylls*, CRC Press: Boca Raton, FL, 1991.
2. H. Brockmann Jr., *The Porphyrins*, D. Dolphin, Ed., Academic Press, New York, 1978, p. 288.
3. F.-P. Montforts, B. Gerlach and F. Höper, *Chem. Rev.* **1994**, *94*, 327.
4. P. H. Hynninen, *Chlorophylls*, H. Scheer, Ed., CRC Press: Boca Raton, FL, 1991.
5. P. H. Hynninen, *Kemia-Kemi* **1990**, *17*, 241.
6. I. Fleming, *Nature* (London) **1967**, *216*, 151.
7. H.-C. Chow, R. Serlin and C. E. Strouse, *J. Am. Chem. Soc.* **1975,** *97*, 7230.
8. W.-D. Schubert, O. Klukas, N. Krauss, W. Saenger, P. Fromme and H. T. Witt, *J. Mol. Biol.* **1997**, *272*, 741.
9. K.-H. Rhee, E. P. Morris, D. Zheleva, B. Hankamer, W. Kühlbrandt and J. Barber, *Nature* **1997**, *389*, 522.
10. W. W. Parson, *Chlorophylls*, H. Scheer, Ed., CRC Press: Boca Raton, FL, 1991, p. 1153.
11. U. Ermler, G. Fritzsch, S. K. Buchanan and H. Michel, *Structure* **1994**, *2*, 925.
12. J. Deisenhofer, O. Epp, R. Miki and H. Michel, *Nature* **1985**, *318*, 618.
13. M. Mac, N. R. Bowlby, G. T. Babcock and J. McCracken, *J. Am. Chem. Soc.* **1998**, *120*, 13215.
14. M. R. A. Blomberg, P. E. M. Siegbahn and G. T. Babcock, *J. Am. Chem. Soc.* **1998**, *120*, 8812.
15. D. Gust and T. A. Moore, *Top. Curr. Chem.* **1991**, *159*, 103.
16. H. Kurreck and M. Huber, *Angew. Chem. Int. Ed. Eng.* **1995**, *34*, 849.
17. W. W. Kalisch, M. O. Senge and K. Ruhlandt-Senge, *Photochem. Photobiol.* **1998**, *67*, 312 and references therein.
18. M. R. Wasielewski, *Chem. Rev.* **1992**, *92*, 435.
19. E. D. Sternberg, D. Dolphin and C. Brückner, *Tetrahedron* **1998**, *54*, 4151.
20. M. Lahav, T. Gabriel, A. N. Shipway and I. Willner, *J. Am. Chem. Soc.* **1999**, *121*, 258 and references therein.
21. F.-P. Montforts and U. M. Schwartz, *Liebigs Ann. Chem.* **1991**, 709.
22. H. Friebolin, *Basic One- and Two-Dimensional NMR spectroscopy*, VCH, Weinheim, 1991.
23. H. Günther, *NMR Spectroscopy: Basic Principles, Concepts, and Applications in Chemistry*, 2nd ed, Wiley, Chichester, 1995.
24. G. E. Martin and A. S. Zektzer, *Two-Dimensional NMR Methods for Establishing Molecular Connectivity*, VCH, New York, 1988.
25. C. Griesinger, H. Schwalbe, J. Schleucher and M. Sattler, in *Proton-Detected Heteronuclear and Multidimensional NMR in Two Dimensional NMR Spectroscopy, Applications for Chemists and Biochemists,* W. R. Croasmun and R. M. Carlson, Eds., VCH, New York, 1994, p. 357.
26. L. Müller, A. Kumar and R. R. Ernst, *J. Chem. Phys.* **1975**, *63*, 5490.
27. L. Braunschweiler and R. R. Ernst*, J. Magn. Reson.* **1983**, *53*, 521.
28. S. Macura, Y. Huang, D. Suter and R. R. Ernst, *J. Magn. Reson.* **1981**, *43*, 259.
29. A. A. Bothner-By, R. L. Stephens, J. Lee, C. D. Warren and R. W. Jeanloz, *J. Am. Chem. Soc.* **1984**, *106*, 811.
30. A. Bax, R. H. Griffey and B. L. Hawkings, *J. Am. Chem. Soc.* **1983**, *105*, 7188.
31. G. Bodenhausen and D. J. Ruben, *Chem. Phys. Lett.* **1980**, *69*, 185.
32. M. F. Summers, L. G. Marzilli and A. Bax, *J. Am. Chem. Soc.* **1987**, *109*, 566.
33. T. Parella, *Magn. Reson. Chem.* **1998**, *36*, 467.

34. T. Parella, J. Belloc, F. Sánchez-Ferrendo and A. Virgilli, *Magn. Reson. Chem.* **1998**, *36*, 715.
35. G. E. Martin and C. E. Hadden, *J. Nat. prod.* **2000**, *63*, 543.
36. G. Zhu, X. Kong and K. Sze, *J. Magn. Reson.* **1998**, *135*, 232.
37. K Furihata and H. Seto, *Tetrahedron Lett.* **1998**, *39*, 7337.
38. R. Wagner and S. Berger, *Magn. Reson. Chem.* **1998**, *36*, S44.
39. G. E. Martin, C. E. Hadden, R. C. Crouch and V. V. Krishnamurthy, *Magn. Reson. Chem.* **1999**, *37*, 517.
40. C. E. Hadden, G. E. Martin and V. V. Krishnamurthy, *J. Magn. Reson.* **1999**, *140*, 274.
41. C. E. Hadden, G. E. Martin and V. V. Krishnamurthy, *Magn. Reson. Chem.* **2000**, *38*, 143.
42. M. Karplus, *J. Chem. Phys.* **1959**, *30*, 11.
43. C. A. G. Haasnoot, F. A. A. M. de Leeuw and C. Altona, *Tetrahedron* **1980**, *36*, 2783.
44. E. Ösawa, T. Ouchi, N. Saito, M. Yamato, O. S. Lee and M.-K. Seo, *Magn. Reson. Chem.* **1992**, *30*, 1104.
45. C. Altona, R. Francke, R. de Haan, J. H. Ippel, G. J. Daalmans, A. J. A. Westra Hoekzema and J. van Wijk, *Magn. Reson. Chem.* **1994**, *32*, 670.
46. N. Matsumori, D. Kaneno, M. Murata, H. Nakamura and K. Tachibana, *J. Org. Chem.* **1999**, *64*, 866.
47. D. Neuhaus and M. P. Williamson, *The Nuclear Overhauser Effect in Structural and Conformational Analysis,* VCH, New York, 1991.
48. A. Bax and D. G. Davis, *J. Magn. Reson.* **1985**, *63*, 207.
49. T.-L. Hwang and A. J. Shaka, *J. Magn. Reson., B* **1993**, *102*, 155.
50. J. P. Boven and N. L. Allinger, *Reviews in Computational Chemistry II*, K. B. Lipkowitz and D. B. Boyle, Ed., VCH, 1991, 81.
51. N. L. Alligner, *J. Am. Chem. Soc.* **1977**, *99*, 8127.
52. S. L. Mayo, B. D. Olafson and W. A. Goddard III, *J. Phys. Chem.* **1990**, *94*, 8897.
53. A. K. Rappé, C. J. Casewit, K. S. Colwell, W. A. Goddard III and W. M. Skiff, *J. Am. Chem. Soc.* **1992**, *114*, 10024.
54. HYPERCHEM, Hypercube, http://www.hyper.com
55. P. W. Atkins, *Molecular Quantum Chemistry*, Oxford University Press, Oxford, 1993.
56. M. C. Zerner, *Reviews in Computational Chemistry II*, K. B. Lipkowit7z and D. B. Boyle, Ed., VCH, 1991, 313.
57. W. Kohn, A. D. Becke and R. G. Parr, *J. Chem. Phys.* **1996**, *100*, 12974.
58. J. Weber, H. Huber and H. P. Weber, *Chimia* **1993**, *47*, 57.
59. T. Helgaker, M. Jaszunski and K. Ruud, *Chem. Rev.* **1999**, *99*, 293.
60. R. Zanasi, P. Lazzaretti, M. Malagoli and F. Piccinini, *J. Chem. Phys.* **1995**, *102*, 7150.
61. A. Ligabue, U. Pincelli, P. Lazzeretti and R. Zanasi, *J. Am. Chem. Soc.* **1999**, *121*, 5513.
62. P. von Ragué Schleyer, C. Maerker, A. Dransfeld, H. Jiao and N. J. R. van Eikema Hommes, *J. Am. Chem. Soc.* **1996**, *107*, 6317.
63. J. Jusélius and D. Sundholm, *Phys. Chem. Chem. Phys.* **1999**, *1*, 3429.
64. J. P. P. Stewart, *Reviews in Computational Chemistry*, K. B. Lipkowitz and D. B. Boyle, Ed., VCH, 1990, 45.
65. M. J. S. Dewar and W. Thiel, *J. Am. Chem. Soc.* **1977**, *99*, 4899.

66. M. J. S. Dewar, E. G. Zoebisch, E. F. Healy and J. J. P. Stewart, *J. Am. Chem. Soc.* **1985**, *107*, 3902.
67. J. J. P. Stewart, *J. Comp. Chem.* **1996**, *118*, 3902.
68. N. T. Anh, G. Frison, A. Solladié-Cavallo and P. Metzner, *Tetrahedron* **1998**, *54*, 12841.
69. International Union of Pure and Applied Chemistry (IUPAC) and International Union Of Biochemistry (IUB), *Nomenclature of Tetrapyrroles*, G. B. Moss, Ed., *Pure & Appl. Chem.* **1987**, *59*, p. 779.
70. P. H. Hynninen, *J. Chem. Soc. Perkin trans. 2* **1991**, 669.
71. C. B. Storm and Y. Teklu, *J. Am. Chem. Soc.* **1972**, *94*, 1745.
72. P. H. Hynninen and S. Lötjönen, *Biochim. Biophys. Acta* **1983**, *1183*, 381.
73. P. H. Hynninen, M. R Wasielewski and J. J. Katz, *Acta Chem. Scand.* B **1979**, *33*, 637.
74. F. C. Pennington, H. H. Strain, W. A. Svec and J. J. Katz, *J. Am. Chem. Soc.* **1964**, *86*, 1418.
75. C. A. Hunter and J. K. M. Sanders, *J. Am. Chem. Soc.* **1990**, *112*, 5525.
76. L. J. Boucher and J. J. Katz, *J. Am. Chem. Soc.* **1967**, *89*, 4703.
77. J. March, *Advanced Organic Chemistry*, 4nd ed, Wiley, New York, 1992, p. 40.
78. P. S. Clezy, C. J. R. Fookes and S. Sternhell, *Aust. J. Chem.* **1978**, *31*, 639.
79. P. George, *Chem. Rev.* **1975**, *75*, 85.
80. M. J. Crossley, M. M. Harding and S. Sternhell, *J. Org. Chem.* **1988**, *53*, 1132.
81. M. J. Crossley, M. M. Harding and S. Sternhell, *J. Am. Chem. Soc.* **1992**, *114*, 3266.
82. C. H. Reynolds, *J. Am. Chem. Soc.* **1985**, *53*, 6061.
83. S. Lötjönen and P. H. Hynninen, *Org. Magn. Reson.* **1984**, *22*, 510.
84. R. J. Abraham, S. C. M. Fell and K. M. Smith, *Org. Magn. Reson.* **1977**, *9*, 367.
85. R. J. Abraham, K. M. Smith, D. A. Goff and J.-J. Lai, *J. Am. Chem. Soc.* **1982**, *104*, 4332.
86. M. K. Cyranski, T. M. Krygowski, M. Wisiorowski, N. J. R. van Eikema Hommes and P. von Ragué Schleyer, *Angew. Chem. Int. Ed.* **1998**, *37*, 177.
87. D. Sundholm, H. Konschin and M. Häser, *Chem. Eur. J.* **1999**, *5*, 267.
88. J. Jusélius and D. Sundholm, *Phys. Chem. Chem. Phys.* **2000**, *2*, 2145.
89. A. A. Bothner-By, C. Gayathri, P. C. M. van Zijl, C. MacLean, J.-J. Lai and K. M. Smith, *Magn. Reson. Chem.* **1985**, *23*, 935.
90. C. Gayathri, A. A. Bothner-By, P. C. M. van Zijl and C. MacLean, *Chem. Phys. Lett.* **1982**, *87*, 192.
91. R. J. Abraham and A. E. Rowan, *Chlorophylls*, H. Scheer, Ed., CRC Press: Boca Raton, FL, 1991, p. 797.
92. J. J. Katz and C. E. Brown, *Bull. Magn. Reson.* **1983**, 5, 3.
93. K. Hyvärinen, J. Helaja, P. Kuronen, I. Kilpeläinen and P. H. Hynninen, *Magn. Reson. Chem.* **1995**, *33*, 646.
94. G. Giacometti, D. Carbonera, A. Venzo and S. Mammi, *Gazz. Chim. Ital.* **1991**, *121*, 457.
95. S. Lötjönen and P. H. Hynninen, *Org. Magn. Reson.* **1981**, *16*, 304.
96. S. Lötjönen and P. H. Hynninen, *Org. Magn. Reson.* **1983**, *21*, 757.
97. N. Risch and H. Brockmann, *Tetrahedron Lett.* **1983**, *24*, 173.
98. I. Kilpeläinen, S. Kaltia, P. Kuronen, K. Hyvärinen and P. H. Hynninen, *Magn. Reson. Chem.* **1994**, *32*, 29.
99. J. C. Facelli, *J. Phys. Chem. B* **1998**, *102*, 2111.
100. T. Okazaki and M. Kajivara, *Chem. Pharm. Bull.* **1995**, *43*, 1311.

101. S. G. Boxer, G. L. Closs and J. J. Katz, *J. Am. Chem. Soc.* **1974**, *96*, 9363.
102. S. Gomi, T. Nishizuka, O. Ushiroda, N. Uchida, H. Takahashi and S. Sumi, *Heterocycles* **1998**, *48*, 2231.
103. L. Limantara, Y. Kurimoto, K. Furukawa, T. Shimamura, H. Utsumi, I. Katheder, H. Scheer and Y. Koyama, *Chem. Phys. Lett.* **1995**, *236*, 71.
104. Z.-Y. Wang, M. Umetsu, M. Kobayashi and T. Nozawa, *J. Am. Chem. Soc.* **1999**, *121*, 9363.
105. W. W. Paudler, *Nuclear Magnetic Resonance, General Concepts and Applications*, Wiley, New York, 1987, p. 33.
106. K. M. Smith, D. A. Goff and R. J. Abraham, *Tetrahedron Lett.* **1981**, *22*, 4873.
107. K. M. Smith, D. A. Goff and R. J. Abraham, *Org. Magn. Reson.* **1984**, *22*, 779.
108. K. M. Smith, D. A. Goff and R. J. Abraham, *J. Org. Chem.* **1987**, *52*, 176.
109. S. Lötjönen, T. J. Michalski, J. R. Norris and P. H. Hynninen, *Magn. Reson. Chem.* **1987**, *25*, 670.
110. P. H. Hynninen and S. Lötjönen, *Magn. Reson. Chem.* **1985**, *23*, 605.
111. F. K. Fong and V. J. Koester, *J. Am. Chem. Soc.* **1975**, *97*, 6888.
112. F. K. Fong and V. J. Koester, *J. Am. Chem. Soc.* **1975**, *97*, 6890.
113. R. J. Abraham and K. M. Smith, *Tetrahedron lett.* **1983**, *24*, 2681.
114. R. J. Abraham and K. M. Smith, *J. Am. Chem. Soc.* **1983**, *105*, 5734.
115. R. P. H. Kooyman and T. J. Schaafsma, *J. Am. Chem. Soc.* **1984**, *106*, 551.
116. R. J. Abraham, D. A. Goff and K. M. Smith, *J. Chem. Soc. Perkin trans. I* **1988**, 2443.
117. R. J. Abraham, A. E. Rowan, D. A. Goff, K. E. Mansfield and K. M. Smith, *J. Chem. Soc. Perkin trans. 2* **1989**, 1633.
118. G. L. Closs, J. J. Katz, F. C. Pennington, M. R. Thomas and H. H. Strain, *J. Am. Chem. Soc.* **1963**, *85*, 3809.
119. P. H. Hynninen and S. Lötjönen, *Biochim. Biophys. Acta* **1984**, *22*, 510.
120. Z.-Y. Wang, M. Umetsu, M. Kobayashi and T. Nozawa, *J. Phys. Chem. B* **1999**, *103*, 3742.
121. R. R. Ernst, G. Bodenhausen and A. Wokaun, *Principles of Nuclear Magnetic Resonance in One and Two Dimensions*, Clarendon Press, Oxford, 1990, Chapter 9.
122. S. G. Boxer and G. L. Closs, *J. Am. Chem. Soc.* **1976**, *98*, 5406.
123. S. G. Boxer and R. R. Bucks, *J. Am. Chem. Soc.* **1979**, *101*, 1883.
124. M. R. Wasielewski, W. A. Svec and B. T. Cope, *J. Am. Chem. Soc.* **1978**, *100*, 1961.
125. A. Osuka, Y. Wada and S. Shinoda, *Tetrahedron* **1996**, *52*, 4311.
126. G. Zheng, J. L. Alderfer, M. O. Senge, M. Shibata, T. J. Dougherty and R. K. Pandey, *J. Org. Chem.* **1998**, *63*, 6434.
127. A. N. Kozyrev, G. Zheng, M. Shibata, J .L. Alderfer, T. J. Dougherty and R. K. Pandey, *Org. Lett.* **1999**, *1*,1193.
128. H. Imahori and Y. Sakata, *Eur. J. Org. Chem.* **1999**, 2445.
129. J. von Gersdorff, B. Kirste and H. Kurreck, *Liebigs Ann. Chem.* **1993**, 897.
130. J. Fajer, K. M. Barkigia, D. Melamed, R. M. Sweet, H. Kurreck, J. von Gersdorff, M. Plato, H.-C. Rohland, G. Elger and K. Möbius, *J. Phys. Chem.* **1996**, *100*, 14236.
131. H. Dieks, M. O. Senge, B. Kirste and H. Kurreck, *J. Org. Chem.* **1997**, *62*, 8666.
132. G. M. Sanders, M. van Dijk, A. van Veldhuizen and H. C. van der Plas, *J. Chem. Soc, Chem. Commun.* **1986**, 1311.

133. A. Y. Tauber, R. K. Kostiainen and P .H. Hynninen, *Tetrahedron* **1994**, *50*, 4723.
134. A. Tauber, *Ph.D. Thesis university of Helsinki*, 1996.
135. N. V. Tkachenko, A. Y. Tauber, H. Lemmetyinen and P. H. Hynninen, *Thin Solid Films* **1996**, *280*, 244.
136. M. Prato, T. Suzuki and F. Wudl, *J. Am. Chem. Soc.* **1993**, *115*, 7877.
137. P. D. W. Boyd, M. C. Hodgson, C. E. F. Rickard, A. G. Oliver, L. Chaker, P. J. Brothers, R. D. Bolskar, F. S. Tham and C. A. Reed, *J. Am. Chem. Soc.* **1999**, *121*, 10487.
138. M. J. Hwang, T. P. Stockfisch and A. T. Hagler, *J. Am. Chem. Soc.* **1994**, *116*, 2415.
139. P. A. Liddell, J. P. Sumida, A. N. Macpherson, L. Noss, G. R. Seely, K. N. Clark, A. L. Moore, T. A. Moore and D. Gust, *Photochem. Photobiol.* **1994**, *60*, 537.
140. T. Drovetskaya, C. A. Reed and P. D. W. Boyd, *Tetrahedron Lett.* **1995**, *36*, 7971.
141. D. Kuciauskas, S. Lin, G. R. Seely, A. L. Moore, T. A. Moore, D. Gust, T. Drovetskaya, C. A. Reed and P. D. W. Boyd, *J. Phys. Chem.* **1996**, *100*, 15931.
142. Y. Sun, T. Drovetskaya, R. D. Bolskar, R. Bau, P. D. W. Boyd and C. A. Reed, *J. Org. Chem.* **1997**, *62*, 3642.
143. H. Imahori, K. Hagiwara, M. Aoki, T. Akiyama, S. Taniguchi, T. Okada, M. Shirakawa and Y. Sakata, *J. Am. Chem. Soc.* **1996**, *118*, 11771.
144. R. Bonnett, B. D. Djelal, G. E. Hawkes, P. Haycock and F. Pond, *J. Chem. Soc. Perkin trans. 2* **1994**, 1839.
145. T. Nozava, M. Nishimura, M. Hatano and M. Sato, *Bull. Chem. Soc, Jpn.* **1993**, *66*, 692.
146. J. Almlöf, T. H. Fischer, P. G. Gassman, A. Ghosh and H. Häser, *J. Phys. Chem.* **1993,** *97,* 10964.
147. A. Gosh, *J. Phys. Chem. B* **1997,** *101,* 3290.
148. D. K. Maity, R. L. Bell, and T. N. Truong, *J. Am. Chem. Soc.* **2000,** *122,* 897 and references therein.
149. J. Braun, M. Schlabach, B. Werhle, M. Köcher, E. Vogel and H.-H. Limbach, *J. Am. Chem. Soc.* **1994,** *116*, 6593 and references therein.
150. M. J. Crossley, L. D. Field, M. M. Harding and S. Sternhell, *J. Am. Chem. Soc.* **1987,** *109,* 2335 and references therein.
151. J. Sandström, *Dynamic NMR Spectroscopy*, Academic Press, London, 1982.
152. Z. Smedarchina, W. Siebrand and F. Zerbetto, *Chem. Phys.* **1989,** *136*, 285.
153. K. M. Merz and C. H. Reynolds, *J. Chem. Soc. Chem. Commun.* **1988**, 90.
154. T. X. Lü, J. R. Reimers, M. J. Crossley and N. S. Hush, *J. Phys. Chem.* **1994**, *98,* 11878.
155. J. R. Reimers, T. X. Lü, M. J. Crossley and N. S. Hush, *J. Am. Chem. Soc.* **1995,** *117,* 2855.
156. J. Baker, P. M. Kozlowski, A. A. Jarzecki, P. Pulay, *Theor. Chem. Acc*. **1997**, *97*, 59.
157. J. Braun, H.-H. Limbach, P. G. Williams, H. Morimoto and D. E. Wemmer, *J. Am. Chem. Soc.* **1996,** *118,* 7231.
158. P. H. Hynninen, *Acta Chem. Scand.* **1977**, *31B*, 829.
159. R. J. Laatikainen and M. Niemitz, PERCH project. Department of Chemistry, University of Kuopio.
160. J. Helaja, unpublished results.

161. A. Y. Tauber, J. Helaja, N. V. Tkachenko, H. Lemmetyinen, I. Kilpeläinen and P. H. Hynninen, in Photosynthesis: from Light to Biosphere, P. Mathis, Ed., Vol. VI, Kuwer, Dordrecht, 1995, p. 815.
162. N. V. Tkachenko, L. Rantala, A. Y. Tauber, J. Helaja, P. H. Hynninen and H. Lemmetyinen, *J. Am. Chem. Soc.* **1999,** *121*, 9378.